

Studies of Strong-Field Gravity: Testing the Black Hole Hypothesis and Investigating Spin-Curvature Coupling

by

Sarah Jane Vigeland

B.A., Carleton College (2006)

Submitted to the Department of Physics
in partial fulfillment of the requirements for the degree of

Doctor of Philosophy in Physics

at the

MASSACHUSETTS INSTITUTE OF TECHNOLOGY

June 2012

© Massachusetts Institute of Technology 2012. All rights reserved.

Author
Department of Physics
May 17, 2012

Certified by.....
Scott A. Hughes
Associate Professor
Thesis Supervisor

Accepted by.....
Krishna Rajagopal
Professor of Physics
Associate Department Head for Education

**Studies of Strong-Field Gravity:
Testing the Black Hole Hypothesis and Investigating
Spin-Curvature Coupling**

by

Sarah Jane Vigeland

Submitted to the Department of Physics
on May 17, 2012, in partial fulfillment of the
requirements for the degree of
Doctor of Philosophy in Physics

Abstract

Observations of gravitational systems agree well with the predictions of general relativity (GR); however, to date we have only tested gravity in the weak-field limit. In the next few years, observational advances may make it possible for us to observe motion in the strong field for the first time. This thesis is concerned with two probes of strong-field gravity: whether the spacetime of a black hole has the structure predicted by GR, and the effect of spin-curvature coupling on orbital motion in the large mass-ratio limit.

The first two-thirds of this thesis develop a formalism for determining whether a candidate black hole is described by the Kerr metric, as predicted by GR for all black holes in vacuum. In the first chapter, we describe how to construct a “bumpy black hole,” an object whose spacetime is almost, but not quite, the Kerr metric. We define perturbations to the mass and spin moments and relate the changes in the moments to changes in the orbital frequencies using canonical perturbation theory. In the second chapter, we extend the bumpy black hole formalism to include black holes in non-GR theories of gravity, which leads to additional functional degrees of freedom.

The final chapter investigates the effects of spin-curvature coupling. For a small body with spin moving around a massive black hole, the spin of the small body couples to the background curvature, and its trajectory deviates from a geodesic. To date, there has been relatively little work that considers this effect except in the special cases of aligned spins and circular, equatorial orbits. We compute the perturbation to the trajectory and the spin precession due to spin-curvature coupling for generic orbits of Kerr and arbitrary initial spin orientations.

Thesis Supervisor: Scott A. Hughes
Title: Associate Professor

Acknowledgments

I'd like to begin by thanking my advisor, Scott Hughes, for all of his support and guidance over the years. I'd also like to thank Nico Yunes who has been a valuable collaborator and mentor. Thank you to my committee members Eddie Farhi and Saul Rappaport for their helpful comments and suggestions.

I've been lucky to have some made some wonderful friends over the last few years. I'd like to thank my academic siblings, the other students in Scott's group: Ryan Lang, Pranesh Sundararajan, Leo Stein, Stephen O'Sullivan, Uchupol Ruangsri, and Bogdan Stoica. Thanks to my fellow astrograds, especially Ben Cain, Kat Deck, Robyn Sanderson Grier, Scott Hertel, Adrien Liu, Mike Matejek, Leslie Rogers, Nick Smith-Lefebvre, Chris Williams, and Phil Zukin. You made graduate school a lot more fun.

During my time at MIT, the Women in Physics group has been a wonderful social outlet and source of advice. In particular, I'd like to thank Bonna Newman and Shelby Kimmel. Thanks also to my fellow bartenders at the Muddy Charles Pub and our manager Mike Grenier.

I started my physics career at Carleton College, where I was fortunate to have some wonderful mentors and friends. I'd like to thank my undergraduate advisors Nelson Christensen and Joel Weisberg, who introduced me to the joys and frustrations of physics research. I'd also like to thank Mara Morgenstern Orescanin and Alex Petroff, with whom I've enjoyed many hours of conversation and commiseration. Hans Bantilan has been a colleague and good friend for almost eight years, and I'm looking forward to many more.

I could not have done any of this without the love and support of my family. Thank you to my parents, Deborah and Robert Vigeland, who have done so much to make sure I got a great education. When you bought that picture book about black holes, you probably didn't think that someday I would write a Ph.D. thesis about them. Thanks to my wonderful siblings, Karen, Christine, and John, who are always a source of support, advice, and fun. I'd also like to thank my grandparents, Jane

and Kenneth Browne, for their love and encouragement.

Finally, I'd like to thank Jonathan Malmaud, who makes everything a little better. I'm so lucky to have you in my life.

The research in this thesis was supported by NSF Grants No. PHY-0449884 and No. PHY-1068720, and by NASA Grants No. NNG05G105G and No. NNX08AL42G. During my first year of graduate school, I was supported by a Whiteman Fellowship thanks to the generosity of Dr. George Elbaum.

Contents

1	Introduction	15
1.1	Motivation	15
1.2	Astrophysics of black holes	17
1.3	Motion in black hole spacetimes	18
1.3.1	Equations of motion	19
1.3.2	Constants of the motion and separability	20
1.3.3	Orbital frequencies	26
1.4	Outline of this thesis	28
2	Bumpy black holes	31
2.1	Introduction	31
2.1.1	Motivation: Precision tests of the black hole hypothesis	31
2.1.2	Bumpy black holes: Previous work	34
2.1.3	This analysis	36
2.1.4	Organization and overview	38
2.2	Computing the Geroch-Hansen moments	40
2.3	Bumpy black hole spacetimes	44
2.3.1	Bumpy Schwarzschild	45
2.3.2	Bumpy Kerr	48
2.4	Motion in bumpy black hole spacetimes	52
2.5	Perturbations to the mass moments: Schwarzschild background	55
2.5.1	$l = 2$ mass perturbation	57
2.5.2	$l = 3$ mass perturbation	59

2.5.3	$l = 4$ mass perturbation	61
2.6	Perturbations to the mass moments: Kerr background	63
2.6.1	$l = 2$ mass perturbation	64
2.6.2	$l = 3$ mass perturbation	67
2.7	Perturbations to the spin moments: Schwarzschild background	68
2.7.1	$l = 1$ spin perturbation (linearized Kerr)	68
2.7.2	$l = 2$ spin perturbation	69
2.7.3	$l = 3$ spin perturbation	70
2.8	Perturbations to the spin moments: Kerr background	71
2.8.1	$l = 2$ spin perturbation	72
2.8.2	$l = 3$ spin perturbation	73
2.9	Summary and future work	75
3	Bumpy black holes in alternative theories of gravity	79
3.1	Introduction	79
3.2	Generalized bumpy Kerr formalism	83
3.2.1	From standard to generalized bumpy black holes	84
3.2.2	Existence conditions for the Carter constant	86
3.3	Deformed Kerr formalism	90
3.3.1	Deformed Kerr geometry	90
3.3.2	Existence conditions for the Carter constant	93
3.4	Relating parameterizations	96
3.4.1	To each other	96
3.4.2	To alternative theories	99
3.5	Motion in alternative theories of gravity	102
3.6	Summary and future work	106
4	Spin-curvature coupling	109
4.1	Introduction	109
4.2	Derivation of the Papapetrou equations	113
4.2.1	Overview	113

4.2.2	Motion of a single-pole body	115
4.2.3	Motion of a pole-dipole body	117
4.3	Results: Orbits in Schwarzschild	121
4.3.1	Case 1: Initial spin $\vec{S}_0 = \mu^2 \hat{\theta}$	123
4.3.2	Case 2: Initial spin $\vec{S}_0 = \mu^2 \hat{\phi}$	125
4.4	Results: Orbits in Kerr	126
4.4.1	Case 1: Equatorial orbit, initial spin $\vec{S}_0 = \mu^2 \hat{\theta}$	129
4.4.2	Case 2: Inclined orbit, initial spin $\vec{S}_0 = \mu^2 \hat{\theta}$	130
4.4.3	Case 3: Inclined orbit, initial spin $\vec{S}_0 = \mu^2 \hat{\phi}$	132
4.5	Summary and future work	134
A Averaging functions along black hole orbits		137
B Newtonian precession frequencies		139
B.1	Quadrupole shift ($l = 2$)	141
B.2	Octupole shift ($l = 3$)	142
B.3	Hexadecapole shift ($l = 4$)	143
C Definitions of the modified gravity bumpy Kerr metrics		145

List of Figures

- 2-1 Shifts to black hole orbital frequencies due to an $l = 2$ bump. The shifts $\delta\Omega^{r,\theta,\phi}$ are normalized by the bumpiness parameter B_2 , and are scaled by $p^{7/2}$; this is because in the Newtonian limit, $\delta\Omega^{r,\theta,\phi} \propto p^{-7/2}$. The Newtonian result (dashed lines) describes the exact calculations (solid lines) well in the large p limit, however, the Newtonian result substantially underestimates the shifts in the strong field. Notice that the radial frequency shift changes sign in the strong field, typically at $p \sim (10 - 13)M$, depending slightly on parameters. This behavior is starkly different from the weak field limit. 58
- 2-2 Shifts to black hole orbital frequencies due to an $l = 4$ bump. The shifts $\delta\Omega^{r,\theta,\phi}$ are normalized by the bumpiness parameter B_4 and are scaled by $p^{11/2}$, which sets the scaling in the Newtonian limit. As in the $l = 2$ case (Fig. 2-1), exact results and the Newtonian limit coincide at large p , but there are significant differences in the strong field. The functional behavior of the radial frequency shift can be especially complicated in this case. 62

2-3 Shifts to Kerr black hole orbital frequencies for an $l = 2$ bump. As with the Schwarzschild results presented in Fig. 2-1, the shifts $\delta\Omega^{r,\theta,\phi}$ are normalized by the bumpiness B_2 and scaled by $p^{7/2}$. Rather than examining a variety of orbital geometries, we here examine a few black hole spins, showing results for $a = 0.1M$, $a = 0.5M$, and $a = 0.9M$. Qualitatively, the results are very similar to what we find for the Schwarzschild case. The major difference is that the last stable orbit is located at smaller p , so that these orbits can get deeper into the strong field. The overall impact of the bumps is greater in these cases which reach deeper into the strong field. 66

4-1 Comparison between the trajectory of a body with mass $\mu = 10^{-5}M$ and initial spin vector $\vec{S}_0 = \mu^2 \hat{\theta}$ and a geodesic. The background geodesic is an equatorial orbit around a Schwarzschild black hole with orbital parameters $p = 10 M$ and $e = 0.3$. The spin of the small body produces a phase difference between the geodesic and perturbed trajectories, which causes Δr to grow. There is also an accumulated phase difference in the ϕ coordinate. 124

4-2 Comparison between the spin force and the conservative part of the gravitational self-force for an equatorial orbit around a Schwarzschild black hole with orbital parameters $p = 10M$ and $e = 0.3$. The initial spin vector is $\vec{S}_0 = \mu^2 \hat{\theta}$. The spin force is smaller than the gravitational self-force by about an order of magnitude, indicating that influence of the spin of the small body is not negligible compared to the gravitational self-force. 124

- 4-3 Evolution of the spin vector along an equatorial orbit around a Schwarzschild black hole with orbital parameters $p = 10M$ and $e = 0.3$. The initial spin vector is $\vec{S}_0 = \mu^2 \hat{\phi}$. The spin precession is described by the spin angles α and β , defined in Eq. (4.77) and (4.78), and the magnitude of the spatial part of the spin vector, defined in Eq. (4.79). The angles $\alpha = \pi/2$ and β describe a spin vector rotating in the equatorial plane. 126
- 4-4 Comparison between the trajectory of a body with mass $\mu = 10^{-5}M$ and initial spin vector $\vec{S}_0 = \mu^2 \hat{\phi}$ and a geodesic. The background geodesic is an equatorial orbit around a Schwarzschild black hole with orbital parameters $p = 10M$ and $e = 0.3$. The spin of the small body causes the orbit to oscillate around the equatorial plane by an amount $\Delta\theta$. There are also slight differences in the r and ϕ motions. 127
- 4-5 Comparison between the trajectory of a body with mass $\mu = 10^{-5}M$ and initial spin vector $\vec{S}_0 = \mu^2 \hat{\theta}$ and a geodesic. The background geodesic is an equatorial orbit around a Kerr black hole with spin $a = 0.5M$ and orbital parameters $p = 10M$ and $e = 0.3$. The spin of the small body produces a phase difference between the geodesic and perturbed trajectories, which causes Δr to grow. There is also an accumulated phase difference in the ϕ coordinate. 129
- 4-6 Evolution of the spin vector along an equatorial orbit around a Kerr black hole of spin $a = 0.5M$ with orbital parameters $p = 10M$, $e = 0.3$, and $\theta_{\min} = \pi/3$. The initial spin vector is $\vec{S}_0 = \mu^2 \hat{\theta}$. The spin angles α and β describe the orientation of the spin vector, as defined in Eq. (4.77) and (4.78), respectively. The quantity $|S^i|$ is the magnitude of the spatial part of the spin vector [Eq. (4.79)]. 130

- 4-7 Comparison between the trajectory of a body with mass $\mu = 10^{-5}M$ and initial spin vector $\vec{S}_0 = \mu^2 \hat{\theta}$ and a geodesic. The background geodesic is an inclined orbit around a Kerr black hole with spin $a = 0.5M$ and orbital parameters $p = 10M$, $e = 0.3$, and $\theta_{\min} = \pi/3$. The spin of the small body perturbs the motion. There is an accumulated phase difference between the trajectory and the background geodesic in the r , θ , and ϕ coordinates. 131
- 4-8 Evolution of the spin vector along an equatorial orbit around a Kerr black hole of spin $a = 0.5M$ with orbital parameters $p = 10M$, $e = 0.3$, and $\theta_{\min} = \pi/3$. The initial spin vector is $\vec{S}_0 = \mu^2 \hat{\phi}$. The spin precession is described by the spin angles α and β , defined in Eq. (4.77) and (4.78), and the magnitude of the spatial part of the spin vector, defined in Eq. (4.79). 132
- 4-9 Comparison between the trajectory of a body with mass $\mu = 10^{-5}M$ and initial spin vector $\vec{S}_0 = \mu^2 \hat{\phi}$ and a geodesic. The background geodesic is an orbit around a Kerr black hole with orbital parameters $p = 10M$, $e = 0.3$, and $\theta_{\min} = \pi/3$. The spin of the small body causes the orbit to oscillate around the equatorial plane by an amount $\Delta\theta$. There are also perturbations to the r and ϕ coordinates, but there is no accumulated phase difference in r or ϕ 133

Chapter 1

Introduction

1.1 Motivation

Massive black holes (MBHs) with masses $\sim 10^6 - 10^9 M_\odot$ are ubiquitous in the local Universe; they lie at the center of nearly every nearby galaxy [55] and power active galactic nuclei. Gravitational wave (GW) observations of binary coalescences involving MBHs, made possible by future space-based GW detectors, will let us study their origin, growth mechanism, and populations, as well as provide a way to study strong-field gravity. Extreme mass-ratio inspirals (EMRIs), in which a small compact object of $\sim 1 - 100 M_\odot$ falls into a MBH of $\sim 10^6 M_\odot$, are a particularly interesting source of low-frequency GWs. As the small body slowly falls into the MBH, it probes the structure of the surrounding spacetime and the information is encoded into the emitted GWs. A space-based GW detector would be able to observe the emitted waves in the milliHertz band for a timescale of years, during which time the small body would be very near the horizon of the MBH [83]. Observing these GWs would let us make very precise maps of the spacetime surrounding the MBH in the strong-field regime.

Additionally, advances in electromagnetic observations of MBHs are making it possible to study orbital dynamics in the strong-field. Numerous efforts are underway to study the region around the radio source Sgr A*, which is associated with the MBH at the center of our galaxy. Observations of stars orbiting the central object allow

the measurement of its mass, and recent work has shown that as we probe deeper, we may be able to measure the spacetime’s quadrupole moment [60]. The discovery of a pulsar in orbit around Sgr A* would allow us to map the spacetime very precisely through pulsar timing [57]. There has also been work done to image the accretion disk very close to the horizon of the MBH using very long baseline interferometry (VLBI) [30, 18]. Another promising source is the X-ray emission of the accretion disk around a candidate black hole. Steiner et al. measured the spin of the microquasar XTE J 1550-564 using two methods: modeling the thermal continuum spectrum of the accretion disk and modeling the broad red wing of the Fe $K\alpha$ line [89]. As these observational techniques improve, we will be able to make precision measurements of the spacetime around black holes. To prepare for these advances, it is crucial that we understand how to test the structure of black hole spacetimes and how to model the orbital dynamics in these systems.

Another motivation for studying the evolution of EMRIs is the fact that the large mass ratio of the two bodies significantly simplifies the equations of motion, allowing us to perform the calculations analytically or quasi-analytically. To leading order, an EMRI can be modeled as a small body moving on a geodesic around the large body. Higher order effects perturb the orbit of the small body away from a geodesic and cause the orbit to decay. Once we have analytic models for the motion of an EMRI, we can compare those results to numerical simulations and extrapolate to smaller mass ratios to give us insight into the dynamics of generic binaries [100, 9].

In this thesis, we present projects concerned with two aspects of the strong-field gravity of MBHs. In the first aspect, we develop a formalism for testing whether the spacetime of the MBH is described by the Kerr metric, as predicted by GR. There are several reasons why the spacetime might be described by a non-Kerr metric. The presence of matter, such as a companion object or an accretion disk, would perturb the spacetime away from Kerr. The object might not be a black hole but instead be a compact object composed of an exotic form of matter. Also, some alternate theories of gravity predict rotating black hole solutions that differ from Kerr, such as dynamical Chern-Simons extensions to GR [101]. The second aspect we consider is

the effect of the spin of the small body on its trajectory. If the small body has spin, as all known astrophysical bodies do, its spin couples to the background spacetime and the small body no longer moves along a geodesic [68, 29].

This introductory chapter presents a brief discussion of background material relevant to the rest of the thesis. In Sec. 1.2 we discuss the astrophysics of massive black holes. In Sec. 1.3, we review properties of geodesics of the Kerr metric, which in GR describes all black hole spacetimes in vacuum. Section 1.4 gives an outline of the projects discussed in this thesis.

Throughout this thesis, we work in geometrized (“theorist”) units for which $G = c = 1$. In this system, mass, distance, and time are all measured in the same units; a useful conversion factor is $1 M_{\odot} = 4.92 \times 10^{-6} \text{ s} = 1.48 \text{ km}$. Following the notation of Misner, Thorne, and Wheeler [62], when writing tensors we use Greek indices to indicate a spacetime index ($\mu = 0, 1, 2, 3$, with $\mu = 0$ indicating the time dimension), and a Latin letter to indicate a spatial index ($i = 1, 2, 3$). Parenthesis and brackets around indices stand for symmetrization and antisymmetrization, respectively, i.e. $A_{(\mu\nu)} = (A_{\mu\nu} + A_{\nu\mu})/2$ and $A_{[\mu\nu]} = (A_{\mu\nu} - A_{\nu\mu})/2$.

1.2 Astrophysics of black holes

Although we cannot make direct electromagnetic observations of black holes, we can observe them indirectly by looking at matter around the black hole. There is solid observational evidence for black holes between $\sim 5 - 25 M_{\odot}$ [66]. One example is the compact object in the X-ray binary Cyg X-1. Observations show that the mass of the compact object is $\sim 15 - 25 M_{\odot}$, which is much greater than the maximum mass of a neutron star [104]. Models of stellar evolution predict that stellar-mass black holes with masses $\sim 3 - 100 M_{\odot}$ are the end state of massive stars [45]. In some models, after a neutron star forms in a supernova, it accretes matter until it exceeds the maximum mass of a neutron star and collapses into a black hole. In other models, a black hole is formed directly during the collapse of the progenitor.

There is also evidence that the universe contains many MBHs with masses \sim

$10^5 - 10^7 M_\odot$ and supermassive black holes (SMBHs) with masses $\sim 10^7 - 10^9 M_\odot$. The radio source Sgr A* located at the galactic center is believed to be a MBH. By looking at the orbits of stars near the galactic center, we find that the mass of the central object is $\sim 4 \times 10^6 M_\odot$, with the mass constrained to lie within a very small region ($< 10^{-6} \text{ pc}^3$) [37]. Observations of other galaxies suggest all galaxies with central bulges contain MBHs or SMBHs [55, 58]. Quasars, which are powered by accretion onto SMBHs, have been observed out to a redshift of $z \sim 7$ [63]. The formation mechanism for MBHs and SMBHs is not well-understood; they form through a combination of accretion of gas and mergers of smaller black holes, but the masses of these seed black holes are not known. They may form from black holes with masses $\sim 100 M_\odot$ that formed as remnants of Population III stars at a redshift $\gtrsim 20$, or from black holes with masses $\sim 10^5 M_\odot$ that formed at $10 \lesssim z \lesssim 15$ from dynamical instabilities in massive gaseous protogalactic discs [84]. The mergers of these seed black holes are likely triggered by mergers of the black holes' host galaxies.

Intermediate-mass black holes (IMBHs) are defined to have masses $\sim 10^2 - 10^4 M_\odot$; however, there is not as much evidence for the existence of black holes within this mass range. Some ultra-luminous X-ray sources (ULXs) may be accreting IMBHs [24]. Black holes in this mass range may be formed by stellar collisions in globular collisions [73].

1.3 Motion in black hole spacetimes

Since this thesis is concerned with orbital dynamics in black hole spacetimes, in this section we review some basic material on the Kerr solution and its geodesics. More information can be found in a GR textbook, such as [62], and in Schmidt's paper on Kerr dynamics [82]. The most general stationary, axisymmetric black hole solution¹ in GR is the Kerr metric, which in Boyer-Lindquist coordinates (t, r, θ, ϕ) takes the

¹We ignore the astrophysically uninteresting case of a black hole with charge. Charged astrophysical objects should neutralize quickly due to the ubiquity of plasma in most astrophysical environments.

form

$$\begin{aligned}
ds^2 &\equiv g_{\mu\nu} dx^\mu dx^\nu \\
&= - \left(1 - \frac{2Mr}{\Sigma}\right) dt^2 - \frac{4aMr \sin^2 \theta}{\Sigma} dt d\phi + \frac{\Sigma}{\Delta} dr^2 + \Sigma d\theta^2 \\
&\quad + \frac{\sin^2 \theta}{\Sigma} [(r^2 + a^2)^2 - a^2 \Delta \sin^2 \theta] d\phi^2,
\end{aligned} \tag{1.1}$$

where we have introduced the quantities

$$\Sigma \equiv r^2 + a^2 \cos^2 \theta, \tag{1.2a}$$

$$\Delta \equiv r^2 - 2Mr + a^2. \tag{1.2b}$$

This spacetime describes a black hole with mass M and spin angular momentum $|S| = aM$, where a is the Kerr spin parameter with units of length. In the $a = 0$ limit, this reduces to the Schwarzschild solution:

$$ds^2 = - \left(1 - \frac{2M}{r}\right) dt^2 + \left(1 - \frac{2M}{r}\right)^{-1} dr^2 + r^2 d\theta^2 + r^2 \sin^2 \theta d\phi^2, \tag{1.3}$$

which describes a non-rotating black hole with mass M .

1.3.1 Equations of motion

Now that we have defined the background spacetime, we can compute the equations of motion for a test particle of mass m moving on a background worldline $x^\mu = z^\mu(\lambda)$, where λ is an affine parameter. One way to derive these equations is via the action for a non-spinning test-particle (see e.g. [70])

$$S = -m \int_{\gamma} d\lambda \sqrt{-g_{\alpha\beta}(z) \dot{z}^\alpha \dot{z}^\beta}, \tag{1.4}$$

where $\dot{z}^\mu = dz^\mu/d\lambda$ is the tangent to z^μ .

The contribution of this action to the field equations can be obtained by varying it with respect to the metric tensor. Doing so, we obtain the stress-energy for the

test-particle:

$$T^{\alpha\beta}(x^\mu) = m \int \frac{d\tau}{\sqrt{-g}} u^\alpha u^\beta \delta^{(4)}[\mathbf{x} - \mathbf{z}(\tau)], \quad (1.5)$$

where the proper time τ is related to λ by $d\tau = d\lambda \sqrt{-g_{\alpha\beta}(z)\dot{z}^\alpha\dot{z}^\beta}$, $u^\mu = dz^\mu/d\tau$ is the particle's four-velocity, normalized via $g_{\mu\nu}u^\mu u^\nu = -1$ and $\delta^{(4)}$ is the four-dimensional Dirac density, defined via $\int d^4x \sqrt{-g} \delta^{(4)}(\mathbf{x}) = 1$. The divergence of this stress-energy tensor must vanish in GR, which implies that test-particles follow geodesics:

$$\frac{D}{d\tau} \frac{dz^\alpha}{d\tau} = 0, \quad (1.6)$$

where $D/d\tau$ is a covariant derivative. The divergence of the stress-energy tensor vanishes due to local energy-momentum conservation and the equivalence principle [62]. We have assumed here that the particle is non-spinning, so that geodesic motion is simply described by Eq. (1.6); otherwise other terms would arise in the action that would lead to spin-dependent modifications. We will discuss spin effects in Chapter 4.

1.3.2 Constants of the motion and separability

The geodesic equations as written in Eq. (1.6) are in second-order form, but they can be simplified to first-order form if there exist at least three constants of the motion plus a normalization condition on the four-momentum. As first recognized by Carter [22], this is the case for geodesics in the Kerr spacetime. To derive this, we look for Killing vectors ξ^α and Killing tensors $\xi^{\alpha\beta}$ that satisfy Killing's equation:

$$\nabla_{(\mu} K_{\nu_1 \dots \nu_n)} = 0. \quad (1.7)$$

The Kerr metric possesses two Killing vectors and one Killing tensor. The Killing vectors, $t^\alpha = (1, 0, 0, 0)$ and $\phi^\alpha = (0, 0, 0, 1)$, are associated with the stationarity and axisymmetry of the metric, respectively. In addition, the Kerr metric also possesses the Killing tensor:

$$\xi_{\alpha\beta} = \Delta k_{(\alpha} l_{\beta)} + r^2 g_{\alpha\beta}, \quad (1.8)$$

where $\Delta \equiv r^2 - 2Mr + a^2$ as defined in Eq. (1.2), and k^α and l^α are principal null directions:

$$k^\alpha = \left(\frac{r^2 + a^2}{\Delta}, 1, 0, \frac{a}{\Delta} \right), \quad (1.9a)$$

$$l^\alpha = \left(\frac{r^2 + a^2}{\Delta}, -1, 0, \frac{a}{\Delta} \right). \quad (1.9b)$$

Note that although there is a geometric interpretation for the Killing vectors t^α and ϕ^α , there is no simple geometric interpretation for the Killing tensor $\xi_{\alpha\beta}$.

Contracting these Killing vectors and tensors allows us to define three constants of the motion, the energy E , the z -component of the angular momentum L_z , and the ‘‘Carter constant’’ C :

$$E \equiv -t^\alpha p_\alpha, \quad (1.10)$$

$$L_z \equiv \phi^\alpha p_\alpha, \quad (1.11)$$

$$C \equiv \xi_{\alpha\beta} p^\alpha p^\beta. \quad (1.12)$$

It is conventional to define another version of the Carter constant,

$$Q \equiv C - (L_z - aE)^2. \quad (1.13)$$

For a nonrotating black hole, the Carter constant Q has a simple physical interpretation: $Q + L_z^2 = |\vec{L}|^2$, where \vec{L} is the total orbital angular momentum. This is not the case for a rotating black hole; because the spacetime is not spherically symmetric, we cannot really define the total angular momentum.

With these three constants of the motion [either (E, L_z, C) or (E, L_z, Q)] and the normalization condition on the four-momentum, $p^\alpha p_\alpha = -m^2$, we can separate the

geodesic equations and write them in first-order form:

$$\begin{aligned} m^2 \Sigma^2 \left(\frac{dr}{d\tau} \right)^2 &= [(r^2 + a^2)E - aL_z]^2 - \Delta [m^2 r^2 + (L_z - aE)^2 + Q] \\ &\equiv R(r), \end{aligned} \tag{1.14}$$

$$\begin{aligned} m^2 \Sigma^2 \left(\frac{d\theta}{d\tau} \right)^2 &= Q - \cot^2 \theta L_z^2 - a^2 \cos^2 \theta (m^2 - E^2) \\ &\equiv \Theta(\theta), \end{aligned} \tag{1.15}$$

$$\begin{aligned} m \Sigma \left(\frac{d\phi}{d\tau} \right) &= \csc^2 \theta L_z + aE \left(\frac{r^2 + a^2}{\Delta} - 1 \right) - \frac{a^2 L_z}{\Delta} \\ &\equiv \Phi(r, \theta), \end{aligned} \tag{1.16}$$

$$\begin{aligned} m \Sigma \left(\frac{dt}{d\tau} \right) &= E \left[\frac{(r^2 + a^2)^2}{\Delta} - a^2 \sin^2 \theta \right] + aL_z \left(1 - \frac{r^2 + a^2}{\Delta} \right) \\ &\equiv T(r, \theta), \end{aligned} \tag{1.17}$$

where the coordinate τ measures proper time along the test body's worldline.

Given a choice of the constants E , L_z , and Q and a set of initial conditions, Eqs. (1.14) – (1.17) completely describe the geodesic motion of a test body near a Kerr black hole. Implementing Eqs. (1.14) and (1.15) in a numerical integrator can present some problems, however, since the r and θ motion have turning points where $dr/d\tau$ and $d\theta/d\tau$ pass through zero and switch sign. To account for this behavior, it is convenient to reparameterize these motions using angles ψ and χ for the radial and polar motion, respectively, which smoothly vary from 0 to 2π .

Consider first the radial motion. We parametrize r as

$$r = \frac{pM}{1 + e \cos \psi}. \tag{1.18}$$

where p is the semi-latus rectum, e is the eccentricity, and ψ is the true anomaly. The turning points occur at $\psi = 0$ (periapsis) and $\psi = \pi$ (apoapsis). The function $R(r)$

[Eq. (1.14)] is quartic in r and therefore has four roots:

$$\begin{aligned} R(r) &= (E^2 - m^2)r^4 + 2Mr^3 - [a^2(m^2 - E^2) + L_z^2 + Q]r^2 \\ &\quad + 2M[Q + (L_z - aE)^2]r - a^2Q \end{aligned} \quad (1.19)$$

$$= (m^2 - E^2)(r_1 - r)(r - r_2)(r - r_3)(r - r_4). \quad (1.20)$$

We define the roots so that $r_1 \geq r_2 \geq r_3 \geq r_4$. Then r_1 and r_2 correspond to apoapsis and periapsis, respectively:

$$r_1 = \frac{pM}{1 - e}, \quad (1.21a)$$

$$r_2 = \frac{pM}{1 + e}. \quad (1.21b)$$

Similarly, we can map the roots r_3 and r_4 to parameters p_3 and p_4 :

$$r_3 = \frac{p_3M}{1 - e}, \quad (1.22a)$$

$$r_4 = \frac{p_4M}{1 + e}. \quad (1.22b)$$

The roots p_3 and p_4 have no physical meaning. Now the equation of motion of ψ takes a simple form:

$$\begin{aligned} \frac{d\psi}{d\tau} &= \frac{M\sqrt{m^2 - E^2}}{1 - e^2} \frac{1}{\Sigma} [(p - p_3) - e(p + p_3 \cos \psi)]^{1/2} \\ &\quad \times [(p - p_4) + e(p - p_4 \cos \psi)]^{1/2}. \end{aligned} \quad (1.23)$$

This equation has no turning points, so it is easy to numerically integrate; the angle ψ simply accumulates secularly.

Now we turn our attention to the θ motion. We begin by defining $z \equiv \cos \theta$, and then we introduce the parameter χ by setting $z = z_- \cos \chi$. The turning points of the θ motion map to z_- , which we identify by² $z_- \equiv \cos \theta_{\min}$. Then Eq. (1.15) can

²Another common choice is to let $z = \cos^2 \theta = z_- \cos^2 \chi$.

be written

$$\Theta(z) = Q - \frac{z^2}{1-z^2}L_z^2 - a^2z^2(m^2 - E^2) \quad (1.24)$$

$$= \frac{a^2(m^2 - E^2)(z_+^2 - z^2)(z_-^2 - z^2)}{1 - z^2}. \quad (1.25)$$

Like the roots r_3 and r_4 of the radial potential, the root z_+ has no physical meaning.

The geodesic equation for χ is given by

$$\frac{d\chi}{d\tau} = \frac{\sqrt{a^2(m^2 - E^2)(z_+ - z)}}{r^2 + a^2z}, \quad (1.26)$$

This equation of motion for χ has no turning points; like the angle ψ we introduced to describe the radial motion, the angle χ accumulates secularly.

We can relate the constants of the motion E , L_z , and Q to the orbital parameters p , e , and θ_{\min} by looking at the turning points of the r and θ motion. Our derivation here follows the approach of Schmidt in Appendix B of [82]. First we look at the θ motion, described in Eq. (1.24). The θ potential has a turning point at $\theta = \theta_{\min}$, i.e., $\Theta(z_-) = 0$, which gives us an expression for Q in terms of E , L_z , and θ_{\min} :

$$Q = L_z^2 \cot^2 \theta_{\min} + a^2(m^2 - E^2) \cos^2 \theta_{\min}. \quad (1.27)$$

Now we turn to the radial motion. Substituting the expression for Q into the radial potential, Eq. (1.19), allows us to write $R(r)$ as a polynomial in E and L_z :

$$R(r) = f(r)E^2 - 2g(r)EL_z - h(r)L_z^2 - d(r), \quad (1.28)$$

where

$$f(r) = r^4 + a^2(r^2 + 2Mr + \cos^2 \theta_{\min} \Delta), \quad (1.29a)$$

$$g(r) = 2aMr, \quad (1.29b)$$

$$h(r) = \frac{r^2 - 2Mr + a^2 \cos^2 \theta_{\min}}{\sin^2 \theta_{\min}} \quad (1.29c)$$

$$d(r) = m^2(r^2 + a^2 \cos^2 \theta_{\min})\Delta. \quad (1.29d)$$

When we evaluate Eq. (1.28) at the radial turning points, we obtain two equations that are quadratic in E and L_z :

$$f_1 E^2 - 2g_1 E L_z - h_1 L_z^2 - d_1 = 0, \quad (1.30a)$$

$$f_2 E^2 - 2g_2 E L_z - h_2 L_z^2 - d_2 = 0, \quad (1.30b)$$

where we have defined the following coefficients:

$$(f_1, g_1, h_1, d_1) = (f(r_1), g(r_1), h(r_1), d(r_1)), \quad (1.31a)$$

$$(f_2, g_2, h_2, d_2) = (f(r_2), g(r_2), h(r_2), d(r_2)). \quad (1.31b)$$

Solving these equations for E and L_z yields

$$E^2 = \frac{\kappa\rho + 2\epsilon \pm 2\sqrt{\sigma(\sigma\epsilon^2 + \rho\epsilon\kappa - \eta\kappa^2)}}{\rho^2 + 4\eta\sigma}, \quad (1.32)$$

$$L_z^2 = \frac{\epsilon\rho^2 + 4\epsilon\eta\sigma - \eta\kappa\rho - 2\eta\epsilon\sigma \pm 2\eta\sqrt{\sigma(\sigma\epsilon^2 + \rho\epsilon\kappa - \eta\kappa^2)}}{\sigma(\rho^2 + 4\eta\sigma)}, \quad (1.33)$$

where the coefficients κ , ϵ , ρ , η , and σ are defined by

$$\kappa = d_1 h_2 - d_2 h_1, \quad (1.34a)$$

$$\epsilon = d_1 g_2 - d_2 g_1, \quad (1.34b)$$

$$\rho = f_1 h_2 - f_2 h_1, \quad (1.34c)$$

$$\eta = f_1 g_2 - f_2 g_1, \quad (1.34d)$$

$$\sigma = g_1 h_2 - g_2 h_1. \quad (1.34e)$$

In the limit of small a and large p , the constants E , L_z , and Q are given by

$$E = m \left[1 - \frac{1 - e^2}{2p} + \frac{3(1 - e^2)^2}{8p^2} - \frac{a(1 - e^2)^2 \sin \theta_{\min}}{M p^{5/2}} \right], \quad (1.35)$$

$$L_z = mM p^{1/2} \sin \theta_{\min} \left[1 + \frac{3 + e^2}{2p} - \frac{a(3 + e^2) \sin \theta_{\min}}{M p^{3/2}} \right], \quad (1.36)$$

$$Q = m^2 M^2 p \cos^2 \theta_{\min} \left[1 + \frac{3 + e^2}{p} - \frac{a 2(3 + e^2) \sin \theta_{\min}}{M p^{3/2}} \right]. \quad (1.37)$$

1.3.3 Orbital frequencies

Now we turn our attention to the orbital frequencies. Our discussion here closely follows that given by Schmidt [82], which uses Hamilton-Jacobi methods to compute black hole orbital frequencies. Separating the motion not only identifies the constants of the motion but also the action variables

$$J_r \equiv \frac{1}{2\pi} \oint p_r dr = \frac{1}{\pi} \int_{r_p}^{r_a} \frac{\sqrt{R(r)}}{\Delta} dr, \quad (1.38)$$

$$J_\theta \equiv \frac{1}{2\pi} \oint p_\theta d\theta = \frac{2}{\pi} \int_{\theta_{\min}}^{\pi/2} \sqrt{\Theta(\theta)} d\theta, \quad (1.39)$$

$$J_\phi \equiv \frac{1}{2\pi} \oint p_\phi d\phi = L_z. \quad (1.40)$$

It is also useful to define

$$J_t \equiv -E. \quad (1.41)$$

This is a slight abuse of the notation since geodesic motion is not cyclic in t and hence we cannot define J_t as a closed integral over time, but is convenient for reasons we will illustrate shortly.

The Hamiltonian for test-body motion is

$$\mathcal{H} \equiv \frac{1}{2} g_{\alpha\beta} p^\alpha p^\beta. \quad (1.42)$$

At least formally, we can rewrite the Hamiltonian in Eq. (1.42) in terms of the action variables J_μ . Let $\mathcal{H}^{(\text{aa})}$ be the Hamiltonian written in terms of the action variables. According to Hamilton-Jacobi theory, the orbital frequencies are the derivatives of $\mathcal{H}^{(\text{aa})}$ with respect to the action variables:

$$m\omega^i = \frac{\partial \mathcal{H}^{(\text{aa})}}{\partial J_i}. \quad (1.43)$$

For black hole orbits, we cannot explicitly rewrite the Hamiltonian; however, we can use the chain rule to write Eq. (1.43) in terms of quantities we can compute. Following

Ref. [82] (modifying its notation slightly), we put

$$P_\beta \doteq (\mathcal{H}, E, L_z, Q). \quad (1.44)$$

We define the matrices \mathcal{A} and \mathcal{B} , whose components are

$$\mathcal{A}_\alpha^\beta = \frac{\partial P_\alpha}{\partial J_\beta}, \quad (1.45a)$$

$$\mathcal{B}_\alpha^\beta = \frac{\partial J_\alpha}{\partial P_\beta}. \quad (1.45b)$$

By the chain rule, these matrices have an inverse relationship:

$$\mathcal{A}_\alpha^\beta \mathcal{B}_\beta^\gamma = \delta_\alpha^\gamma. \quad (1.46)$$

The components of the matrix \mathcal{A} are directly related to the frequencies we wish to compute. In particular, since P_0 is just the invariant Hamiltonian, $m\omega^i = \partial P_0 / \partial J_i \equiv \mathcal{A}_0^i$. However, the components of the matrix \mathcal{B} are written in a way that is fairly easy to work out. We exploit this to write $m\omega^i = (\mathcal{B}^{-1})_0^i$, from which we find

$$m\omega^r = \frac{\partial J_\theta / \partial Q}{(\partial J_r / \partial \mathcal{H})(\partial J_\theta / \partial Q) - (\partial J_r / \partial Q)(\partial J_\theta / \partial \mathcal{H})}, \quad (1.47)$$

$$m\omega^\theta = \frac{-\partial J_r / \partial Q}{(\partial J_r / \partial \mathcal{H})(\partial J_\theta / \partial Q) - (\partial J_r / \partial Q)(\partial J_\theta / \partial \mathcal{H})}, \quad (1.48)$$

$$m\omega^\phi = \frac{(\partial J_r / \partial Q)(\partial J_\theta / \partial L_z) - (\partial J_r / \partial L_z)(\partial J_\theta / \partial Q)}{(\partial J_r / \partial \mathcal{H})(\partial J_\theta / \partial Q) - (\partial J_r / \partial Q)(\partial J_\theta / \partial \mathcal{H})}. \quad (1.49)$$

The frequencies $\omega^{r,\theta,\phi}$ are conjugate to the orbit's *proper* time; they would be measured by an observer who rides on the orbit itself. For our purposes, it will be more useful to convert to frequencies conjugate to the Boyer-Lindquist coordinate time, describing measurements made by a distant observer. The quantity³

$$\Gamma \equiv \frac{1}{m} \frac{\partial \mathcal{H}^{(\text{aa})}}{\partial J_t} = -\frac{1}{m} \frac{\partial \mathcal{H}^{(\text{aa})}}{\partial E} \quad (1.50)$$

³Here we have adjusted notation from Schmidt slightly.

performs this conversion; the frequencies $\Omega^{r,\theta,\phi} = \omega^{r,\theta,\phi}/\Gamma$ are of observational relevance. Going back to Eqs. (1.45) and (1.46), we find $m\Gamma = (\mathcal{B}^{-1})_0^0$, or

$$m\Gamma = \frac{(\partial J_r/\partial E)(\partial J_\theta/\partial Q) - (\partial J_r/\partial Q)(\partial J_\theta/\partial E)}{(\partial J_r/\partial \mathcal{H})(\partial J_\theta/\partial Q) - (\partial J_r/\partial Q)(\partial J_\theta/\partial \mathcal{H})}. \quad (1.51)$$

For a circular, equatorial orbit, the orbital frequency Ω^ϕ takes a simple form:

$$\Omega^\phi = \frac{M^{1/2}}{r^{3/2} + aM^{1/2}}. \quad (1.52)$$

This is the equivalent to Kepler's law for the Kerr metric.

It is useful to have weak-field ($p \gg M$) forms of these frequencies. When we expand to first order in a , and then expand in $1/p$, the orbital frequencies become

$$\Omega^r = \omega^K \left[1 - \frac{3(1-e^2)}{p} + \frac{a}{M} \frac{3(1-e^2) \sin \theta_{\min}}{p^{3/2}} \right], \quad (1.53a)$$

$$\Omega^\theta = \omega^K \left[1 + \frac{3e^2}{p} - \frac{a}{M} \frac{3(1+e^2) \sin \theta_{\min}}{p^{3/2}} \right], \quad (1.53b)$$

$$\Omega^\phi = \omega^K \left[1 + \frac{3e^2}{p} + \frac{a}{M} \frac{2 - 3(1+e^2) \sin \theta_{\min}}{p^{3/2}} \right], \quad (1.53c)$$

where ω_K is the Kepler frequency,

$$\omega^K = \frac{1}{M} \left(\frac{1-e^2}{p} \right)^{3/2}. \quad (1.54)$$

1.4 Outline of this thesis

This thesis is organized as follows. In Chapter 2, based on [93] and [92], we lay out the bumpy black hole formalism, which provides a model-independent way of testing whether a black hole candidate is described by the Kerr metric as predicted by GR. In this chapter, we describe how to generate spacetimes whose mass and spin moments differ from the Kerr metric by introducing two additional functional degrees of freedom. We find that a perturbation function that falls off like $r^{-(l+1)}$ in the weak-field changes the multipole moments of order l and higher while leaving lower-order

moments unchanged. This enables us to use the bumpy black hole formalism to define spacetimes that are identical to the Kerr spacetime up to some arbitrary order L but which differ from Kerr for $l \geq L$. We also show how these perturbations change the orbital frequencies using canonical perturbation theory.

In Chapter 3, based on [94], we extend the bumpy black hole formalism to include black holes in alternate theories of gravity. In alternate theories of gravity, we can no longer make the assumption that the spacetime is vacuum, i.e., that $T_{\mu\nu} = 0$. When we remove this restriction, the perturbations are described by four functions instead of two. We discuss ways of parametrizing these functions for spacetimes that also admit an approximate second-order Killing tensor. This restriction is not necessary, but it is convenient since it allows us to write the equations of motion in first-order form. We then map these perturbation functions to known black hole solutions in alternative theories of gravity, specifically dynamical Chern-Simons gravity and dynamical, quadratic gravity.

Chapter 4 examines another aspect of strong-field gravity, the impact of spin-curvature coupling on orbital dynamics. A small body with spin does not follow a geodesic; instead its motion is described by the Papapetrou equation [68], which includes a force arising from the small body's spin coupling to the background curvature. To date, this effect has not been studied in great detail. Previous work taking into account the spin of the small body has been limited to an analysis of circular, equatorial orbits with the spin of the small body parallel or nearly parallel to the spin of the background object. In this chapter we compute the trajectory and the spin precession for generic orbits around Kerr black holes with arbitrary initial spin orientations. We also compare the magnitude of the spin force to the gravitational self-force, as calculated by Barack and Sago [7], since both the spin force and the gravitational self-force scale as μ^2 , where μ is the mass of the small body. We find that the spin force is smaller than the gravitational self-force by about an order of magnitude, indicating that the impact of spin-curvature coupling is not significantly smaller than the impact of the gravitational self-force. In order to accurately model the GW emission to first order in the mass of the small body, we need to take into

account both of these effects.

Chapter 2

Bumpy black holes

This chapter is based on *Physical Review D* **81**, 024030 (2010), which was written in collaboration with Scott A. Hughes, and *Physical Review D* **82**, 104041 (2010).

2.1 Introduction

2.1.1 Motivation: Precision tests of the black hole hypothesis

Though observations of gravitational systems agree well with the predictions of general relativity (GR), so far the most detailed and quantitative tests have been done in the weak field. (“Weak field” means that the dimensionless Newtonian potential $\phi \equiv GM/rc^2 \ll 1$, where M is a characteristic mass scale and r a characteristic distance.) This is largely because many of the most precise tests are done in our solar system (e.g., [11]). Even the celebrated tests which use binary neutron stars (e.g., [56]) are essentially weak-field: for those systems, $M \sim$ several M_\odot , orbital separation \sim several R_\odot , so $\phi \sim$ a few $\times GM_\odot/R_\odot c^2 \sim$ a few $\times 10^{-6}$.

This situation is on the verge of changing. Observational technology is taking us to a regime where we either are or soon will be probing motion in strong gravity, with $\phi \gtrsim 0.1$. Examples of measurements being made now include radio studies of accretion flows near the putative black hole in our galactic center [30] and X-ray studies of hot accretion that allow precise measurements of accretion disk geometries

[78, 64]. Future measurements include the possible discovery of a black hole-pulsar system, perhaps with the Square Kilometer Array [85], and gravitational-wave (GW) observations of small bodies spiraling into massive black holes due to the backreaction of GW emission [2].

For weak-field studies, a well-developed paradigm for testing gravity has been developed. The parameterized post-Newtonian (PPN) expansion [62, 96] quantifies various measurable aspects of relativistic gravity. For example, the PPN parameter γ (whose value is 1 in GR) quantifies the amount of spatial curvature produced by a unit of rest mass. Other PPN parameters quantify a theory’s nonlinearity, the degree to which it incorporates preferred frames, and the possible violation of conservation laws. See Ref. [96], Chap. 4 for a detailed discussion. Unfortunately, no similar framework exists for strong-field studies. If we hope to use observations as tools for testing the nature of strong gravity objects and strong-field gravity, we need to rectify this.

Black holes are a particularly interesting tool for studying strong-field gravity. Aside from having the strongest accessible gravitational fields of any object in the Universe¹, within GR they have an amazingly simple spacetime structure: the “no-hair” theorems [48, 23, 79, 74, 75] guarantee that the exterior spacetime of any black hole is completely described by only two numbers, its mass M and spin parameter a . Any deviation from that simplicity points to a failure either in our understanding of gravity or in the nature of ultracompact objects.

A useful way to describe black hole spacetimes is in terms of multipole moments. In many areas of physics, multipolar expansions are used as tools for describing the shape of a distribution of matter or energy, or for describing the behavior of a potential function. Multipole moments are most commonly used to describe fields whose governing equations are linear, since the functions describing the angular behavior

¹More accurately, they have the largest potential $\phi \sim GM/Rc^2$. One may also categorize weak or strong gravity using spacetime curvature or tides; arguably this is a more fundamental measure for assessing whether GR is likely to be accurate or not. From this perspective, black holes are actually *not* such “strong gravity” objects; indeed, the tidal field just outside a $10^8 M_\odot$ black hole’s event horizon is not much different from the tidal field at the surface of the Earth. See Ref. [78] for further discussion of this point.

are typically eigenfunctions of the angular piece of the governing differential operator. For example, the Newtonian gravitational potential Φ arising from a matter distribution ρ must satisfy Poisson's equation:

$$\nabla^2\Phi = \begin{cases} 4\pi G\rho & (\text{interior}), \\ 0 & (\text{exterior}). \end{cases} \quad (2.1)$$

In the exterior region, we can write Φ as a sum over multipolar contributions:

$$\Phi(r, \theta, \phi) = -G \sum_{lm} \frac{M_{lm} Y_{lm}(\theta, \phi)}{r^{l+1}}. \quad (2.2)$$

The coefficients M_{lm} are mass multipole moments. By matching the expansion of Φ on the boundary to a similar expansion for the interior, they can be shown to describe the angular distribution of the mass of the source. (Throughout this chapter, we will restrict ourselves to axisymmetric spacetimes, for which the axial index m must be zero; we ignore it in what follows.)

Geroch [36] and Hansen [42] developed an analogous multipolar description for spacetimes of isolated, stationary, axisymmetric objects in GR in terms of scalar multipoles. Their definition applies to spacetimes that are asymptotically flat; for such spacetimes there is a well-defined “large r ” limit in which multipoles can be defined in a way that roughly accords with our usual intuition. When one computes the Geroch-Hansen moments of a source, one finds that its spacetime is described by a family of mass moments M_l , very similar to those appearing in our Newtonian expansions in Eq. (2.2), as well as a family of *current* moments S_l . For a fluid body, the current moments describe how the matter flow is distributed through the compact body, much as magnetic moments describe how electric current is distributed through an electromagnetic source. These moments can be conveniently combined in the complex moment

$$\mathcal{M}_l = M_l + iS_l. \quad (2.3)$$

For a generic source, the moments \mathcal{M}_l are unconstrained.² As we show in Sec. 2.2, for a Kerr black hole the moments take a particularly simple form:

$$\mathcal{M}_l = M(ia)^l, \quad (2.4)$$

where \mathcal{M}_l is the l th moment, M is the total mass of the black hole, and a is its spin parameter defined by $a = |\vec{S}|/M$. (We neglect the astrophysically uninteresting possibility of a black hole with macroscopic charge.) This is a statement of the “no-hair” theorem: the spacetime of a Kerr black hole is completely described by its mass and spin [48, 23, 79].

Testing the hypothesis that an object is a Kerr black hole can thus be framed as a null experiment. First, measure the putative black hole spacetime’s multipoles. Using the moments M_0 and S_1 , determine the parameters M and a . If the spacetime is Kerr, all moments for $l \geq 2$ must be given by Eq. (2.4). The null hypothesis is that any deviation from those Kerr moments is zero. Failure of the null hypothesis means the black hole candidate is not a Kerr black hole, and may indicate a failure of strong-field GR.

2.1.2 Bumpy black holes: Previous work

The sharply constrained nature of the Kerr multipoles in Eq. (2.4) suggests that this relation may be useful as a test of black hole spacetimes: if the spacetime is Kerr, then knowledge of only two moments is needed to determine all of the others. Ryan [80] was the first to build a scheme to test this idea, constructing spacetimes in which all of the moments were arbitrary. This scheme was sufficient to prove the principle of the idea, but did not work well for building spacetimes that are good deep into the strong field. Collins and Hughes [25] noted that, if GR correctly describes black hole candidates, then testing their nature amounts to trying to falsify the hypothesis that they are Kerr black holes. They suggested formulating black hole tests as a null

²If we assume the spacetime is reflection symmetric, then only the even mass moments and odd spin moments can be nonzero. In this chapter, we do not restrict ourselves to reflection symmetric spacetimes.

experiment by examining spacetimes for which

$$\mathcal{M}_l = M(ia)^l + \delta\mathcal{M}_l, \quad (2.5)$$

and using measurements to test whether $\delta\mathcal{M}_l = 0$, as it should if they are Kerr black holes.

To this end, Collins and Hughes [25] introduced the bumpy black hole: a spacetime that deviates in a small, controllable manner from the exact black holes of GR. By construction, the bumpy black hole includes “normal” black holes as a limit. This is central to testing the black hole hypothesis by a null experiment. Spacetimes of other proposed massive, compact objects (for example, boson stars [26, 81]) typically do not include black holes as a limiting case. This limits their utility if black hole candidates are, in fact, GR’s black holes. Measurements of black holes using observables formulated in a bumpy black hole spacetime should simply measure the spacetime’s “bumpiness” (defined more precisely below) to be zero.

Though a useful starting point, the bumpy black holes developed in Ref. [25] had three major shortcomings. First, the changes to the spacetime that were introduced to modify its mass multipole moments were not smooth. The worked example presented in Ref. [25] is interpreted as a Schwarzschild black hole perturbed by an infinitesimally thin ring of positive mass around its equator and by a pair of negative mass infinitesimal points near its poles. Though this changes the spacetime’s mass quadrupole moment (the desired outcome of this construction), it gives the spacetime a pathological strong-field structure. This is reflected in the fact that non-equatorial strong-field orbits are ill-behaved in this construction [77]. Also, Ref. [25] only considered perturbations to the mass moments and left the spin moments unchanged. In order to construct the most general bumpy black holes, we must be able to perturb both the mass and the spin moments.

Finally, Ref. [25] only examined bumpy Schwarzschild black holes. Glampedakis and Babak [38] rectified this deficiency with their introduction of a “quasi-Kerr” spacetime. Their construction uses the exterior Hartle-Thorne metric [43, 44] de-

scribing the exterior of any slowly rotating, axisymmetric, stationary body. It includes the Kerr metric to $\mathcal{O}(a^2)$ as a special case. Identifying the influence of the mass quadrupole moment in the Hartle-Thorne form of the Kerr metric, they then introduce a modification to the full Kerr spacetime that changes the black hole’s mass quadrupole moment from its canonical value.

2.1.3 This analysis

The goal of this work is to introduce smooth perturbations to both the mass and spin moments, and to extend the bumpy black hole concept to include spinning black holes. Dealing with the non-smooth nature of the bumps is, as we show in Secs. 2.3, 2.5, and 2.6, quite straightforward. It simply requires introducing perturbations to the black hole background that are smooth rather than discontinuous. In essence, rather than having bumps that correspond to infinitesimal points and rings, the bumps we use here are smeared into pure multipoles.

Extending Ref. [25] to spinning black holes is more of a challenge. Given that Ref. [38] already introduced a bumpy-black-hole-like spacetime that encompasses spacetimes with angular momentum, one might wonder why another construction is needed. A key motivation is that we would like to be able to make an arbitrary modification to a black hole’s moments. Although showing that a black hole candidate has a non-Kerr value for the mass quadrupole moment would be sufficient to falsify its black hole nature (at least within the framework of GR), one can imagine scenarios in which the first L moments of a black hole candidate agree with the Kerr value, but things differ for $l > L$. For example, Yunes et al. have shown that in Chern-Simons modifications to GR, slowly rotating black hole solutions have the multipolar structure of Kerr for $l < 4$, but differ for $l \geq 4$ [101, 87]. There are many ways in which black hole candidates might differ from the black holes of GR; we need to develop a toolkit sufficiently robust that it can encompass these many potential points of departure.

Our technique for making bumpy Kerr holes is based on the Newman-Janis algorithm [65]. This algorithm transforms a Schwarzschild spacetime into Kerr by

“rotating” the spacetime in a complex configuration space³. In this chapter, we construct bumpy Kerr black holes by applying the Newman-Janis algorithm to bumpy Schwarzschild black holes. The outcome of this procedure is a spacetime whose mass moments are deformed relative to Kerr. When the bumpiness is set equal to zero, we recover the Kerr metric.

Once one has constructed a bumpy black hole spacetime, one then needs to show how its bumps are encoded in observables. The most detailed quantitative tests will come from orbits near black hole candidates. As such, it is critical to know how orbital frequencies change as a function of a spacetime’s bumpiness. More generally, we are faced with the problem of understanding motion in general stationary axisymmetric vacuum spacetimes. Brink [14] has recently published a very detailed analysis of this problem, with a focus on understanding whether and for which situations the spacetimes admit integrable motion. She has found evidence that geodesic motion in such spacetimes may, in many cases, be integrable. If so, the problem of mapping general spacetimes (not just “nearly black hole” spacetimes) may be tractable. Gair, Li, and Mandel [35] have similarly examined orbital characteristics in the Manko-Novikov spacetime [59], which has a particular tunable non-Kerr structure. They show how orbits change in such spacetimes, and how its bumpiness colors observable characteristics.

For this analysis, we confine ourselves to the simpler problem of motion in bumpy black hole spacetimes, addressing this challenge in Secs. 2.5 and 2.6 using canonical perturbation theory. As is now well known (and was shown rather spectacularly by Schmidt [82]), Hamilton-Jacobi methods let us write down closed-form expressions for the three orbital frequencies (Ω^r , Ω^θ , Ω^ϕ) which completely characterize the behavior of bound Kerr black hole orbits. Since bumpy black hole spacetimes differ only perturbatively from black hole spacetimes, canonical perturbation theory lets us characterize how a spacetime’s bumps shift those frequencies, and thus are encoded in observables. Similar techniques were used by Glampedakis and Babak [38] to see

³This complex “rotation” is made most clear by framing the discussion using the Ernst potential [33]. Transforming from Schwarzschild to Kerr corresponds to adding an imaginary part to a particular potential.

how frequencies are shifted in a quasi-Kerr metric, and were also used by Hinderer and Flanagan [46] in a two-timescale analysis of inspiral into Kerr black holes.

2.1.4 Organization and overview

The organization of this chapter is as follows. We begin in Sec. 2.2 by reviewing in detail how Geroch-Hansen moments are calculated, and we demonstrate the procedure on the Kerr spacetime. Sec. 2.3 is an overview of bumpy spacetimes. We start with the axially symmetric and stationary Weyl line element. We review the Einstein field equations in this representation, introduce the Schwarzschild limit, and describe first order perturbations. The spacetime’s bumpiness is set by choosing potential functions ψ_1 and σ_1 which control how the spacetime deviates from the black hole limit. Specifically, the function ψ_1 describes the mass perturbations while σ_1 describes the spin perturbations. We initially leave these functions arbitrary except for the requirement that they be small enough that we can only consider first-order terms. Later, we discuss specific choices for ψ_1 and σ_1 . Following our discussion of bumpy Schwarzschild spacetimes, we show how to use the Newman-Janis algorithm to build bumpy Kerr black holes.

We discuss geodesic motion in these spacetimes in Sec. 2.4, where we show how to calculate the orbital frequencies of bumpy black holes using canonical perturbation theory. Canonical perturbation theory requires averaging a bump’s shift to an orbit’s Hamiltonian. This averaging was developed in Ref. [32] and is summarized in Appendix A.

In Secs. 2.5 – 2.8, we focus on specific choices for the perturbation functions and compute the resulting changes in the orbital frequencies and multipole moments. We consider mass perturbations on a Schwarzschild and Kerr background in Secs. 2.5 and 2.6, respectively. We take $\sigma_1 = 0$ and ψ_1 to be a pure multipole in the Weyl sector, construct the spacetime, and numerically compute the shifts in Ω^r , Ω^θ , and Ω^ϕ . Detailed results are given for $l = 2$, $l = 3$, and $l = 4$, and some examples of the frequency shifts we find are shown in Figs. 2-1 ($l = 2$, Schwarzschild), 2-2 ($l = 4$, Schwarzschild) and 2-3 ($l = 2$, Kerr). There is no reason in principle to stop there,

though the results quickly become repetitive.

A few results are worth highlighting. First, we find that in the weak field, the exact numerical results for frequency shifts correctly reproduce the Newtonian limit, which we derive in Appendix B. In the strong field, the frequency shifts are significantly greater. The shift to the radial frequency is particularly interesting: it tends to oscillate, shifting between an enhancement and a decrement as orbits move into the strong field. This behavior appears to be a robust signature of non-Kerr multipole structure in black hole strong fields. Interestingly, it turns out that black hole spin does not have a very strong impact on the bumpiness-induced shifts to orbital frequencies. Spin's main effect is to change the location of the last stable orbit. For large spin, orbits reach deeper into the strong field, amplifying the bumps' impact on orbital frequencies. Aside from the change to the last stable orbits, the impact of a particular multipolar bump looks largely the same across all spin values.

We also compute the changes to the Geroch-Hansen moments $\delta\mathcal{M}_l$. Our goal is to demonstrate that our choice for ψ_1 maps in a natural way to the spacetime's Geroch-Hansen moments. For example, a bump which is built from an $l = 2$ spherical harmonic changes the even Geroch-Hansen moments above the $l = 2$ moment. In principle, one could construct a change to a single Geroch-Hansen mass moment by including multiple appropriately weighted spherical harmonic terms in the bumpy black hole spacetime.

We then turn our attention to spin perturbations in Secs. 2.7 and 2.8, for which $\psi_1 = 0$. We show that the spin perturbations map to changes in the Geroch-Hansen moments similarly to the mass moment perturbations; if we add an order l spin moment perturbation, which we define in Secs. 2.7 and 2.8, we leave the spin moments unchanged up to order l .

Finally, we summarize our analysis and suggest some directions for future work in Sec. 2.9. We do not discuss in this analysis the issue of measurability. Turning these foundations for mapping the multipole moment structure of black holes into a practical measurement program (for instance, via gravitational-wave measurements, timing of a black hole-pulsar binary, or precision mapping in radio or x-rays of accretion

flows) will take a substantial effort.

In this chapter, when we discuss bumpy black holes, we will always use a “hat” accent to denote quantities which are calculated in the pure black hole background spacetimes. For example, we write the orbital frequencies as $\Omega = \hat{\Omega} + \delta\Omega$, where $\hat{\Omega}$ is the frequency of an orbit in the black hole background and $\delta\Omega$ denotes the shift due to the black hole’s bumps.

2.2 Computing the Geroch-Hansen moments

We begin our analysis by showing how to compute the Geroch-Hansen moments for the spacetime of a compact object. As an important example, we demonstrate the procedure on the Kerr metric, which in Boyer-Linquist coordinates is given by

$$\begin{aligned}
 ds^2 = & - \left(1 - \frac{2Mr}{\Sigma}\right) dt^2 - \frac{4aMr \sin^2 \theta}{\Sigma} dt d\phi + \frac{\Sigma}{\Delta} dr^2 + \Sigma d\theta^2 \\
 & + [(r^2 + a^2)^2 - a^2 \Delta \sin^2 \theta] \frac{\sin^2 \theta}{\Sigma} d\phi^2,
 \end{aligned} \tag{2.6}$$

where $\Delta \equiv r^2 - 2Mr + a^2$ and $\Sigma \equiv r^2 + a^2 \cos^2 \theta$.

In order to compute the Geroch-Hansen moments, the spacetime must have a timelike Killing vector and be asymptotically flat. Let the spacetime’s Killing tensor be K^α , and let the manifold V be the 3-surface orthogonal to this vector. The metric on V can be written

$$h_{ij} = \lambda g_{ij} + K_i K_j, \tag{2.7}$$

where $\lambda = -K^\alpha K_\alpha$ is the norm of K^α . To calculate the moments, we perform a conformal transformation to map infinity onto a point Λ . The space is asymptotically flat if it can be conformally mapped to a 3-space \tilde{V} which satisfies [36]

- (i) $\tilde{V} = V \cup \Lambda$, where Λ is a single point;
- (ii) $\tilde{h}_{ij} = \Omega^2 h_{ij}$ is the conformal metric;
- (iii) $\Omega|_\Lambda = 0$, $\tilde{D}_i \Omega|_\Lambda = 0$, $\tilde{D}_i \tilde{D}_j \Omega|_\Lambda = 2\tilde{h}_{ij}$;

where Ω is the conformal factor and \tilde{D}_i is the derivative operator associated with \tilde{h}_{ij} . The conformal metric has the form [4]

$$ds^2 = dr^2 + r^2 d\theta^2 + r^2 \sin^2 \theta e^{-2\beta(r,\theta)} d\phi^2. \quad (2.8)$$

The function $\beta(r, \theta)$ parametrizes the deviation of the conformal metric from sphericity.

In order to construct the spacetime's Geroch-Hansen moments, we need its Ernst potential [33] and the conformal factor Ω . We begin with the Ernst potential, which we build from the norm λ and twist ω of K^α . For the Kerr metric, the norm is given by

$$\lambda = 1 - \frac{2Mr}{\Sigma}. \quad (2.9)$$

The twist is related to the “generalized curl”⁴ of the timelike Killing vector,

$$\omega_\alpha = \epsilon_{\alpha\beta\gamma\delta} K^\beta \nabla^\gamma K^\delta. \quad (2.10)$$

From the Bianchi identities, we can write the curl as [36]

$$\nabla_{[\alpha} \omega_{\beta]} = -\epsilon_{\alpha\beta\gamma\delta} K^\gamma R^\delta{}_\nu K^\nu. \quad (2.11)$$

For a spacetime that is vacuum in GR, the condition $R_{\mu\nu} = 0$ implies that $\nabla_{[\alpha} \omega_{\beta]} = 0$. This allows us to write $\omega_\alpha = \nabla_\alpha \omega$, where the scalar function ω is the twist of K^α . (If $R_{\mu\nu} \neq 0$, we cannot construct the Ernst potential. We will discuss this issue in more detail in Sec. 2.6 and 2.8.) For the Kerr spacetime, we find

$$\omega = -\frac{2Ma \cos \theta}{\Sigma}. \quad (2.12)$$

⁴Normally, the curl of a vector is only defined in a 3-dimensional vector space; we follow the lead of Ref. [34] in generalizing the notion of the curl to higher dimensions.

We then combine the norm and twist into the complex quantity

$$\epsilon = \lambda + i\omega \quad (2.13)$$

$$= 1 - \frac{2Mr}{\Sigma} - i \frac{2Ma \cos \theta}{\Sigma}, \quad (2.14)$$

where on the second line we have specialized to Kerr. From this, two definitions of the Ernst potential appear in the literature: Ref. [33] defines it as

$$\Xi = \frac{1 + \epsilon}{1 - \epsilon}, \quad (2.15)$$

while Ref. [34] defines the Ernst potential as

$$\xi = \frac{1 - \epsilon}{1 + \epsilon}. \quad (2.16)$$

These definitions are simply related to one another ($\xi = \Xi^{-1}$). We find the potential ξ to be most useful for computing multipoles of bumpy black hole spacetimes, but we use Ξ to perturb a spacetime's current multipoles.

Next, we must find the conformal factor Ω . We begin by defining a new radial coordinate \bar{R} according to

$$r = \bar{R}^{-1} \left(1 + M\bar{R} + \frac{M^2 - a^2}{4} \bar{R}^2 \right). \quad (2.17)$$

The point Λ corresponds to $\bar{R} = 0$. The conformal factor is given by

$$\Omega = \frac{\bar{R}^2}{\sqrt{\left(1 - \frac{M^2 - a^2}{4} \bar{R}^2\right)^2 - a^2 \bar{R}^2 \sin^2 \theta}}, \quad (2.18)$$

and the conformal metric is given by

$$ds^2 = d\bar{R}^2 + \bar{R}^2 d\theta^2 + \bar{R}^2 \sin^2 \theta d\phi^2 \left[1 - \left(\frac{4a\bar{R} \sin \theta}{4 - (M^2 - a^2)\bar{R}^2} \right)^2 \right]^{-1}. \quad (2.19)$$

This corresponds to β equal to

$$\beta = \frac{1}{2} \ln \left[1 - \left(\frac{4a\bar{R} \sin \theta}{4 - (M^2 - a^2)\bar{R}^2} \right)^2 \right]. \quad (2.20)$$

As shown by Bäckdahl and Herberthson [4], the multipole moments can be computed from derivatives of a function y , which we now describe. Begin by defining $\tilde{\phi}$, a conformally weighted variant of the Ernst potential ξ ,

$$\tilde{\phi} = \Omega^{-1/2} \xi, \quad (2.21)$$

and new cylindrical coordinates $\tilde{z} = \bar{R} \cos \theta$ and $\tilde{\rho} = \bar{R} \sin \theta$. We now write the potential $\tilde{\phi}$ as a function of these variables, $\tilde{\phi}(\tilde{z}, \tilde{\rho})$, and introduce yet another variation:

$$\phi_L(\bar{R}) = \tilde{\phi}(\bar{R}, i\bar{R}). \quad (2.22)$$

We need to define a few more functions related to the metric:

$$\beta_L(\bar{R}) = \beta(\bar{R}, i\bar{R}), \quad (2.23)$$

$$\kappa_L(\bar{R}) = -\ln \left[1 - \bar{R} \int_0^{\bar{R}} \frac{e^{2\beta_L(\bar{R}')} - 1}{\bar{R}'^2} d\bar{R}' - \bar{R}C \right] + \beta_L(\bar{R}), \quad (2.24)$$

where β is defined in Eq. (2.8) and C is the integration constant. We can choose the gauge so that $C = 0$. The multipoles are calculated from the function

$$y(\bar{R}) = e^{-\kappa_L(\bar{R})/2} \phi_L(\bar{R}), \quad (2.25)$$

with the l th multipole moment given by

$$\mathcal{M}_l = \frac{2^l l!}{(2l)!} \left. \frac{d^l y}{d\rho^l} \right|_{\rho=0}, \quad (2.26)$$

where $\rho(\bar{R}) = \bar{R}e^{\kappa_L(\bar{R}) - \beta_L(\bar{R})}$. For the Kerr spacetime, the potential ϕ_L is given by

$$\phi_L(\bar{R}) = \frac{M(1 + ia\bar{R})}{(1 + a^2\bar{R}^2)^{3/4}}. \quad (2.27)$$

The functions $\beta_L(\bar{R})$ and $\kappa_L(\bar{R})$ are given by

$$\beta_L(\bar{R}) = \frac{1}{2} \ln [1 + a^2\bar{R}^2], \quad (2.28)$$

$$\kappa_L(\bar{R}) = \frac{1}{2} \ln \left[\frac{1 + a^2\bar{R}^2}{(1 - a^2\bar{R}^2)^2} \right]. \quad (2.29)$$

Then the variable ρ is given by $\rho = \bar{R}(1 - a^2\bar{R}^2)^{-1}$ and

$$y(\bar{R}) = \frac{M\sqrt{1 - a^2\bar{R}^2}}{1 - ia\bar{R}}. \quad (2.30)$$

In this case, the multipoles can be written as

$$\mathcal{M}_l = M(ia)^l. \quad (2.31)$$

2.3 Bumpy black hole spacetimes

We begin with general considerations on the spacetimes we consider. We are interested in stationary, axisymmetric, asymptotically flat spacetimes, which are described by the Weyl metric:

$$ds^2 = -e^{2\psi} dt^2 + e^{2\gamma - 2\psi} (d\rho^2 + dz^2) + e^{-2\psi} \rho^2 d\phi^2. \quad (2.32)$$

The nontrivial vacuum Einstein equations for this metric are given by

$$0 = \frac{\partial^2 \psi}{\partial \rho^2} + \frac{1}{\rho} \frac{\partial \psi}{\partial \rho} + \frac{\partial^2 \psi}{\partial z^2}, \quad (2.33)$$

$$\frac{\partial \gamma}{\partial \rho} = \rho \left[\left(\frac{\partial \psi}{\partial \rho} \right)^2 - \left(\frac{\partial \psi}{\partial z} \right)^2 \right], \quad (2.34)$$

$$\frac{\partial \gamma}{\partial z} = 2\rho \frac{\partial \psi}{\partial \rho} \frac{\partial \psi}{\partial z}. \quad (2.35)$$

Equations (2.33) – (2.35) will be our main tools for building bumpy black hole spacetimes. We expand ψ and γ as $\psi = \psi_0 + \psi_1$ and $\gamma = \gamma_0 + \gamma_1$, with $\psi_1/\psi_0 \ll 1$, and $\gamma_1/\gamma_0 \ll 1$. Before specializing to black hole backgrounds, note that Eq. (2.33) is simply Laplace’s equation. The functions ψ_1 can thus very conveniently be taken to be harmonic functions. This is key to smoothing out the spacetime’s bumps and curing one of the problems with the bumpy black holes defined in [25].

2.3.1 Bumpy Schwarzschild

We begin by building a bumpy Schwarzschild black hole. The Schwarzschild metric is recovered from Eq. (2.32) when $\psi_1 = \gamma_1 = 0$ and we set

$$\psi_0 = \ln \tanh(u/2), \quad (2.36)$$

$$\gamma_0 = -\frac{1}{2} \ln \left(1 + \frac{\sin^2 v}{\sinh^2 u} \right). \quad (2.37)$$

The prolate spheroidal coordinates (u, v) are a remapping of the coordinates (ρ, z) used in Eq. (2.32):

$$\rho = M \sinh u \sin v, \quad (2.38a)$$

$$z = M \cosh u \cos v. \quad (2.38b)$$

Expanding the Einstein equations Eqs. (2.33) – (2.35) about the Schwarzschild values to leading order in ψ_1 and γ_1 , we find the perturbations must satisfy

$$\nabla^2 \psi_1 = 0, \quad (2.39)$$

$$\frac{\partial \gamma_1}{\partial u} = \frac{2[\tan v(\partial \psi_1 / \partial u) + \tanh u(\partial \psi_1 / \partial v)]}{\sinh u(\coth u \tan v + \tanh u \cot v)}, \quad (2.40)$$

$$\frac{\partial \gamma_1}{\partial v} = \frac{2[\tan v(\partial \psi_1 / \partial v) - \tanh u(\partial \psi_1 / \partial u)]}{\sinh u(\coth u \tan v + \tanh u \cot v)}. \quad (2.41)$$

As discussed in [25], Eqs. (2.40) and (2.41) overdetermine the solution; we choose to use Eq. (2.41) to calculate γ_1 .

We introduce a final set of coordinates, the Schwarzschild coordinates r and θ , by

$$r = 2M \cosh^2 \frac{u}{2}, \quad (2.42a)$$

$$\theta = v. \quad (2.42b)$$

The coordinates ρ and z are related to r and θ by

$$\rho = r \sin \theta \sqrt{1 - \frac{2M}{r}}, \quad (2.43a)$$

$$z = (r - M) \cos \theta. \quad (2.43b)$$

Then in Schwarzschild coordinates, the metric is given by

$$ds^2 = -(1 + 2\psi_1) \left(1 - \frac{2M}{r}\right) dt^2 + (1 + 2\gamma_1 - 2\psi_1) \left(1 - \frac{2M}{r}\right)^{-1} dr^2 \\ + (1 + 2\gamma_1 - 2\psi_1) r^2 d\theta^2 + (1 - 2\psi_1) r^2 \sin^2 \theta d\phi^2. \quad (2.44)$$

Now we turn our attention to perturbations to the spin moments. When we defined mass perturbations, we based our definition on the multipolar expansion of the gravitational potential in Newtonian gravity. We cannot do the same thing for spin perturbations because in Newtonian gravity, mass currents are not a source of the gravitational field. Instead, we create perturbations to the spin moments by adding an imaginary perturbation to the Ernst potential as defined in Eq. (2.15):

$$\Xi = \Xi_{\text{Schw}} + i\Xi_1, \quad (2.45)$$

where $\Xi_{\text{Schw}} = r/M - 1$ is the Ernst potential for the Schwarzschild spacetime.

For the mass perturbations, we found a natural way of defining order l perturbations when we enforced the vacuum Einstein equations to first order. We want to do something similar for the perturbations to the spin moments. As shown by Ernst [33], enforcing the vacuum Einstein equations to first order gives the following constraint

equation for Ξ_1 :

$$\nabla^2 \left(\frac{\partial^2 \Xi_1}{\partial r^2} \right) = 0. \quad (2.46)$$

As discussed in [33], one class of solutions to this equation includes the linearized Kerr spacetime, which we discuss in Sec. 2.7.1. We define higher order perturbations by considering another class of solutions to Eq. (2.46). Since $(\partial^2 \Xi_1 / \partial r^2)$ satisfies Laplace's equation, we can define an order l spin perturbation as one for which $(\partial^2 \Xi_1 / \partial r^2)$ is an order l spherical harmonic. We relate the perturbation to the Ernst potential to changes in the timelike Killing vector field by inverting Eq. (2.15):

$$\epsilon = 1 - \frac{2M}{r} + i \frac{2M^2}{r^2} \Xi_1. \quad (2.47)$$

The perturbation leaves the norm of the timelike Killing vector unchanged, but it changes the twist of the timelike Killing vector, which was formerly zero, to

$$\omega = \frac{2M^2}{r^2} \Xi_1. \quad (2.48)$$

The metric now has a nonzero $g_{t\phi}$ component,

$$ds^2 = - \left(1 - \frac{2M}{r} \right) dt^2 + 2\sigma_1 dt d\phi + \left(1 - \frac{2M}{r} \right)^{-1} dr^2 + r^2 d\theta^2 + r^2 \sin^2 \theta d\phi^2, \quad (2.49)$$

where σ_1 is related to Ξ_1 by

$$\frac{\partial}{\partial r} \left(\frac{r\sigma_1}{r-2M} \right) = \frac{2M^2 \sin \theta}{(r-2M)^2} \frac{\partial \Xi_1}{\partial \theta}, \quad (2.50)$$

$$\frac{\partial \sigma_1}{\partial \theta} = \frac{2M^2 \sin \theta}{r} \left(2\Xi_1 - r \frac{\partial \Xi_1}{\partial r} \right). \quad (2.51)$$

Equations (2.50) and (2.51) overdetermine σ_1 ; we will use Eq. (2.50) to calculate σ_1

with the boundary conditions

$$\lim_{r \rightarrow \infty} \sigma_1 = 0, \quad (2.52a)$$

$$\lim_{r \rightarrow \infty} \frac{\partial \sigma_1}{\partial r} = 0. \quad (2.52b)$$

Combining the metrics in Eq. (2.44) and Eq. (2.49), we obtain the full bumpy Schwarzschild metric:

$$ds^2 = -(1 + 2\psi_1) \left(1 - \frac{2M}{r}\right) dt^2 + (1 + 2\gamma_1 - 2\psi_1) \left(1 - \frac{2M}{r}\right)^{-1} dr^2 \\ + (1 + 2\gamma_1 - 2\psi_1) r^2 d\theta^2 + (1 - 2\psi_1) r^2 \sin^2 \theta d\phi^2 + 2\sigma_1 dt d\phi. \quad (2.53)$$

We can expand the metric as $g_{\alpha\beta} \equiv g_{\alpha\beta}^{\text{Schw}} + h_{\alpha\beta}$, where $g_{\alpha\beta}^{\text{Schw}}$ is the Schwarzschild metric, and $h_{\alpha\beta}$ is the perturbed metric:

$$h_{tt} = -2\psi_1 \left(1 - \frac{2M}{r}\right), \quad (2.54a)$$

$$h_{t\phi} = \sigma_1, \quad (2.54b)$$

$$h_{rr} = 2(\gamma_1 - \psi_1) \left(1 - \frac{2M}{r}\right)^{-1}, \quad (2.54c)$$

$$h_{\theta\theta} = 2(\gamma_1 - \psi_1) r^2, \quad (2.54d)$$

$$h_{\phi\phi} = -2\psi_1 r^2 \sin^2 \theta. \quad (2.54e)$$

All other components of $h_{\alpha\beta}$ are related by symmetry or are zero. It is clear that we recover the normal Schwarzschild black hole in the limit $\psi_1 \rightarrow 0$, $\gamma_1 \rightarrow 0$, $\sigma_1 \rightarrow 0$. As we discuss further in Sec. 2.5 and 2.7, the potentials ψ_1 and γ_1 perturb the mass moments while σ_1 perturbs the spin moments.

2.3.2 Bumpy Kerr

We now use the Newman-Janis algorithm [65] to transform bumpy Schwarzschild into bumpy Kerr. We begin with the bumpy Schwarzschild metric from Eq. (2.53), and

we use Eq. (2.42) to write the metric in prolate spheroidal coordinates:

$$\begin{aligned}
ds^2 &= -(1 + 2\psi_1) \tanh^2(u/2) dt^2 + 2\sigma_1 dt d\phi \\
&\quad + (1 + 2\gamma_1 - 2\psi_1) 4M^2 \cosh^4(u/2) (du^2 + dv^2) \\
&\quad + (1 - 2\psi_1) 4M^2 \cosh^4(u/2) \sin^2 v d\phi^2.
\end{aligned} \tag{2.55}$$

We decompose the metric in terms of a complex null tetrad with legs l^μ , n^ν , m^ν :

$$g^{\mu\nu} = -l^\mu n^\nu - l^\nu n^\mu + m^\mu \bar{m}^\nu + m^\nu \bar{m}^\mu, \tag{2.56}$$

where an overbar denotes complex conjugate, and the legs are given by

$$\begin{aligned}
l^\mu &= (1 - \psi_1) \coth^2(u/2) \delta_t^\mu + (1 + \psi_1 - \gamma_1) \frac{1}{M} \operatorname{csch} u \delta_u^\mu \\
&\quad - \sigma_1 \frac{1}{M^2} \operatorname{csch}^2 u \csc^2 v \delta_\phi^\mu,
\end{aligned} \tag{2.57a}$$

$$\begin{aligned}
n^\mu &= \frac{1}{2} \left[(1 - \psi_1) \delta_t^\mu - (1 + \psi_1 - \gamma_1) \frac{1}{M} \operatorname{csch} u \tanh^2(u/2) \delta_u^\mu \right. \\
&\quad \left. - \sigma_1 \frac{1}{M^2} \operatorname{csch}^2 u \tanh^2(u/2) \csc^2 v \delta_\phi^\mu \right],
\end{aligned} \tag{2.57b}$$

$$m^\mu = \frac{1}{2\sqrt{2}M} (1 + \psi_1) \operatorname{sech}^2(u/2) \left[(1 - \gamma_1) \delta_v^\mu + i \csc v \delta_\phi^\mu \right]. \tag{2.57c}$$

We use the Kronecker delta δ_ν^μ to indicate components.

Next, following the key step of the Newman-Janis algorithm, we allow the coor-

dinate u to be complex, and rewrite l^μ , n^μ , and m^μ as

$$\begin{aligned}
l^\mu &= (1 - \psi_1) \frac{2}{\tanh^2(u/2) + \tanh^2(\bar{u}/2)} \delta_t^\mu \\
&\quad + (1 + \psi_1 - \gamma_1) \frac{1}{M \sqrt{\cosh u \cosh \bar{u} - 1}} \delta_u^\mu \\
&\quad - \sigma_1 \frac{\csc^2 v}{M^2 (\cosh u \cosh \bar{u} - 1)} \delta_\phi^\mu, \tag{2.58a}
\end{aligned}$$

$$\begin{aligned}
n^\mu &= \frac{1}{2} (1 - \psi_1) \delta_t^\mu - (1 + \psi_1 - \gamma_1) \frac{\tanh^2(u/2) + \tanh^2(\bar{u}/2)}{4M \sqrt{\cosh u \cosh \bar{u} - 1}} \delta_u^\mu \\
&\quad - \sigma_1 \frac{\csc^2 v}{8M^2} \operatorname{sech}^2(u/2) \operatorname{sech}^2(\bar{u}/2) \delta_\phi^\mu, \tag{2.58b}
\end{aligned}$$

$$m^\mu = \frac{1}{2\sqrt{2}M} (1 + \psi_1) \operatorname{sech}^2(\bar{u}/2) [(1 - \gamma_1) \delta_v^\mu + i \csc v \delta_\phi^\mu]. \tag{2.58c}$$

Notice that we recover the original tetrad when we force $u = \bar{u}$. Further discussion of this seemingly *ad hoc* procedure (and an explanation of how it uniquely generates the Kerr spacetime) is given in Ref. [31].

Next, we change coordinates. We rewrite the tetrad using coordinates (U, r, θ, ϕ) given by

$$U = t - 2M \cosh^2(u/2) - 2M \ln [\sinh^2(u/2)] - ia \cos \theta, \tag{2.59a}$$

$$r = 2M \cosh^2(u/2) + ia \cos \theta, \tag{2.59b}$$

$$\theta = v. \tag{2.59c}$$

The axial coordinate ϕ is the same in both coordinate systems. At this point, a is

just a parameter. The result of this transformation is

$$l^\mu = (\gamma_1 - 2\psi_1) \left(1 - \frac{2Mr}{\Sigma}\right)^{-1} \delta_U^\mu + (1 + \psi_1 - \gamma_1) \delta_r^\mu - \sigma_1 \frac{\csc^2 \theta}{\Sigma - 2Mr} \delta_\phi^\mu, \quad (2.60a)$$

$$n^\mu = \left(1 - \frac{1}{2}\gamma_1\right) \delta_U^\mu - \frac{1}{2}(1 + \psi_1 - \gamma_1) \left(1 - \frac{2Mr}{\Sigma}\right) \delta_r^\mu - \sigma_1 \frac{\csc^2 \theta}{2\Sigma} \delta_\phi^\mu, \quad (2.60b)$$

$$m^\mu = \frac{(1 + \psi_1 - \gamma_1)}{\sqrt{2}(r + ia \cos \theta)} \left[ia \sin \theta (\delta_U^\mu - \delta_r^\mu) + \delta_\theta^\mu + \gamma_1 i \csc \theta \delta_\phi^\mu \right]. \quad (2.60c)$$

Making one additional coordinate transformation,

$$dU = dt - \frac{r^2 + a^2}{\Delta} dr, \quad (2.61a)$$

$$d\phi = d\phi' - \frac{a}{\Delta} dr, \quad (2.61b)$$

leads to the bumpy Kerr black hole metric in Boyer-Lindquist coordinates:

$$\begin{aligned} ds^2 = & - \left[(1 + 2\psi_1) \left(1 - \frac{2Mr}{\Sigma}\right) + \frac{4aMr}{\Sigma^2} \sigma_1(r, \theta) \right] dt^2 \\ & - \gamma_1 \frac{4a^2 Mr \sin^2 \theta}{\Delta \Sigma} dt dr - \left\{ (1 + 2\psi_1 - \gamma_1) \frac{4aMr \sin^2 \theta}{\Sigma} \right. \\ & \left. + 4\sigma_1 \left[\frac{(r^2 + a^2)2Mr}{\Sigma^2} + \frac{\Delta}{\Sigma} - \frac{\Delta}{2\Sigma - 4Mr} \right] \right\} dt d\phi \\ & + (1 + 2\gamma_1 - 2\psi_1) \frac{\Sigma}{\Delta} dr^2 + 2\gamma_1 \left[1 + \frac{2Mr(r^2 + a^2)}{\Delta \Sigma} \right] a \sin^2 \theta dr d\phi \\ & + (1 + 2\gamma_1 - 2\psi_1) \Sigma d\theta^2 + [(r^2 + a^2)^2 - a^2 \Delta \sin^2 \theta \\ & + (\gamma_1 - \psi_1) \frac{8a^2 M^2 r^2 \sin^2 \theta}{\Sigma - 2Mr} - 2\psi_1 \frac{\Sigma^2 \Delta}{\Sigma - 2Mr} \\ & \left. + \frac{4aMr}{\Sigma - 2Mr} \sigma_1 \left(\Delta + \frac{2Mr(r^2 + a^2)}{\Sigma} \right) \right] \frac{\sin^2 \theta}{\Sigma} d\phi^2, \end{aligned} \quad (2.62)$$

where we have dropped the prime on ϕ . Notice that Eq. (2.62) reduces to the Kerr metric when $\psi_1 \rightarrow 0$, $\gamma_1 \rightarrow 0$, $\sigma_1 \rightarrow 0$, and it reduces to the bumpy Schwarzschild metric [Eq. (2.53)] for $a \rightarrow 0$. The parameter a is seen to be the spin angular momentum of the black hole, $|\vec{S}|/M$. Writing the bumpy Kerr metric in the form

$g_{\alpha\beta} = g_{\alpha\beta}^{\text{Kerr}} + h_{\alpha\beta}$, where $g_{\alpha\beta}^{\text{Kerr}}$ is the Kerr metric, we read out of Eq. (2.62)

$$h_{tt} = -2 \left(1 - \frac{2Mr}{\Sigma} \right) \psi_1 - \frac{4aMr}{\Sigma^2} \sigma_1, \quad (2.63a)$$

$$h_{tr} = -\gamma_1 \frac{2a^2 Mr \sin^2 \theta}{\Delta \Sigma}, \quad (2.63b)$$

$$h_{t\phi} = (\gamma_1 - 2\psi_1) \frac{2aMr \sin^2 \theta}{\Sigma} + \sigma_1 \left[\frac{4Mr(r^2 + a^2)}{\Sigma^2} + \frac{2\Delta}{\Sigma} - \frac{\Delta}{\Sigma - 2Mr} \right], \quad (2.63c)$$

$$h_{rr} = 2(\gamma_1 - \psi_1) \frac{\Sigma}{\Delta}, \quad (2.63d)$$

$$h_{r\phi} = \gamma_1 a \sin^2 \theta \left[1 + \frac{2Mr(r^2 + a^2)}{\Delta \Sigma} \right], \quad (2.63e)$$

$$h_{\theta\theta} = 2(\gamma_1 - \psi_1) \Sigma, \quad (2.63f)$$

$$h_{\phi\phi} = \frac{\sin^2 \theta}{\Sigma} \left\{ (\gamma_1 - \psi_1) \frac{8a^2 M^2 r^2 \sin^2 \theta}{\Sigma - 2Mr} - 2\psi_1 \Sigma \Delta \left(1 - \frac{2Mr}{\Sigma} \right)^{-1} + \sigma_1 \frac{4aMr}{\Sigma - 2Mr} \left[\Delta + \frac{2Mr(r^2 + a^2)}{\Sigma} \right] \right\}. \quad (2.63g)$$

All other components are related by symmetry or are zero. By inspection, we see that $h_{\alpha\beta} \rightarrow 0$ as $\psi_1 \rightarrow 0$, $\gamma_1 \rightarrow 0$, $\sigma_1 \rightarrow 0$.

Before moving on, we summarize our procedure. To build a bumpy black hole spacetime, we first select functions ψ_1 (for mass bumps) and σ_1 (for spin bumps) which satisfy the necessary constraint equations [Eq. (2.33) for mass bumps; Eqs. (2.46), (2.50), and (2.51) for spin bumps]. We use Eqs. (2.40) and (2.41) to find the function γ_1 that corresponds to the background spacetime and our chosen ψ_1 . Finally, we apply the Newman-Janis algorithm to “rotate” the spacetime to nonzero a . The resulting metric is given by Eq. (2.62).

2.4 Motion in bumpy black hole spacetimes

We now discuss motion in these spacetimes. We focus on the frequencies associated with oscillations in the radial coordinate r , the polar angle θ , and rotations in ϕ about the symmetry axis. These frequencies are typically the direct observables of

black hole orbits; it is from measuring these frequencies and their evolution that one can hope to constrain the properties of black hole candidates.

For motion in a bumpy black hole space-time, the Hamiltonian \mathcal{H} remains conserved with value $-m^2/2$, but its functional form is shifted:

$$\begin{aligned}\mathcal{H} &= \frac{1}{2}g^{\alpha\beta}p_\alpha p_\beta = -\frac{m^2}{2} \\ &= \hat{\mathcal{H}} + \mathcal{H}_1,\end{aligned}\tag{2.64}$$

where $\hat{\mathcal{H}}$ is the original (non-bumpy) Hamiltonian and \mathcal{H}_1 describes the influence of the spacetime's bumpiness. To first order in the perturbation,

$$\mathcal{H}_1 = -\frac{1}{2}b_{\mu\nu}p^\mu p^\nu = -\frac{m^2}{2}b_{\mu\nu}\frac{dx^\mu}{d\tau}\frac{dx^\nu}{d\tau}.\tag{2.65}$$

For a bumpy spacetime, the motion is no longer separable (except for the special case of equatorial motion) and the techniques used in Sec. 1.3.3 for computing orbital frequencies do not work. However, since the spacetime is “close to” the exact black hole spacetime in a well-defined sense, the motion is likewise “close to” the integrable motion. We can thus take advantage of canonical perturbation theory as described in, for example, Goldstein [39], to calculate how the spacetime's bumps change the frequencies.

The shifts to the frequencies can be found by averaging \mathcal{H}_1 :

$$m\delta\omega^i = \frac{\partial\langle\mathcal{H}_1\rangle}{\partial\hat{J}_i},\tag{2.66a}$$

$$m\delta\Gamma = \frac{\partial\langle\mathcal{H}_1\rangle}{\partial\hat{J}_0}.\tag{2.66b}$$

Notice that the derivatives are taken with respect to the action variables of the background motion; the averaging, which we denote with angular brackets, is likewise done with respect to orbits in the background. Then the observable frequencies are given by

$$\Omega^i \equiv \hat{\Omega}^i + \delta\Omega^i = \frac{\hat{\omega}^i + \delta\omega^i}{\hat{\Gamma} + \delta\Gamma}\tag{2.67}$$

or

$$\frac{\delta\Omega^i}{\Omega^i} = \frac{\delta\omega^i}{\hat{\omega}^i} - \frac{\delta\Gamma}{\hat{\Gamma}}. \quad (2.68)$$

The averaging used in Eq. (2.66) is described in detail in Appendix A. This procedure uses the fact that the r and θ portions of the background motion can be separated, and thus can be averaged independently. As described in Appendix A, $\langle\mathcal{H}_1\rangle$ is given by

$$\langle\mathcal{H}_1\rangle = \frac{1}{\Upsilon^t(2\pi)^2} \int_0^{2\pi} dw^r \int_0^{2\pi} dw^\theta \mathcal{H}_1 [r(w^r), \theta(w^\theta)] T [r(w^r), \theta(w^\theta)], \quad (2.69)$$

where $T(r, \theta)$ is defined in Eq. (1.17); $w^{r,\theta}$ are the angles associated with the separated r and θ motions, as defined in Eq. (A.8); and Υ^t is the averaged value of the function $T(r, \theta)$, as defined in Eq. (A.9). The perturbed Hamiltonian \mathcal{H}_1 can be expanded as

$$\begin{aligned} \mathcal{H}_1 &= -\frac{m^2}{2} \left[b_{tt} \left(\frac{dt}{d\tau} \right)^2 + b_{rr} \left(\frac{dr}{d\tau} \right)^2 + b_{\theta\theta} \left(\frac{d\theta}{d\tau} \right)^2 + b_{\phi\phi} \left(\frac{d\phi}{d\tau} \right)^2 \right. \\ &\quad \left. + 2b_{tr} \frac{dt}{d\tau} \frac{dr}{d\tau} + 2b_{r\phi} \frac{dr}{d\tau} \frac{d\phi}{d\tau} + 2b_{t\phi} \frac{dt}{d\tau} \frac{d\phi}{d\tau} \right] \\ &= -\frac{m^2}{2} \left[b_{tt} \left(\frac{dt}{d\tau} \right)^2 + b_{rr} \left(\frac{dr}{d\tau} \right)^2 + b_{\theta\theta} \left(\frac{d\theta}{d\tau} \right)^2 + b_{\phi\phi} \left(\frac{d\phi}{d\tau} \right)^2 \right. \\ &\quad \left. + 2b_{t\phi} \frac{dt}{d\tau} \frac{d\phi}{d\tau} \right] \\ &= -\frac{1}{2\Sigma^2} \left[b_{tt}T(r, \theta)^2 + b_{rr}R(r) + b_{\theta\theta}\Theta(\theta) + b_{\phi\phi}\Phi(r, \theta)^2 \right. \\ &\quad \left. + 2b_{t\phi}T(r, \theta)\Phi(r, \theta) \right], \end{aligned} \quad (2.70)$$

where $R(r)$, $\Theta(\theta)$, $T(r, \theta)$, and $\Phi(r, \theta)$ are defined in Eqs. (1.14) – (1.17). In going from the first line to the second, we use the fact that terms linear in $dr/d\tau$ average to zero because the radial motion switches sign after half a cycle.

In computing this average, we end up with $\langle\mathcal{H}_1\rangle$ as a function of p , e , and θ_{\min} . We likewise compute the actions J_μ using these parameters, and then compute the shifts to the frequencies and Γ using the chain rule. To set up this calculation, we

define an array b_β which contains all the system's physical parameters:

$$b_\beta \doteq (m, p, e, \theta_{\min}) . \quad (2.71)$$

Next, we define the matrix \mathcal{J} , the Jacobian of the actions with respect to these parameters:

$$(\mathcal{J})_\alpha^\beta = \frac{\partial J_\alpha}{\partial b_\beta} . \quad (2.72)$$

Then

$$\delta\omega^i = \frac{\partial \langle \mathcal{H}_1 \rangle}{\partial b_\alpha} (\mathcal{J}^{-1})_\alpha^i , \quad (2.73a)$$

$$\delta\Gamma = \frac{\partial \langle \mathcal{H}_1 \rangle}{\partial b_\alpha} (\mathcal{J}^{-1})_\alpha^0 , \quad (2.73b)$$

where \mathcal{J}^{-1} is the matrix inverse of the Jacobian \mathcal{J} .

2.5 Perturbations to the mass moments: Schwarzschild background

We now examine the spacetimes and orbits of bumpy Schwarzschild black holes for specific choices of ψ_1 with $\sigma_1 = 0$. Because ψ_1 satisfies the Laplace equation [Eq. (2.39)], we can take it to be a pure multipole in Weyl coordinates (ρ, z) [i.e., in the coordinates of Eq. (2.32)]. As we show in this section and the next, this smooths out the bumps and cures the strong-field pathologies associated with orbits in the perturbations used in [25].

Note that a pure multipole in the Weyl sector will not correspond to a pure Geroch-Hansen moment of the black hole. For example, taking ψ_1 to be proportional to an $l = 2$ spherical harmonic does not change only M_2 Geroch-Hansen moment [Eq. (2.5)]. However, as we show below, taking ψ_1 to be proportional to a spherical harmonic Y_{l0} does not change any of the Geroch-Hansen moments lower than M_l . Furthermore, since the equations governing ψ_1 and γ_1 are linear in these fields, one can choose ψ_1

to be a combination of multipoles such that the resulting spacetime puts its “bump” into a single Geroch-Hansen moment. In this way, one can arbitrarily adjust the Geroch-Hansen moments of a spacetime, provided the adjustments are small.

In order to calculate the Geroch-Hansen moments of the bumpy Schwarzschild spacetime, we need to construct the Ernst potential. The norm and twist of the timelike Killing vector field, to first order in the perturbation, are given by

$$\lambda = (1 + 2\psi_1) \left(1 - \frac{2M}{r}\right), \quad (2.74)$$

$$\omega = 0. \quad (2.75)$$

Then the Ernst potential is

$$\xi = \frac{M}{r - M} - \left[1 - \left(\frac{M}{r - M}\right)^2\right] \psi_1. \quad (2.76)$$

Notice that ψ_1 only changes the real part of the Ernst potential. This means the perturbation only changes the mass moments and leaves the spin moments unchanged. The conformal factor becomes

$$\Omega = \bar{R}^2 \left(1 - \frac{M^2}{4} \bar{R}^2\right)^{-1} (1 - \gamma_1), \quad (2.77)$$

and the conformal metric is

$$ds^2 = d\bar{R}^2 + \bar{R}^2 d\theta^2 + (1 - 2\gamma_1) \bar{R}^2 \sin^2 \theta d\phi^2, \quad (2.78)$$

where \bar{R} has the same definition as for an unperturbed Schwarzschild spacetime,

$$r = \bar{R}^{-1} \left(1 + M\bar{R} + \frac{M^2 \bar{R}^2}{4}\right). \quad (2.79)$$

Now we are ready to consider specific choices of ψ_1 and γ_1 .

2.5.1 $l = 2$ mass perturbation

We begin by considering an $l = 2$ perturbation in the Weyl sector. The perturbation ψ_1 which satisfies Eq. (2.39) and has an $l = 2$ spherical harmonic form is

$$\psi_1^{l=2}(\rho, z) = B_2 M^3 \frac{Y_{20}(\theta_{\text{Weyl}})}{(\rho^2 + z^2)^{3/2}} = \frac{B_2 M^3}{4} \sqrt{\frac{5}{\pi}} \left[\frac{3 \cos^2 \theta_{\text{Weyl}} - 1}{(\rho^2 + z^2)^{3/2}} \right], \quad (2.80)$$

where $\cos \theta_{\text{Weyl}} = z/\sqrt{\rho^2 + z^2}$. The dimensionless constant B_2 sets the magnitude of the bumpiness. Since we are treating the bumpiness as a perturbation, $B_2 \ll 1$. Transforming to Schwarzschild coordinates by Eq. (2.43), we find

$$\psi_1^{l=2}(r, \theta) = \frac{B_2 M^3}{4} \sqrt{\frac{5}{\pi}} \frac{1}{d(r, \theta)^3} \left[\frac{3(r - M)^2 \cos^2 \theta}{d(r, \theta)^2} - 1 \right], \quad (2.81)$$

where

$$d(r, \theta) \equiv (r^2 - 2Mr + M^2 \cos^2 \theta)^{1/2}. \quad (2.82)$$

As a useful aside, the mapping from (ρ, z) to (r, θ) implies that any Weyl sector ψ_1 can be transformed into Schwarzschild coordinates by putting

$$\rho^2 + z^2 \rightarrow d(r, \theta), \quad (2.83a)$$

$$\cos \theta_{\text{Weyl}} \rightarrow \frac{(r - M) \cos \theta}{d(r, \theta)}. \quad (2.83b)$$

Integrating the constraint [Eq. (2.41)] and imposing the condition $\gamma_1(r \rightarrow \infty) = 0$ gives

$$\gamma_1^{l=2}(r, \theta) = B_2 \sqrt{\frac{5}{\pi}} \left[\frac{(r - M) c_{20}(r) + c_{22}(r) \cos^2 \theta}{2 d(r, \theta)^5} - 1 \right], \quad (2.84)$$

where

$$c_{20}(r) = 2(r - M)^4 - 5M^2(r - M)^2 + 3M^4, \quad (2.85a)$$

$$c_{22}(r) = 5M^2(r - M)^2 - 3M^4. \quad (2.85b)$$

Figure 2-1 shows the impact of an $l = 2$ bump on orbital frequencies as a function

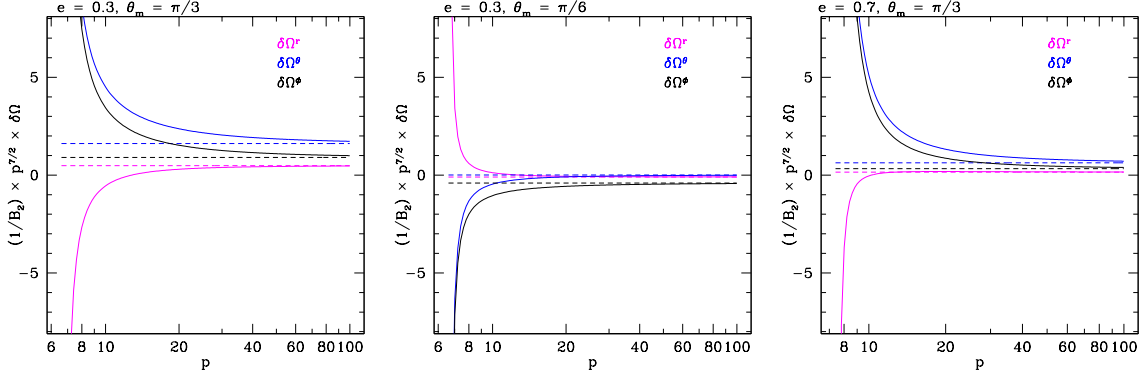


Figure 2-1: Shifts to black hole orbital frequencies due to an $l = 2$ bump. The shifts $\delta\Omega^{r,\theta,\phi}$ are normalized by the bumpiness parameter B_2 , and are scaled by $p^{7/2}$; this is because in the Newtonian limit, $\delta\Omega^{r,\theta,\phi} \propto p^{-7/2}$. The Newtonian result (dashed lines) describes the exact calculations (solid lines) well in the large p limit, however, the Newtonian result substantially underestimates the shifts in the strong field. Notice that the radial frequency shift changes sign in the strong field, typically at $p \sim (10 - 13)M$, depending slightly on parameters. This behavior is starkly different from the weak field limit.

of p for a few choices of e and θ_m . We show the three shifts $\delta\Omega^{r,\theta,\phi}$, normalized by the bumpiness B_2 and rescaled by the asymptotic weak-field dependence $\delta\Omega_{l=2}^{r,\theta,\phi} \propto p^{-7/2}$, which we derive in Appendix B. As we move to the weak field, the numerical results (solid lines) converge to the weak-field forms (dashed lines). The frequency shifts generically get substantially larger as we move into the strong field. The bumps have a very strong influence near the last stable orbit, $p_{\text{LSO}} = (6 + 2e)$, although the behavior is smooth and non-pathological.

We calculate the multipole moments for the bumpy Schwarzschild spacetime by following the procedure laid out in Sec. 2.2. The changes to the few multipole mo-

ments are listed below:

$$\delta\mathcal{M}_0 = 0, \quad (2.86a)$$

$$\delta\mathcal{M}_1 = 0, \quad (2.86b)$$

$$\delta\mathcal{M}_2 = -\frac{1}{2}B_2M^3\sqrt{\frac{5}{\pi}}, \quad (2.86c)$$

$$\delta\mathcal{M}_3 = 0, \quad (2.86d)$$

$$\delta\mathcal{M}_4 = \frac{4}{7}B_2M^5\sqrt{\frac{5}{\pi}}, \quad (2.86e)$$

$$\delta\mathcal{M}_5 = 0, \quad (2.86f)$$

$$\delta\mathcal{M}_6 = -\frac{19}{66}B_2M^7\sqrt{\frac{5}{\pi}}. \quad (2.86g)$$

An $l = 2$ mass perturbation in the Weyl sector changes only the even Geroch-Hansen mass moments with $l \geq 2$. The bumpiness parameter B_2 controls the magnitude of the perturbations.

2.5.2 $l = 3$ mass perturbation

Next, consider an $l = 3$ perturbation. In Weyl coordinates, we put

$$\psi_1^{l=3}(\rho, z) = B_3M^4\frac{Y_{30}(\theta_{\text{Weyl}})}{(\rho^2 + z^2)^2}; \quad (2.87)$$

in Schwarzschild coordinates, this becomes

$$\psi_1^{l=3}(r, \theta) = \frac{B_3M^4}{4}\frac{1}{d(r, \theta)^4}\sqrt{\frac{7}{\pi}}\left[\frac{5(r-M)^3\cos^3\theta}{d(r, \theta)^3} - \frac{3(r-M)\cos\theta}{d(r, \theta)}\right]. \quad (2.88)$$

From the constraint equation [Eq. (2.41)] and the condition $\gamma_1(r \rightarrow \infty) = 0$, we find

$$\begin{aligned} \gamma_1^{l=3}(r, \theta) &= \frac{B_3M^5}{2}\sqrt{\frac{7}{\pi}}\cos\theta \\ &\times \left[\frac{c_{30}(r) + c_{32}(r)\cos^2\theta + c_{34}(r)\cos^4\theta + c_{36}(r)\cos^6\theta}{d(r, \theta)^7}\right], \quad (2.89) \end{aligned}$$

where

$$c_{30}(r) = -3r(r - 2M), \quad (2.90a)$$

$$c_{32}(r) = 10r(r - 2M) + 2M^2, \quad (2.90b)$$

$$c_{34}(r) = -7r(r - 2M), \quad (2.90c)$$

$$c_{36}(r) = -2M^2. \quad (2.90d)$$

Notice that $\psi_1^{l=3}$ and $\gamma_1^{l=3}$ are proportional to $\cos\theta$; their contribution to the averaged Hamiltonian $\langle \mathcal{H}_1 \rangle$ is zero, and there is no secular shift to orbital frequencies from $l = 3$ bumps. This is identical to the result in Newtonian gravity, as discussed in Appendix B, and holds for all odd values of l . There will be non-secular shifts to the motion which cannot be described by our orbit-averaged approach. These shifts would be apparent in a direct (time-domain) evolution of the geodesics of spacetimes with odd l bumps. It would be a useful exercise to examine these effects and ascertain under which conditions odd l spacetime bumps could, in principle, have an observable impact.

The changes to the first few multipole moments from this perturbation are listed below:

$$\delta\mathcal{M}_0 = 0, \quad (2.91a)$$

$$\delta\mathcal{M}_1 = 0, \quad (2.91b)$$

$$\delta\mathcal{M}_2 = 0, \quad (2.91c)$$

$$\delta\mathcal{M}_3 = -\frac{1}{2}B_3M^4\sqrt{\frac{7}{\pi}}, \quad (2.91d)$$

$$\delta\mathcal{M}_4 = 0, \quad (2.91e)$$

$$\delta\mathcal{M}_5 = \frac{2}{3}B_3M^6\sqrt{\frac{7}{\pi}} \quad (2.91f)$$

$$\delta\mathcal{M}_6 = 0. \quad (2.91g)$$

An $l = 3$ mass perturbation in the Weyl sector changes only the odd Geroch-Hansen mass moments with $l \geq 3$ by an amount proportional to B_3 .

2.5.3 $l = 4$ mass perturbation

We conclude our discussion of Schwarzschild bumps with $l = 4$:

$$\psi_1^{l=4}(\rho, z) = B_4 M^5 \frac{Y_{40}(\theta_{\text{Weyl}})}{(\rho^2 + z^2)^5}, \quad (2.92)$$

from which we obtain

$$\begin{aligned} \psi_1^{l=4}(r, \theta) &= \frac{B_4 M^5}{16} \frac{1}{d(r, \theta)^5} \sqrt{\frac{9}{\pi}} \\ &\times \left[\frac{35(r-M)^4 \cos^4 \theta}{d(r, \theta)^4} - \frac{30(r-M)^2 \cos^2 \theta}{d(r, \theta)^2} + 3 \right]. \end{aligned} \quad (2.93)$$

Solving for γ_1 as before, we find

$$\gamma_1^{l=4}(r, \theta) = B_4 \sqrt{\frac{9}{\pi}} \left[\frac{(r-M) c_{40}(r) + c_{42}(r) \cos^2 \theta + c_{44}(r) \cos^4 \theta}{8 d(r, \theta)^9} - 1 \right], \quad (2.94)$$

where

$$\begin{aligned} c_{40}(r) &= 8(r-M)^8 - 36M^2(r-M)^6 + 63M^4(r-M)^4 \\ &\quad - 50M^6(r-M)^2 + 15M^8, \end{aligned} \quad (2.95a)$$

$$\begin{aligned} c_{42}(r) &= 36M^2(r-M)^6 - 126M^4(r-M)^4 + 120M^6(r-M)^2 \\ &\quad - 30M^8, \end{aligned} \quad (2.95b)$$

$$c_{44}(r) = 63M^4(r-M)^4 - 70M^6(r-M)^2 + 15M^8. \quad (2.95c)$$

Figure 2-2 presents the shifts in the orbital frequencies due to an $l = 4$ bump for the same orbital parameters as are shown in Fig. 2-1. The shifts are normalized by the bumpiness B_4 and rescaled by the weak-field form $\delta\Omega_{l=4}^{r,\theta,\phi} \propto p^{-11/2}$. The qualitative behavior is largely the same as for the quadrupole bump. In particular, we see once again that there are no strong-field pathologies in the orbit shifts, and that the degree of shift due to spacetime bumps is especially strong near the last stable orbit. The strong-field radial oscillations in $\delta\Omega^r$ are even more pronounced than they were in the $l = 2$ case. This appears to be a robust signature of non-Kerr multipoles in the

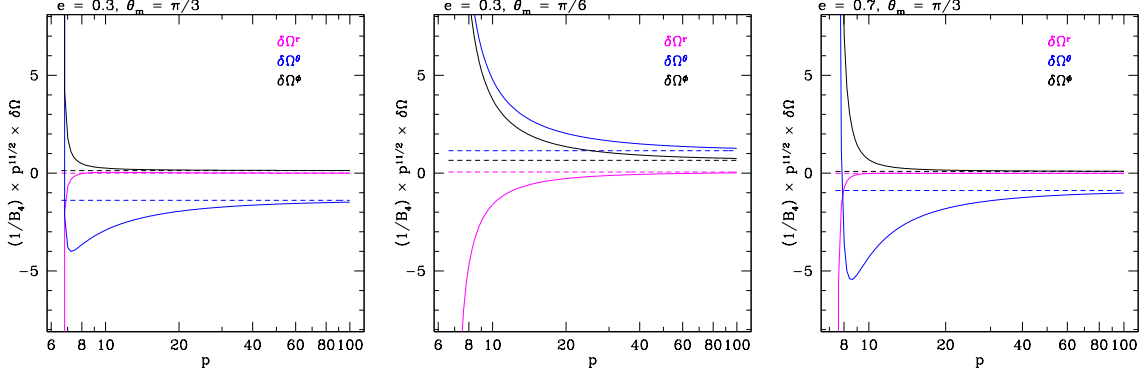


Figure 2-2: Shifts to black hole orbital frequencies due to an $l = 4$ bump. The shifts $\delta\Omega^{r,\theta,\phi}$ are normalized by the bumpiness parameter B_4 and are scaled by $p^{11/2}$, which sets the scaling in the Newtonian limit. As in the $l = 2$ case (Fig. 2-1), exact results and the Newtonian limit coincide at large p , but there are significant differences in the strong field. The functional behavior of the radial frequency shift can be especially complicated in this case.

strong-field.

The first few changes to the multipole moments from this perturbation are

$$\delta\mathcal{M}_0 = 0, \quad (2.96a)$$

$$\delta\mathcal{M}_1 = 0, \quad (2.96b)$$

$$\delta\mathcal{M}_2 = 0, \quad (2.96c)$$

$$\delta\mathcal{M}_3 = 0, \quad (2.96d)$$

$$\delta\mathcal{M}_4 = \frac{2}{5}B_4M^5\sqrt{\frac{9}{\pi}}, \quad (2.96e)$$

$$\delta\mathcal{M}_5 = 0, \quad (2.96f)$$

$$\delta\mathcal{M}_6 = -\frac{5}{11}B_4M^7\sqrt{\frac{9}{\pi}}. \quad (2.96g)$$

An $l = 4$ mass perturbation changes only the even mass moments with $l \geq 4$, with the perturbation proportional to the parameter B_4 .

2.6 Perturbations to the mass moments: Kerr background

Now we repeat this procedure for a bumpy Kerr black hole with perturbed mass moments. As with the bumpy Schwarzschild case, we need to compute the conformal factor and the Ernst potential for the spacetime. The conformal factor is

$$\Omega = \bar{R}^2 \left[\left(1 - \frac{M^2 - a^2}{4} \bar{R}^2 \right)^2 - a^2 \bar{R}^2 \sin^2 \theta \right]^{-1/2} (1 - \gamma_1). \quad (2.97)$$

To compute the Ernst potential, we need to compute the norm and the twist of the timelike Killing vector. The norm is straightforward; it is given by

$$\lambda = \left(1 - \frac{2Mr}{\Sigma} \right) (1 + 2\psi_1). \quad (2.98)$$

Notice that the portion of the norm proportional to the perturbation falls off as $r^{-(l+1)}$.

Computing the twist is much trickier. Formally, it does not exist; the construction detailed in Sec. 2.3.2 for making a bumpy Kerr black hole does not leave the spacetime vacuum in GR. Consider, for example, the $l = 2$ perturbation, described in more detail below. If we compute the Einstein tensor and enforce the Einstein equation $G_{\mu\nu} = 8\pi T_{\mu\nu}$, we find that, in the large r limit and to leading order in a , the spacetime has a stress-energy tensor whose only non-vanishing components are

$$T_{\theta\phi} = \frac{3}{8\pi} a B_2 M^4 \sqrt{\frac{5}{\pi}} \frac{(3 - 5 \cos^2 \theta) \cos \theta \sin^3 \theta}{r^5}. \quad (2.99)$$

It may be possible to generalize Geroch-Hansen moments to nonvacuum spacetimes, but that is beyond the scope of this chapter. For our purposes, it is sufficient to say that for the kinds of perturbations we have considered, the spacetime approaches vacuum very rapidly in the region where we need to use the twist. In general, since the stress-energy tensor is constructed from two derivatives of the metric, an order

l perturbation to the metric produces a non-zero stress-energy tensor which falls off as $r^{-(l+3)}$. This enables us to define the spacetime's twist to the order necessary to define the Geroch-Hansen moments to order $l + 1$.

We divide the curl into two parts: the gradient of a scalar function ω' plus some correction term v_α :

$$\omega_\alpha = \nabla_\alpha \omega' + v_\alpha. \quad (2.100)$$

For an order l mass perturbation, the scalar function ω' is the same as for the unperturbed Kerr spacetime:

$$\omega' = -\frac{2aM \cos \theta}{\Sigma}. \quad (2.101)$$

The correction term v_α falls off as $r^{-(l+3)}$. Since, at large r , the portion of the norm proportional to the perturbation falls off as $r^{-(l+1)}$, the correction to the curl can be neglected. We thus treat ω' as the spacetime's twist.

2.6.1 $l = 2$ mass perturbation

We begin with an $l = 2$ perturbation in the Weyl sector, starting with Eq. (2.80).

Transforming to prolate spheroidal coordinates by Eq. (2.38), ψ_1 becomes

$$\begin{aligned} \psi_1^{l=2}(u, v) &= \frac{B_2}{4} \sqrt{\frac{5}{\pi}} \left(\frac{3 \cosh^2 u \cos^2 v}{\sinh^2 u \sin^2 v + \cosh^2 u \cos^2 v} - 1 \right) \\ &\quad \times (\sinh^2 u \sin^2 v + \cosh^2 u \cos^2 v)^{-3/2}. \end{aligned} \quad (2.102)$$

The corresponding γ_1 is

$$\gamma_1^{l=2}(u, v) = B_2 \sqrt{\frac{5}{\pi}} \left\{ \frac{\cosh u [4 - \cos 2v + (5 \cos 2v - 1) \cosh 2u + \cosh 4u]}{8 (\sinh^2 u \sin^2 v + \cosh^2 u \cos^2 v)^{5/2}} - 1 \right\}. \quad (2.103)$$

Following the procedure of the Newman-Janis algorithm, we allow u to be complex, and we replace $\cosh^2 u$ with $\cosh u \cosh \bar{u}$ and $\sinh^2 u$ with $(\cosh u \cosh \bar{u} - 1)$. Making

the coordinate transformation

$$\cosh u = \frac{r - ia \cos \theta}{M} - 1, \quad (2.104a)$$

$$v = \theta, \quad (2.104b)$$

puts the perturbation in Boyer-Lindquist coordinates:

$$\psi_1^{l=2}(r, \theta) = \frac{B_2 M^3}{4} \sqrt{\frac{5}{\pi}} \frac{1}{d(r, \theta, a)^3} \left[\frac{3L(r, \theta, a)^2 \cos^2 \theta}{d(r, \theta, a)^2} - 1 \right], \quad (2.105)$$

$$\begin{aligned} \gamma_1^{l=2}(r, \theta) = & \frac{B_2}{2} \sqrt{\frac{5}{\pi}} \{ L(r, \theta, a) [c_{20}(r, a) + c_{22}(r, a) \cos^2 \theta \\ & + c_{24}(r, a) \cos^4 \theta] d(r, \theta, a)^{-5} - 2 \}, \end{aligned} \quad (2.106)$$

where

$$d(r, \theta, a) = \sqrt{r^2 - 2Mr + (M^2 + a^2) \cos^2 \theta}, \quad (2.107)$$

$$L(r, \theta, a) = \sqrt{(r - M)^2 + a^2 \cos^2 \theta}, \quad (2.108)$$

and

$$c_{20}(r, a) = 2(r - M)^4 - 5M^2(r - M)^2 + 3M^4, \quad (2.109a)$$

$$c_{22}(r, a) = 5M^2(r - M)^2 - 3M^4 + a^2 [4(r - M)^2 - 5M^2], \quad (2.109b)$$

$$c_{24}(r, a) = a^2(2a^2 + 5M^2). \quad (2.109c)$$

Note that the result for ψ_1 can be found by taking the perturbation in Weyl coordinates [Eq. (2.80)] and substituting

$$\rho^2 + z^2 \rightarrow d(r, \theta, a), \quad (2.110a)$$

$$\cos \theta_{\text{Weyl}} \rightarrow \frac{L(r, \theta, a)}{d(r, \theta, a)} \cos \theta. \quad (2.110b)$$

This is the Kerr analog to the mapping described in Eq. (2.83).

Figure 2-3 shows how an $l = 2$ bump changes Kerr orbital frequencies. We focus

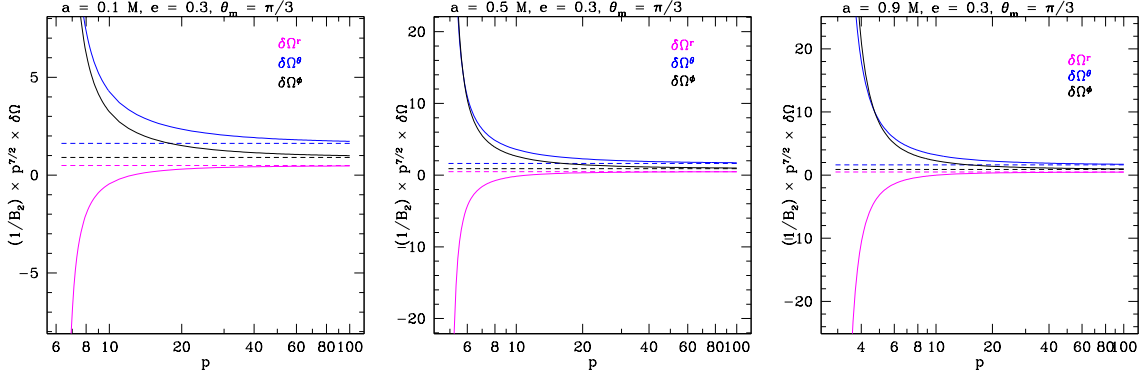


Figure 2-3: Shifts to Kerr black hole orbital frequencies for an $l = 2$ bump. As with the Schwarzschild results presented in Fig. 2-1, the shifts $\delta\Omega^{r,\theta,\phi}$ are normalized by the bumpiness B_2 and scaled by $p^{7/2}$. Rather than examining a variety of orbital geometries, we here examine a few black hole spins, showing results for $a = 0.1M$, $a = 0.5M$, and $a = 0.9M$. Qualitatively, the results are very similar to what we find for the Schwarzschild case. The major difference is that the last stable orbit is located at smaller p , so that these orbits can get deeper into the strong field. The overall impact of the bumps is greater in these cases which reach deeper into the strong field.

here on how black hole spin affects our results, presenting results for a single orbit geometry ($e = 0.3$, $\theta_m = \pi/3$). The primary impact of black hole spin is to change the value of p at which orbits become unstable. For large spin, orbits can reach deeper into the strong field, accumulating larger anomalous shifts to their orbital frequencies. Aside from this behavior, spin has relatively little effect on the shifts: the three panels are similar to one another and to the Schwarzschild result (compare left-most panel of Fig. 2-1).

Now we compute the changes to the multipole moments following the procedure outlined in the previous sections. The changes to the multipole moments are

$$\delta\mathcal{M}_0 = 0, \quad (2.111a)$$

$$\delta\mathcal{M}_1 = 0, \quad (2.111b)$$

$$\delta\mathcal{M}_2 = -\frac{1}{2}B_2M^3\sqrt{\frac{5}{\pi}}, \quad (2.111c)$$

$$\delta\mathcal{M}_3 = 0. \quad (2.111d)$$

The lowest order multipole that is affected is the $l = 2$ mass moment, and the change

is the same as for an $l = 2$ mass perturbation on a Schwarzschild background. The multipole moments are well-defined up to the \mathcal{M}_3 moment; the higher order moments are not well-defined because the stress-energy tensor is nonzero.

2.6.2 $l = 3$ mass perturbation

For the $l = 3$ Kerr bump, we begin with Eq. (2.87), then follow the same procedure to take it to Boyer-Linquist coordinates as described for the $l = 2$ Kerr bump. The result is

$$\begin{aligned} \psi_1^{l=3}(r, \theta) &= \frac{B_3 M^4}{4} \sqrt{\frac{7}{\pi}} \frac{1}{d(r, \theta, a)^4} \\ &\times \left[\frac{5L(r, \theta, a)^3 \cos^3 \theta}{d(r, \theta, a)^3} - \frac{3L(r, \theta, a) \cos \theta}{d(r, \theta, a)} \right], \end{aligned} \quad (2.112)$$

$$\begin{aligned} \gamma_1^{l=3}(r, \theta) &= \frac{B_3 M^5}{2} \sqrt{\frac{7}{\pi}} \cos \theta \frac{1}{d(r, \theta, a)^7} [c_{30}(r, a) + c_{32}(r, a) \cos^2 \theta \\ &+ c_{34}(r, a) \cos^4 \theta + c_{36}(r, a) \cos^6 \theta], \end{aligned} \quad (2.113)$$

where

$$c_{30}(r, a) = -3r(r - 2M), \quad (2.114a)$$

$$c_{32}(r, a) = 10r(r - 2M) + 2M^5 - 3a^2, \quad (2.114b)$$

$$c_{34}(r, a) = -7r(r - 2M) + 10a^2, \quad (2.114c)$$

$$c_{36}(r, a) = -2M^2 - 7a^2. \quad (2.114d)$$

As with the Schwarzschild $l = 3$ bumps, $\psi_1^{l=3}$ and $\gamma_1^{l=3}$ are proportional to $\cos \theta$, and therefore $\langle \mathcal{H}_1 \rangle = 0$. Thus there is no secular shift to orbital frequencies for $l = 3$, or any other odd value of l . We emphasize again that there will be non-secular shifts to the motion which our orbit-averaged approach misses by construction, and that it would be worthwhile to investigate their importance in future work.

The changes to the multipole moments from this perturbation are

$$\delta\mathcal{M}_0 = 0, \tag{2.115a}$$

$$\delta\mathcal{M}_1 = 0, \tag{2.115b}$$

$$\delta\mathcal{M}_2 = 0, \tag{2.115c}$$

$$\delta\mathcal{M}_3 = -\frac{1}{2}B_3M^4\sqrt{\frac{7}{\pi}}, \tag{2.115d}$$

$$\delta\mathcal{M}_4 = 0. \tag{2.115e}$$

The perturbation changes the $l = 3$ mass multipole, and the change is the same as for an $l = 3$ mass perturbation on a Schwarzschild background. The lower order multipoles are unchanged.

2.7 Perturbations to the spin moments: Schwarzschild background

Now we turn our attention to bumpy Schwarzschild black holes for which $\psi_1 = \gamma_1 = 0$ and σ_1 is nonzero. For these spacetimes, the norm of the timelike Killing vector is unchanged while the twist is perturbed away from zero. Therefore, only the imaginary part of the Ernst potential depends on σ_1 , which means that σ_1 perturbs the spin moments while leaving the mass moments unchanged. We consider specific choices of σ_1 below.

2.7.1 $l = 1$ spin perturbation (linearized Kerr)

One solution for a current perturbation is the linearized Kerr spacetime, i.e., the Kerr metric expanded to leading order in the spin parameter a . In our notation, this spacetime is described by Eq. (2.49) with

$$\sigma_1 = -\frac{2aM \sin^2 \theta}{r}. \tag{2.116}$$

Here we demonstrate that our framework includes the linearized Kerr spacetime; however, it requires a modification to the procedure we use to define higher-order spin perturbations.

To begin, we note that one family of solutions to Eq. (2.46) can be written

$$\Xi_1 = Af_0(\theta) + Brf_1(\theta). \quad (2.117)$$

Let us choose a solution with $B = 0$ and $f_0 = \cos \theta$. We calculate σ_1 by enforcing Eq. (2.51):

$$\frac{\partial \sigma_1}{\partial \theta} = \frac{4AM^2 \sin \theta \cos \theta}{r}, \quad (2.118)$$

which we can easily integrate:

$$\sigma_1 = \frac{2AM^2 \sin^2 \theta}{r}. \quad (2.119)$$

It is simple to verify that this value of σ_1 also satisfies Eq. (2.50). Comparing this solution to the definition of the linearized Kerr spacetime in Eq. (2.116), we relate the parameter A to the spin parameter according to $A = -a/M$.

2.7.2 $l = 2$ spin perturbation

We define an $l = 2$ spin perturbation by specifying a solution to Eq. (2.46) that has the form of an $l = 2$ spherical harmonic:

$$\frac{\partial^2 \Xi_1}{\partial r^2} = \frac{S_2 M}{4} \sqrt{\frac{5}{\pi}} \frac{1}{(\rho^2 + z^2)^{3/2}} \left(\frac{3z^2}{\rho^2 + z^2} - 1 \right). \quad (2.120)$$

We can use Eq. (2.43) to rewrite Eq. (2.120) in terms of Schwarzschild coordinates:

$$\frac{\partial^2 \Xi_1}{\partial r^2} = \frac{S_2 M}{4} \sqrt{\frac{5}{\pi}} \frac{1}{d(r, \theta)^3} \left[\frac{3(r - M)^2 \cos^2 \theta}{d(r, \theta)} - 1 \right], \quad (2.121)$$

where $d(r, \theta)$ is defined in Eq. (2.82). Integrating and imposing the boundary conditions in Eq. (2.52) yields

$$\Xi_1(r, \theta) = \frac{S_2}{4} \sqrt{\frac{5}{\pi}} \frac{[d(r, \theta)^2 - (r - M)d(r, \theta) + M^2 \cos^2 \theta]}{Md(r, \theta)}. \quad (2.122)$$

From the perturbation to Ξ , we can calculate the perturbation to the metric σ_1 :

$$\sigma_1 = \frac{S_2 M}{2} \sqrt{\frac{5}{\pi}} \cos \theta \left[\frac{2d(r, \theta)}{r} - \frac{r - M}{d(r, \theta)} - \left(1 - \frac{2M}{r} \right) \right]. \quad (2.123)$$

The changes to the first few multipole moments due to this perturbation are:

$$\delta \mathcal{M}_0 = 0, \quad (2.124a)$$

$$\delta \mathcal{M}_1 = 0, \quad (2.124b)$$

$$\delta \mathcal{M}_2 = i \frac{1}{4} S_2 M^3 \sqrt{\frac{5}{\pi}}, \quad (2.124c)$$

$$\delta \mathcal{M}_3 = 0, \quad (2.124d)$$

$$\delta \mathcal{M}_4 = -i \frac{1}{28} S_2 M^5 \sqrt{\frac{5}{\pi}}, \quad (2.124e)$$

$$\delta \mathcal{M}_5 = 0. \quad (2.124f)$$

An $l = 2$ spin perturbation changes the even spin moments for $l \geq 2$, but it leaves the odd spin moments and all of the mass moments unchanged.

2.7.3 $l = 3$ spin perturbation

Consider an $l = 3$ spin perturbation:

$$\frac{\partial^2 \Xi_1}{\partial r^2} = \frac{S_3 M^2}{4} \sqrt{\frac{7}{\pi}} \frac{1}{(\rho^2 + z^2)^2} \left[\frac{5z^3}{(\rho^2 + z^2)^{3/2}} - \frac{3z}{(\rho^2 + z^2)^{1/2}} \right]. \quad (2.125)$$

Then the perturbation to the Ernst potential Ξ_1 is given by

$$\Xi_1 = i \frac{S_3}{12} \sqrt{\frac{7}{\pi}} \cos \theta \left\{ 3 - \frac{(r - M)[3d(r, \theta)^2 - M^2 \cos^2 \theta]}{d(r, \theta)^3} \right\}. \quad (2.126)$$

This corresponds to a perturbation to the metric given by

$$\sigma_1 = \frac{S_3 M}{6} \sqrt{\frac{7}{\pi}} \left[\left(1 - \frac{2M}{r}\right) \frac{r^2(2r - 3M) - 3Mr(r - 2M) \cos^2 \theta - 2M^3 \cos^4 \theta}{d(r, \theta)^3} - \frac{2r - M - 3M \cos^2 \theta}{r} \right]. \quad (2.127)$$

The changes to the first few multipole moments are listed below:

$$\delta \mathcal{M}_0 = 0, \quad (2.128a)$$

$$\delta \mathcal{M}_1 = 0, \quad (2.128b)$$

$$\delta \mathcal{M}_2 = 0, \quad (2.128c)$$

$$\delta \mathcal{M}_3 = i \frac{1}{12} S_3 M^4 \sqrt{\frac{7}{\pi}}, \quad (2.128d)$$

$$\delta \mathcal{M}_4 = 0, \quad (2.128e)$$

$$\delta \mathcal{M}_5 = -i \frac{1}{36} S_3 M^6 \sqrt{\frac{7}{\pi}}. \quad (2.128f)$$

The $l = 3$ spin perturbation changes only the odd Geroch-Hansen moments for $l \geq 3$.

2.8 Perturbations to the spin moments: Kerr background

Now we consider a bumpy spacetime consisting of a spin perturbation on a Kerr background. The norm of the timelike Killing vector for this spacetime is

$$\lambda = 1 - \frac{2Mr}{\Sigma} + \frac{4aMr}{\Sigma^2} \sigma_1(r, \theta). \quad (2.129)$$

However, as in Sec. 2.6, we cannot define the twist because the spacetime is not vacuum. For example, in the large r limit and expanding in a , the stress-energy tensor of the Kerr spacetime with an $l = 2$ spin perturbation, which we define in the

following section, has nonzero terms

$$T_{\theta\theta} = -\frac{39}{8\pi}aS_2M^4\sqrt{\frac{5}{\pi}}\frac{\cos\theta\sin^2\theta}{r^5}, \quad (2.130a)$$

$$T_{\phi\phi} = -\frac{27}{8\pi}aS_2M^4\sqrt{\frac{5}{\pi}}\frac{\cos\theta\sin^4\theta}{r^5}. \quad (2.130b)$$

In general, an order l spin perturbation creates nonzero terms in the stress-energy tensor that fall off like $r^{-(l+3)}$. As in Sec. 2.6, this allows us to define the Geroch-Hansen moments up to order $l + 1$. The twist depends on the perturbation, so we cannot continue the calculation without choosing a particular perturbation. Below we consider specific choices for the perturbation.

2.8.1 $l = 2$ spin perturbation

We define an $l = 2$ spin perturbation with the perturbation potential

$$\begin{aligned} \sigma_1(r, \theta) = & -\frac{S_2M}{2}\sqrt{\frac{5}{\pi}}\cos\theta\left[\frac{M}{L(r, \theta, a) + M}\frac{L(r, \theta, a) + M\sin^2\theta}{d(r, \theta, a)}\right. \\ & \left. + \frac{L(r, \theta, a) - M - d(r, \theta, a)}{L(r, \theta, a) + M}\right], \end{aligned} \quad (2.131)$$

where $d(r, \theta, a)$ and $L(r, \theta, a)$ are defined in Eqs. (2.107) and (2.108), respectively. Now we need to construct the Ernst potential. The norm of the timelike Killing vector is given by Eq. (2.129). As discussed in Sec. 2.6, we can write the curl of a nonvacuum spacetime in the form of Eq. (2.100). We define ω' by ignoring all terms of order aS_2 in the curl. This yields

$$\omega' = -\frac{2aM\cos\theta}{\Sigma} - \frac{S_2M}{2}\sqrt{\frac{5}{\pi}}\frac{1}{r}\left[\frac{r^2 - 2Mr + 2M^2\cos^2\theta}{r d(r, \theta)} - \left(1 - \frac{M}{r}\right)\right]. \quad (2.132)$$

In this case, v_α falls off like r^{-5} , so we are justified in treating ω' as the twist. The Ernst potential is

$$\begin{aligned} \xi = & \frac{M}{r - M - ia \cos \theta} + i \frac{S_2 M}{4} \sqrt{\frac{5}{\pi}} \\ & \times \left[\frac{r(r - 2M) - (r - M) d(r, \theta) + 2M^2 \cos^2 \theta}{(r - M)^2 d(r, \theta)} \right]. \end{aligned} \quad (2.133)$$

Applying the procedure from the previous sections gives the changes to the multipole moments:

$$\delta \mathcal{M}_0 = 0, \quad (2.134a)$$

$$\delta \mathcal{M}_1 = 0, \quad (2.134b)$$

$$\delta \mathcal{M}_2 = i \frac{1}{4} S_2 M^3 \sqrt{\frac{5}{\pi}}, \quad (2.134c)$$

$$\delta \mathcal{M}_3 = 0. \quad (2.134d)$$

The perturbation changes the $l = 2$ spin moment by the same amount as an $l = 2$ spin perturbation on a Schwarzschild background, and it leaves lower order moments unchanged.

2.8.2 $l = 3$ spin perturbation

We consider an $l = 3$ spin perturbation:

$$\begin{aligned} \sigma_1(r, \theta) = & \frac{S_3 M}{6} \sqrt{\frac{7}{\pi}} \left[\frac{L(r, \theta, a) - M s_{30}(r, a) + s_{32}(r, a) \cos^2 \theta + s_{34}(r, a) \cos^4 \theta}{L(r, \theta, a) + M} \frac{1}{d(r, \theta, a)^3} \right. \\ & \left. - \frac{2L(r, \theta, a) - M(3 \cos^2 \theta - 1)}{L(r, \theta, a) + M} \right], \end{aligned} \quad (2.135)$$

where

$$s_{30}(r, a) = 2L(r, \theta, a)^3 + 3r(r - 2M) + 2M^3, \quad (2.136a)$$

$$s_{32}(r, a) = -3M(r(r - 2M) - a^2), \quad (2.136b)$$

$$s_{34}(r, a) = -2M^3 - 3a^2 M. \quad (2.136c)$$

Now we construct the Ernst potential. The norm of the timelike Killing vector is given by Eq. (2.129). As discussed in Sec. 2.6, we can write the curl of a nonvacuum spacetime in the form of Eq. 2.100. We define ω' by ignoring all terms of order aS_3 in the curl. This yields

$$\begin{aligned} \omega' = & -\frac{2aM \cos \theta}{\Sigma} + \frac{S_3 M^2}{6} \sqrt{\frac{7}{\pi}} \frac{\cos \theta}{r^2} \\ & \times \left[\frac{(r-M)(3r^2 - 6Mr + 2M^2 \cos^2 \theta)}{d(r, \theta)^3} - 3 \right]. \end{aligned} \quad (2.137)$$

We see that v_α falls off like r^{-6} , so we are justified in treating ω' as the twist. The Ernst potential is

$$\begin{aligned} \xi = & \frac{M}{r - M - ia \cos \theta} + i \frac{S_3 M^2}{12} \sqrt{\frac{7}{\pi}} \cos \theta \\ & \times \left\{ \frac{3r(r - 2M)[d(r, \theta) - r + M] + M^2 \cos^2 \theta [3d(r, \theta) - 2r + 2M]}{(r - M)^2 d(r, \theta)^3} \right\}. \end{aligned} \quad (2.138)$$

Applying the procedure from the previous sections gives the multipole moments:

$$\delta \mathcal{M}_0 = 0, \quad (2.139a)$$

$$\delta \mathcal{M}_1 = 0, \quad (2.139b)$$

$$\delta \mathcal{M}_2 = 0, \quad (2.139c)$$

$$\delta \mathcal{M}_3 = i \frac{1}{12} S_3 M^4 \sqrt{\frac{7}{\pi}}, \quad (2.139d)$$

$$\delta \mathcal{M}_4 = 0. \quad (2.139e)$$

As in the case of an $l = 3$ spin perturbation on a Schwarzschild background, the perturbation changes the $l = 3$ spin moment but leaves lower order moments unchanged.

2.9 Summary and future work

This analysis significantly extends the bumpy black hole formalism introduced by Collins and Hughes [25]. We define smooth bumps with well-behaved strong-field structure, and we extend the formalism to include Kerr black holes. We consider two kinds of static, axisymmetric perturbations: those that perturb the mass moments and those that perturb the spin moments. We map these perturbations to changes in the Geroch-Hansen moments and show that an order l perturbation changes the Geroch-Hansen moments above \mathcal{M}_l but leaves lower order moments unchanged. This allows us to build spacetimes whose multipoles agree with those of the Kerr spacetime up to some arbitrary order L but differ for $l \geq L$. We also demonstrate how Hamilton-Jacobi theory can be applied to orbits in bumpy spacetimes to categorize the anomalous precessions arising from their bumps. In principle, bumpy black holes can now be used as the foundation for strong-gravity tests with astrophysical data.

It's worth re-emphasizing why we propose to use bumpy black holes, rather than using exact solutions which include black holes as a limit (for example, the Manko-Novikov spacetime [59] used in Ref. [35]). In large part, our choice is a matter of taste. Our goal is to tweak a black hole's moments in an arbitrary manner, so that the non-Kerr nature is entirely under our control. From the standpoint of formulating a null experiment, it arguably makes no difference whether the Kerr deviation takes one particular form or another; *any* falsifiable non-Kerr form is good enough to formulate the test. To our minds, a nice feature of this approach is that it is agnostic as to the identify of the compact object. There are several possible reasons why the spacetime of a candidate black hole might differ from the Kerr metric. The presence of matter, such as a companion object or an accretion disk, would perturb the spacetime away from Kerr. The object might not be a black hole but instead be a compact object composed of an exotic form of matter. Finally, it might indicate a breakdown of GR. Some alternative theories of gravity predict rotating black hole solutions that differ from Kerr, such as dynamical Chern-Simons extensions to GR [101].

In this analysis, we defined the perturbations by enforcing the vacuum Einstein

equations in the Schwarzschild limit. These perturbations are fine for describing some possible deviations from the Kerr metric, but they are not sufficient to describe all possible perturbed Kerr spacetimes, particularly those arising from non-GR theories of gravity. In Chapter 3, we extend the bumpy formalism to include black holes in alternate theories of gravity. We find that relaxing this condition leads to additional functional degrees of freedom that describe the perturbations.

The next major step in this program will be to use these foundations to formulate actual strong-field gravity tests that can be applied to astrophysical data. We imagine several directions that would be interesting to follow:

- *Extreme mass ratio inspiral (EMRI)*: The capture and inspiral of stellar mass compact into massive black holes at galaxy centers is one of the original motivations of this work. Much of the recent literature on testing and mapping black hole spacetimes has centered on understanding the character of orbits in non-Kerr black hole candidate spacetimes [13, 14, 3], with an eye on application to gravitational-wave measurement of EMRIs.

The full analysis of EMRIs in non-Kerr spacetimes is, in principle, quite complicated since their non-Kerr-ness breaks the Petrov Type-D character of Kerr black holes. As such, it may be quite difficult to accurately compute their radiation emission. It may not be quite so difficult in bumpy black hole spacetimes. Thanks to the smallness of their non-Kerr character, it may be fruitful to use a “hybrid” approach in which the short timescale motion is computed in the bumpy spacetime, but the radiation generation and backreaction is computed in the Kerr spacetime. Given that our goal is to formulate a null experiment, this hybrid may be good enough for a useful test, in lieu of solving the entire radiation reaction problem in non-Kerr spacetimes.

- *Black hole-pulsar systems*: One of the goals of the planned Square Kilometer Array (SKA) [85] is the discovery of a black hole-pulsar binary system. If such a system is discovered, detailed observation over many years should be able to tease the multipole structure of the black hole from the data. Similar

observations of neutron star-pulsar binary systems have already allowed us to make exquisite measurements of neutron star properties and gravitational-wave emission [88]. The tools developed here may already be adequate for doing this analysis since such binaries will have a relatively slow inspiral time.

- *Accretion flows on black hole candidate:* Programs to observe the (presumed) black hole at the center of our galaxy are maturing very quickly; programs to study accretion flows onto stellar mass black holes in x-rays are already quite mature. In our galactic center, the most precise measurements come from millimeter wavelength radio emission from gas accreting onto this central object. The precision of these measurements is increasing to the point where we will soon be able to use them to map the detailed strong-field spacetime structure of the spacetime near Sagittarius A*. Johannsen and Psaltis showed that perturbations to the mass quadrupole moment shift the location of the innermost stable circular orbit (ISCO), which can be observed by looking at the X-ray emission of the accretion disk surrounding the black hole [50]. They also showed that these perturbations change the shapes of the image of the black hole and the bright ring around the black hole shadow [51]. So far, only the effects of changes to the mass quadrupole moment have been considered. Although the effects of higher-order moments are probably small, it is important to measure as many moments as possible to determine if the spacetime satisfies the no-hair theorem. Just as Johannsen and Psaltis found that perturbations to the mass quadrupole moment change the shape of the image of the black hole, perturbations to higher-order mass moments and the spin moments may also leave a unique observable signature.

Chapter 3

Bumpy black holes in alternative theories of gravity

This chapter is based on *Physical Review D* **83**, 104027 (2011), which was written in collaboration with Nicolás Yunes and Leo C. Stein.

3.1 Introduction

Gravitational waves (GWs) will be powerful tools for learning about source astrophysics and testing strong field gravity [83, 86]. The Laser Interferometer Space Antenna (LISA) [10, 28, 27, 76] is expected to be sensitive to roughly a few radians or better of GW phase in a one-year observation. Such levels of precision are achieved through matched filtering, where the data are cross-correlated with a family of waveform models (see eg. [49]). If a signal is present in the data, this cross-correlation acts as a filter that selects the member of the waveform family that most closely resembles the signal.

Extreme mass-ratio inspirals (EMRIs) are ideal astrophysical sources to perform precision GW tests of strong field gravity with LISA [2, 83]. These sources consist of a small compact object that spirals into a massive black hole (MBH) in a generic orbit, producing millions of radians in GW phase inside LISA's sensitivity band. These waves carry detailed information about the spacetime geometry in which the small

compact object moves, thus serving as a probe to test general relativity (GR).

Tests of strong field gravity cannot rely on waveform families that assume GR is correct *a priori*. Instead, such tests must employ more generic waveforms that allow for GR deviations. Recently, Yunes and Pretorius [102] proposed the parameterized post-Einsteinian (ppE) framework, in which analytic waveforms that represent comparable mass-ratio coalescences in GR are parametrically deformed. For specific values of the ppE parameters, one recovers GR waveforms; otherwise they describe waveforms in non-GR theories. The ppE scheme has been shown to be sufficiently flexible to map all known alternative theory predictions for comparable mass-ratio coalescences [102].

PpE deformations of EMRI waveforms have not yet been constructed because of the complexities associated with the computation of such waveforms. EMRIs are not amenable to post-Newtonian (PN) approximation schemes [12, 98, 97, 99, 100], from which many GR templates are analytically constructed. Instead, to build EMRI waveforms one must solve geodesic-like equations, enhanced with a radiation-reaction force that induces an inspiral. The solution of these differential equations can only be found numerically (see eg. [5] for a recent review of the self-force problem).

One can parametrically deform EMRI waveforms by introducing non-GR deviations in the numerical scheme used to build such waveforms. Two main ingredients can then be modified: the conservative sector, which controls the shape of non-radiative orbits, and the dissipative sector, which controls the rate of inspiral and the GW generation mechanism. The conservative sector, to leading order in the mass-ratio, depends only on the background spacetime metric, the Kerr metric, on which the small compact object moves like a test-particle.

The goal of this work is to find a parametric deformation of the Kerr metric that allows for non-GR deviations while retaining a smooth Kerr limit, i.e. as the deformation parameters go to zero, the deformed Kerr metric reduces smoothly and exactly to Kerr. This limit then guarantees that the main properties of the Kerr background survive to the deformation, such as the existence of an event horizon, an ergosphere, and, in particular, three constants of the motion, such that the geodesic

equations can be separated into first-order form.

Although motion in alternative theories of gravity need not be geodesic, we will assume here that the geodesic equations hold to leading order in the mass ratio. This allows us to focus only on metric deformations that correct the conservative sector of EMRI waveforms. This assumption is justified for theories that derive from certain diffeomorphism-covariant Lagrangians [40], as is the case, for example, in dynamical Chern-Simons (CS) modified gravity [1], in Einstein-Dilaton-Gauss-Bonnet theory [53, 91, 54, 72, 67], and in dynamical quadratic gravity [21, 61, 103]. We are not aware of any alternative theory where this is not the case to leading order in the mass ratio (neglecting spins), although it is not hard to imagine that one may exist.

As discussed in Chapter 2, a framework already exists to parametrically deform the metric tensor through the construction of “bumpy spacetimes” [25, 93, 92]. These metrics are deformations of the Kerr metric, where the bumps are required to satisfy the Einstein equations in the $a = 0$ limit and to first order in the perturbation. Because of this last condition, bumpy black holes are not sufficiently generic to represent black holes in certain alternative theories of gravity (e.g. solutions that are not Ricci flat). A better interpretation is to think of these bumps as representing exterior matter distributions. The bumpy black hole formalism then allows tests of whether compact objects are truly described by the vacuum Kerr metric or by some more general tensor with external matter sources, assuming GR still holds.

In this chapter, we propose two generalizations of the bumpy black hole formalism to allow for metric deformations that can represent vacuum black hole solutions in alternative theories. The first approach, the generalized bumpy Kerr (BK) scheme, takes the standard bumpy metric and relaxes the requirement that the bumps satisfy the Einstein equations. The second approach, the generalized deformed Kerr (DK) scheme, perturbs the most general stationary, axisymmetric metric in Lewis-Papapetrou form and transforms it to Boyer-Lindquist coordinates without assuming the deformations satisfy the Einstein equations. In both cases, the metric is equivalent to the Kerr metric to zeroth order in the deformation parameter, but it deviates from Kerr at first order through a set of arbitrary functions.

The metric deformation is then restricted by requiring that the full metric still possesses three constants of the motion: a conserved energy (associated with time invariance), a conserved angular momentum component (associated with azimuthal rotational invariance), and an approximate second-order Killing tensor that leads to a conserved Carter constant. These conditions restrict the set of arbitrary functions that parameterize the metric deformations to have a certain functional form. It is these conditions that select the appropriate “bumps” instead of the imposition of the Einstein equations.

The restrictions imposed above are not strictly necessary, as there is no guarantee that black holes in alternative theories of gravity will continue to have three conserved quantities. However, all black hole solutions in alternative theories of gravity known to date and that are not pathological (i.e. they are stationary, axisymmetric, asymptotically flat, and contain no spacetime regions with closed time-like curves outside the horizon) possess three constants of the motion [19]. Examples include the slowly-rotating solution found in dynamical CS gravity [101] and the spherically symmetric solution found in dynamical quadratic gravity [103].

Much effort has gone into finding spacetimes with an exact second-order (or higher-order) generalized “Carter constant,” thus allowing for the separation of the equations of motion [13, 14, 15, 16, 17]. That work demonstrates that, for a broad class of spacetimes, such separation can be done provided that the Carter constant is quartic in the orbit’s 4-momentum (i.e., the constant is $C = \xi_{\alpha\beta\gamma\delta} p^\alpha p^\beta p^\gamma p^\delta$, where $\xi_{\alpha\beta\gamma\delta}$ is a 4th-rank Killing tensor and p^α is the 4-momentum). In this analysis, we show that one can in fact find an approximate Carter constant that is quadratic in the 4-momentum, $C = \xi_{\alpha\beta} p^\alpha p^\beta$, for many relevant spacetimes, provided they differ from Kerr only perturbatively.

Finally, we gain insight on the different proposed parameterizations by studying certain key limits. First, we show that the BK and DK deformations are related to each other by a gauge transformation. Second, we show that both the BK and DK metrics can be exactly mapped to specific non-GR black hole metrics, the dynamical CS gravity one and the dynamical quadratic one. Third, we study the structure that

the deformations must take when only deforming frame-dragging or the location of the event horizon. Finally, we separate the geodesic equations into first-order form in both the BK and DK metrics, and calculate the modified Kepler law. This modification corrects the dissipative dynamics through the conversion of radial quantities to frequency space.

The parameterized metrics (BK and DK) proposed in this chapter lay the foundations for a systematic construction and study of ppE EMRI waveforms. With these metrics and their associated separated equations of motion, one can now study modified small compact object trajectories and see how these impact the GW observable. Numerical implementation and a detailed data analysis study will be presented in a forthcoming publication.

This chapter is organized as follows. Sec. 3.2 introduces the BK formalism, which generalizes the bumpy black hole formalism. Sec. 3.3 presents the DK parameterized metric. Sec. 3.4 compares the parameterizations to each other and to alternative theory predictions. In Sec. 3.5 we discuss motion in alternative theories of gravity and derive the first-order form of the geodesic equations. We conclude in Sec. 3.6 by discussing some general properties of the parameterizations and outlining future work. In this chapter, background quantities are denoted with an overhead hat; for example, the full metric $g_{\mu\nu} = \hat{g}_{\mu\nu} + \epsilon b_{\mu\nu}$ can be decomposed into a background metric $\hat{g}_{\mu\nu}$ plus a small deformation $b_{\mu\nu}$, where $\epsilon \ll 1$ is a book-keeping parameter. The background spacetime is always taken to be the Kerr metric.

3.2 Generalized bumpy Kerr formalism

We here introduce the standard bumpy black hole formalism [25, 93, 92] and generalize it to the BK framework. The bumps are constrained by requiring that an approximate, second-order Killing tensor exists. We then rewrite the geodesic equations in first-order form.

3.2.1 From standard to generalized bumpy black holes

Let us first review the basic concepts associated with the bumpy black hole formalism [25, 93, 92]. This framework was initially introduced by Collins and Hughes [25] to model deformations of the Schwarzschild metric and expanded by Vigeland and Hughes [93] to describe deformations on a Kerr background. In this formalism, the metric is expanded perturbatively as

$$g_{\mu\nu} = \hat{g}_{\mu\nu} + \epsilon b_{\mu\nu}^{\text{SBK}}, \quad (3.1)$$

where ϵ is a book-keeping parameter that reminds us that $|b_{\mu\nu}^{\text{SBK}}|/|g_{\mu\nu}| \ll 1$. The background metric $\hat{g}_{\mu\nu}$ is the Kerr solution [Eq. (1.1)], while in the standard bumpy formalism, the metric functions $b_{\mu\nu}^{\text{SBK}}$ are parameterized via

$$b_{tt} = -2 \left(1 - \frac{2Mr}{\Sigma} \right) \psi_1 - \frac{4aMr}{\Sigma^2} \sigma_1, \quad (3.2a)$$

$$b_{tr} = -\gamma_1 \frac{2a^2 Mr \sin^2 \theta}{\Delta \Sigma}, \quad (3.2b)$$

$$b_{t\phi} = (\gamma_1 - 2\psi_1) \frac{2aMr \sin^2 \theta}{\Sigma} + \sigma_1 \left[\frac{4Mr(r^2 + a^2)}{\Sigma^2} + \frac{2\Delta}{\Sigma} - \frac{\Delta}{\Sigma - 2Mr} \right], \quad (3.2c)$$

$$b_{rr} = 2(\gamma_1 - \psi_1) \frac{\Sigma}{\Delta}, \quad (3.2d)$$

$$b_{r\phi} = \gamma_1 a \sin^2 \theta \left[1 + \frac{2Mr(r^2 + a^2)}{\Delta \Sigma} \right], \quad (3.2e)$$

$$b_{\theta\theta} = 2(\gamma_1 - \psi_1) \Sigma, \quad (3.2f)$$

$$b_{\phi\phi} = \frac{\sin^2 \theta}{\Sigma} \left\{ (\gamma_1 - \psi_1) \frac{8a^2 M^2 r^2 \sin^2 \theta}{\Sigma - 2Mr} - 2\psi_1 \Sigma \Delta \left(1 - \frac{2Mr}{\Sigma} \right)^{-1} + \sigma_1 \frac{4aMr}{\Sigma - 2Mr} \left[\Delta + \frac{2Mr(r^2 + a^2)}{\Sigma} \right] \right\}. \quad (3.2g)$$

where $\Delta \equiv r^2 - 2Mr + a^2$ and $\Sigma \equiv r^2 + a^2 \cos^2 \theta$. The bumps are defined by the perturbation functions ψ_1^{SBK} , γ_1^{SBK} , and σ_1^{SBK} , which are functions of r and θ .

A few comments are due at this point. First, notice that this metric contains only three arbitrary functions (ψ_1^{SBK} , γ_1^{SBK} , σ_1^{SBK}), instead of four, as one would expect from

the most general stationary and axisymmetric metric. This is because of the specific way Eq. (3.2) is derived, which assumes a Ricci-flat metric in the $a = 0$ limit. Second, note that many metric components are non-vanishing: apart from the components g_{tt} , $g_{t\phi}$, g_{rr} , $g_{\theta\theta}$, and $g_{\phi\phi}$ that are nonzero in the Kerr metric, Eq. (3.2) also has non-vanishing g_{tr} and $g_{r\phi}$ components.

The derivation of this spacetime, as discussed in Sec. 2.3, begins with the most general stationary and spherically symmetric metric in Lewis-Pappapetrou form that is Ricci-flat. One then perturbs the two arbitrary functions in this metric and maps it to Schwarzschild coordinates. Through the Newman-Janis procedure, one then performs a complex rotation of the tetrad associated with this metric to transform it into a deformed Kerr spacetime. At no stage in this procedure is one guaranteed that the resulting spacetime will still possess a Carter constant or that it will remain vacuum. In fact, the metric constructed from Eq. (3.2) does not have a Carter constant, nor does it satisfy the vacuum Einstein equations, leading to a nonzero effective stress-energy tensor.

Such features make the standard bumpy formalism not ideal for null-tests of GR. One would prefer to have a framework that is generic enough to allow for non-GR tests while still possessing a smooth GR limit, such that as the deformations are taken to zero, one recovers exactly the Kerr metric. This limit implies that the deformed metric will retain many of the nice properties of the Kerr background, such as the existence of an event horizon, an ergosphere, and a Carter constant.

This can be achieved by generalizing the bumpy black hole formalism by relaxing the initial assumption that the metric be Ricci-flat prior to the Newman-Janis procedure. In this section, inspired by [25, 93, 92], we do this by promoting the non-vanishing components of the metric perturbation, i.e., $(b_{tt}^{\text{BK}}, b_{tr}^{\text{BK}}, b_{t\phi}^{\text{BK}}, b_{rr}^{\text{BK}}, b_{r\phi}^{\text{BK}}, b_{\theta\theta}^{\text{BK}}, b_{\phi\phi}^{\text{BK}})$, to arbitrary functions of r and θ . These functions are restricted only by requiring that an approximate second-order Killing tensor still exists. This restriction is not strictly necessary, but it is appealing on several fronts. First, the few analytic non-GR black hole solutions that are known happen to have a Carter constant, at least perturbatively as an expansion in the non-Kerr deviation. Second, a Carter constant

allows for the separation of the equations of motion into first-order form, which then renders the system easily integrable with already developed numerical techniques.

3.2.2 Existence conditions for the Carter constant

Let us now investigate what conditions must be enforced on the metric perturbation $b_{\alpha\beta}^{\text{BK}}$ so that a Killing tensor $\xi_{\alpha\beta}$ and its associated Carter constant exist, at least perturbatively to $\mathcal{O}(\epsilon)$. Killing's equations can be used to infer some fairly general properties that such a tensor must have. First, this tensor must be non-vanishing in the same components as the metric perturbation. For the generalized bumpy metric, this means the components of the Killing tensor ($\xi_{t\theta}$, $\xi_{r\theta}$, and $\xi_{\theta\phi}$) must all vanish. Furthermore, if we expand the Killing tensor as

$$\xi_{\alpha\beta} = \hat{\xi}_{\alpha\beta} + \epsilon \delta\xi_{\alpha\beta}, \quad (3.3)$$

we then find that $\delta\xi_{\alpha\beta}$ must have the same parity as $\hat{\xi}_{\alpha\beta}$ for the full Killing tensor to have a definite parity. For the generalized bumpy metric, this means the components ξ_{tt} , ξ_{rr} , $\xi_{\theta\theta}$, $\xi_{\phi\phi}$, and $\xi_{t\phi}$ must be even under reflection: $\theta \rightarrow \theta - \pi$.

These conditions imply that of the ten independent degrees of freedom in $\delta\xi_{\alpha\beta}$, only seven are truly necessary. With this in mind, we parameterize the Killing tensor as in Eq. (1.8), namely

$$\xi_{\alpha\beta} = \Delta k_{(\alpha} l_{\beta)} + r^2 g_{\alpha\beta}. \quad (3.4)$$

Notice that $\xi_{\alpha\beta}$ depends here on the full metric $g_{\alpha\beta}$ and on null vectors k^α and l^α that are not required to be the Kerr ones or the principal congruences of the full spacetime: $k^\alpha \neq \hat{k}^\alpha$ and $l^\alpha \neq \hat{l}^\alpha$. We decompose these vectors via

$$k^\alpha = \hat{k}^\alpha + \epsilon \delta k^\alpha, \quad (3.5a)$$

$$l^\alpha = \hat{l}^\alpha + \epsilon \delta l^\alpha, \quad (3.5b)$$

where \hat{k}^α and \hat{l}^α are the principal null vectors of the Kerr spacetime, given in Eq. (1.9).

Then we can expand the tensor $\xi_{\alpha\beta}$ as

$$\xi_{\alpha\beta} = \hat{\xi}_{\alpha\beta} + \epsilon \delta\xi_{\alpha\beta}, \quad (3.6)$$

where $\hat{\xi}_{\alpha\beta}$ is the Killing tensor of the Kerr space-time, given in Eq. (1.8), and $\delta\xi_{\alpha\beta}$ is given by

$$\delta\xi_{\alpha\beta} \equiv \Delta \left[\delta k_{(\alpha} l_{\beta)} + \delta l_{(\alpha} k_{\beta)} + 2b_{\delta(\alpha}^{\text{BK}} \hat{k}_{\beta)} \hat{l}^{\delta} \right] + 3r^2 b_{\alpha\beta}^{\text{BK}}. \quad (3.7)$$

All lowering and raising of indices is carried out with the background metric. Although this particular ansatz only allows six independent degrees of freedom (as the vectors are assumed to be null), we will see it suffices to find a Carter constant.

With this ansatz, the tensor Killing equation [Eq. (1.7)] becomes

$$\partial_{(\mu} \delta\xi_{\alpha\beta)} - 2\hat{\Gamma}_{(\mu\alpha}^{\delta} \delta\xi_{\beta)\delta} = 2\delta\Gamma_{(\mu\alpha}^{\delta} \hat{\xi}_{\beta)\delta}. \quad (3.8)$$

The system of equations one must solve is truly formidable and in fact overconstrained. Equation (3.8) is a set of 20 partial differential equations, while the normalization conditions $l^{\alpha} l_{\alpha} = 0 = k^{\alpha} k_{\alpha}$ add two additional algebraic equations. This means there are a total of 13 degrees of freedom (seven in $b_{\alpha\beta}^{\text{BK}}$ and six in δl^{α} and δk^{α} after imposing the normalization condition) but 20 partial differential equations to solve.

In spite of these difficulties, we have solved this system of equations with MAPLE and the GRTENSORII package¹ and found that the perturbation to the null vectors must satisfy

$$\delta k_{\text{BK}}^{\alpha} = \left(\frac{r^2 + a^2}{\Delta} \delta k_{\text{BK}}^r + \delta_1, \delta k_{\text{BK}}^r, 0, \frac{a}{\Delta} \delta k_{\text{BK}}^r + \delta_2 \right), \quad (3.9a)$$

$$\delta l_{\text{BK}}^{\alpha} = \left(\frac{r^2 + a^2}{\Delta} \delta k_{\text{BK}}^r + \delta_3, \delta k_{\text{BK}}^r + \delta_4, 0, \frac{a}{\Delta} \delta k_{\text{BK}}^r + \delta_5 \right), \quad (3.9b)$$

where the functions $\delta_i \equiv \delta_i(r)$ are arbitrary functions of r , generated upon solving the

¹This is a package which runs within MAPLE but distinct from packages distributed with MAPLE. It is distributed freely from the following address: <http://grtensor.org>.

differential system. These functions are fully determined by the metric perturbation, which is given by

$$\begin{aligned}
b_{tt}^{\text{BK}} &= -\frac{a}{2M} \frac{\Sigma^2 \Delta}{P_1^{\text{BK}}} \frac{\partial b_{t\phi}^{\text{BK}}}{\partial r} - \frac{a}{M} \frac{P_2^{\text{BK}}}{P_1^{\text{BK}}} b_{t\phi}^{\text{BK}} - \frac{a^2 \sin^2 \theta (\Sigma - 4Mr) \Delta^2}{4M P_1^{\text{BK}}} \left(\frac{\partial \delta_1}{\partial r} + \frac{\partial \delta_3}{\partial r} \right) \\
&\quad - \frac{a}{4M} \Delta^2 \sin^2 \theta \frac{P_3^{\text{BK}}}{P_1^{\text{BK}}} \left(\frac{\partial \delta_2}{\partial r} + \frac{\partial \delta_5}{\partial r} \right) + \frac{\Delta P_4^{\text{BK}}}{\Sigma P_1^{\text{BK}}} (\delta_1 + \delta_3) \\
&\quad - \frac{a}{2M} \frac{\Delta P_5^{\text{BK}}}{\Sigma P_1^{\text{BK}}} (\delta_2 + \delta_5) + \frac{\Delta (r^2 + a^2) \bar{\Sigma}}{\Sigma P_1^{\text{BK}}} \Theta_1, \tag{3.10a}
\end{aligned}$$

$$b_{tr}^{\text{BK}} = \frac{1}{2} \left(1 - \frac{2Mr}{\Sigma} \right) (\delta_1 - \delta_3) + \frac{aMr \sin^2 \theta}{\Sigma} (\delta_2 - \delta_5) - \frac{1}{2} \delta_4, \tag{3.10b}$$

$$b_{rr}^{\text{BK}} = -\frac{\Theta_1}{\Delta} + \frac{\Sigma}{\Delta} \delta_4, \tag{3.10c}$$

$$\begin{aligned}
b_{r\phi}^{\text{BK}} &= \frac{aMr \sin^2 \theta}{\Sigma} (\delta_1 - \delta_3) - \frac{\sin^2 \theta}{2\Sigma} (P_3^{\text{BK}} - 2a^2 Mr \sin^2 \theta) (\delta_2 - \delta_5) \\
&\quad + \frac{a}{2} \sin^2 \theta \delta_4, \tag{3.10d}
\end{aligned}$$

$$b_{\theta\theta}^{\text{BK}} = -\Theta_1 + \Sigma \Theta_2, \tag{3.10e}$$

$$\begin{aligned}
b_{\phi\phi}^{\text{BK}} &= -\frac{(r^2 + a^2)^2}{a^2} b_{tt}^{\text{BK}} - \frac{2(r^2 + a^2)}{a} b_{t\phi}^{\text{BK}} + \frac{\Delta}{a^2} \Theta_1 + \frac{\Delta^2}{a^2} (\delta_1 + \delta_3) \\
&\quad - \frac{\Delta^2 \sin^2 \theta}{a} (\delta_2 + \delta_5), \tag{3.10f}
\end{aligned}$$

$$\begin{aligned}
\frac{\partial^2 b_{t\phi}^{\text{BK}}}{\partial r^2} &= \left(\frac{\partial^2 \delta_2}{\partial r^2} + \frac{\partial^2 \delta_5}{\partial r^2} \right) P_6^{\text{BK}} + \left(\frac{\partial^2 \delta_1}{\partial r^2} + \frac{\partial^2 \delta_3}{\partial r^2} \right) P_7^{\text{BK}} + \left(\frac{\partial \delta_2}{\partial r} + \frac{\partial \delta_5}{\partial r} \right) \frac{P_8^{\text{BK}}}{P_{15}^{\text{BK}}} \\
&\quad + \left(\frac{\partial \delta_1}{\partial r} + \frac{\partial \delta_3}{\partial r} \right) \frac{P_{15}^{\text{BK}}}{P_{15}^{\text{BK}}} + (\delta_2 + \delta_5) \frac{P_{10}^{\text{BK}}}{P_{15}^{\text{BK}}} + (\delta_1 + \delta_3) \frac{P_{11}^{\text{BK}}}{P_{15}^{\text{BK}}} \\
&\quad + \frac{\partial b_{t\phi}^{\text{BK}}}{\partial r} \frac{P_{12}^{\text{BK}}}{P_{15}^{\text{BK}}} + b_{t\phi}^{\text{BK}} \frac{P_{13}^{\text{BK}}}{P_{15}^{\text{BK}}} + \Theta_1 \frac{P_{14}^{\text{BK}}}{P_{15}^{\text{BK}}}, \tag{3.10g}
\end{aligned}$$

where $\Delta \equiv r^2 - 2Mr + a^2$, $\Sigma \equiv r^2 + a^2 \cos^2 \theta$, and $\bar{\Sigma} \equiv r^2 - a^2 \cos^2 \theta$. The functions $\Theta_{1,2} \equiv \Theta_{1,2}(\theta)$ are functions of θ , and P_i^{BK} are polynomials in r and $\cos \theta$, which are given explicitly in Appendix C [Eqs. (C.1) – (C.15)]. Notice that δk_{BK}^r does not appear in the metric perturbation at all, so we are free to set $\delta k_{\text{BK}}^r = 0$.

With this at hand, given some metric perturbation $b_{\alpha\beta}^{\text{BK}}$ that satisfies Eq. (3.10), one can construct the arbitrary functions δ_i and Θ_i and thus build the null directions of the perturbed spacetime, such that a Killing tensor and a Carter constant exist to first order. We have verified that the conditions described above satisfy the generic Killing tensor properties, described at the beginning of this subsection.

Non-rotating limit

Let us now investigate the nonrotating limit $a \rightarrow 0$. To do so, we expand all arbitrary functions via

$$\mathcal{F}_i = \mathcal{F}_{i,0} + a\mathcal{F}_{i,1} + \mathcal{O}(a^2), \quad (3.11)$$

where \mathcal{F}_i is any of $\delta_i(r)$ or $\Theta_i(\theta)$. We also expand the metric components in a similar fashion, i.e.

$$b_{\alpha\beta}^{\text{BK}}(r, \theta) = b_{\alpha\beta,0}^{\text{BK}}(r, \theta) + a b_{\alpha\beta,1}^{\text{BK}}(r, \theta) + \mathcal{O}(a^2). \quad (3.12)$$

The following choices

$$\Theta_{1,0} = 0, \quad (3.13a)$$

$$\Theta_{2,n} = 0, \quad (3.13b)$$

$$\delta_{1,0} = \frac{b_{rr,0}^{\text{BK}}}{2} + \frac{b_{tt,0}^{\text{BK}}}{2f^2}, \quad (3.13c)$$

$$\delta_{2,0} = 0, \quad (3.13d)$$

$$\delta_{2,1} = -\frac{r - 4M}{2r^3 f^2} b_{tt,0}^{\text{BK}}, \quad (3.13e)$$

$$\delta_{3,0} = -\frac{b_{rr,0}^{\text{BK}}}{2} + \frac{b_{tt,0}^{\text{BK}}}{2f^2}, \quad (3.13f)$$

$$\delta_{4,0} = f b_{rr,0}^{\text{BK}}, \quad (3.13g)$$

$$\delta_{5,0} = 0, \quad (3.13h)$$

$$\delta_{5,1} = -\frac{r - 4M}{2r^3 f^2} b_{tt,0}^{\text{BK}}, \quad (3.13i)$$

$$(3.13j)$$

where $f \equiv 1 - 2M/r$, force the metric components to take the form

$$b_{tt}^{\text{BK}} = b_{tt,0}^{\text{BK}}(r), \quad (3.14a)$$

$$b_{rr}^{\text{BK}} = b_{rr,0}^{\text{BK}}(r), \quad (3.14b)$$

where we have set all integration constants to zero. All other components of the metric vanish to this order. To obtain this result, it is crucial to use the slow-rotation expansion postulated above, as some of the conditions in Eq. (3.10) have seemingly

divergent pieces. We see then that in the non-rotating limit, one can always choose free functions δ_i and Θ_i such that the only two independent metric perturbations are b_{tt}^{BK} and b_{rr}^{BK} .

The Killing tensor is then given by Eq. (3.4), with the perturbed null vector components

$$\delta k_{\text{BK}}^\alpha = \left[\frac{b_{rr,0}^{\text{BK}}}{2} + \frac{b_{tt,0}^{\text{BK}}}{2f^2}, 0, 0, \mathcal{O}(a) \right], \quad (3.15a)$$

$$\delta l_{\text{BK}}^\alpha = \left[-\frac{b_{rr,0}^{\text{BK}}}{2} + \frac{b_{tt,0}^{\text{BK}}}{2f^2}, f b_{rr,0}^{\text{BK}}, 0, \mathcal{O}(a) \right], \quad (3.15b)$$

where we have set $\delta k_{\text{BK}}^r = 0$. Composing the Killing tensor, we find that all $\mathcal{O}(\epsilon)$ terms vanish in the $a \rightarrow 0$ limit. This result makes perfect sense, considering that the Schwarzschild Killing tensor, $\hat{\xi}_{\alpha\beta} = r^2 \Omega_{\alpha\beta}$ with $\Omega_{\alpha\beta} \equiv \text{diag}(0, 0, r^2, r^2 \sin^2 \theta)$, is also a Killing tensor for the most generic static and spherically symmetric spacetime with arbitrary g_{tt} and g_{rr} components.

3.3 Deformed Kerr formalism

In the previous section, we generalized the bumpy black hole framework at the cost of introducing a large number of arbitrary functions, later constrained by the requirement of the existence of a Carter constant. In this section, we investigate a different parameterization (DK) that isolates the physically independent degrees of freedom from the start so as to minimize the introduction of arbitrary functions.

3.3.1 Deformed Kerr geometry

Let us first consider the most general spacetime metric that one can construct for a stationary and axisymmetric spacetime. In such a geometry, there will exist two Killing vectors, t^a and ϕ^a , that represent invariance under a time and azimuthal coordinate transformation. Because these Killing vectors are independent, they will commute satisfying $t_{[a}\phi_b\nabla_c t_{d]} = 0 = t_{[a}\phi_b\nabla_c \phi_{d]}$. Let us further assume the integra-

bility condition

$$t^a R_a^{[b} t^c \phi^{d]} = 0, \quad (3.16a)$$

$$\phi^a R_a^{[b} t^c \phi^{d]} = 0. \quad (3.16b)$$

This condition guarantees that the 2-planes orthogonal to the Killing vectors t^a and ϕ^a are integrable. Generic stationary and axisymmetric solutions to modified field equations do not need to satisfy Eq. (3.16). However, all known analytic solutions in GR and in alternative theories do happen to satisfy this condition. We will assume it holds here as well.

Given these conditions, the most general stationary, axisymmetric line element can be written in Lewis-Papapetrou canonical form, using cylindrical coordinates (t, ρ, ϕ, z) :

$$ds^2 = -V (dt - w d\phi)^2 + V^{-1} \rho^2 d\phi^2 + \Omega^2 (d\rho^2 + \Lambda dz^2), \quad (3.17)$$

where (V, w, Ω, Λ) are arbitrary functions of (ρ, z) . The Einstein equations restrict the form of these arbitrary functions: [52]

$$\hat{V} = \frac{(r_+ + r_-)^2 - 4M^2 + \frac{a^2}{M^2 - a^2} (r_+ - r_-)^2}{(r_+ + r_- + 2M)^2 + \frac{a^2}{M^2 - a^2} (r_+ - r_-)^2}, \quad (3.18a)$$

$$\hat{w} = \frac{2aM \left(M + \frac{r_+ + r_-}{2} \right) \left(1 - \frac{(r_+ - r_-)^2}{4(M^2 - a^2)} \right)}{\frac{1}{4} (r_+ + r_-)^2 - M^2 + a^2 \frac{(r_+ - r_-)^2}{4(M^2 - a^2)}}, \quad (3.18b)$$

$$\hat{\Lambda} = 1, \quad (3.18c)$$

$$\hat{\Omega} = V \frac{(r_+ + r_-)^2 - 4M^2 + \frac{a^2}{M^2 - a^2} (r_+ - r_-)^2}{4r_+ r_-}, \quad (3.18d)$$

where r_{\pm} is defined by

$$r_{\pm} = \sqrt{\rho^2 + \left(z \pm \sqrt{M^2 - a^2} \right)^2}. \quad (3.19)$$

One can map from this coordinate system to Boyer-Lindquist coordinates (t, r, θ, ϕ)

via the transformation $\rho = \sqrt{\Delta} \sin \theta$ and $z = (r - M) \sin \theta$ to obtain the Kerr metric.

We will not impose Ricci-flatness here, as we wish to model alternative theory deviations from Kerr. We therefore work directly with Eq. (3.17), keeping (V, w, Ω, Λ) as arbitrary functions, but transforming this to Boyer-Lindquist coordinates. Let us then re-parametrize $\Omega^2 \equiv \gamma$, $\lambda \equiv \gamma \Lambda$, and $q \equiv Vw$, and perturb the metric functions via

$$V = \hat{V} + \delta V, \quad (3.20a)$$

$$q = \hat{q} + \delta q, \quad (3.20b)$$

$$\lambda = \hat{\lambda} + \delta \lambda, \quad (3.20c)$$

$$\gamma = \hat{\gamma} + \delta \gamma. \quad (3.20d)$$

The metric then becomes

$$g_{\mu\nu} = \hat{g}_{\mu\nu} + b_{\mu\nu}^{\text{DK}}, \quad (3.21)$$

where the perturbation is given by

$$b_{tt}^{\text{DK}} = -\delta V, \quad (3.22a)$$

$$b_{t\phi}^{\text{DK}} = \delta q, \quad (3.22b)$$

$$b_{rr}^{\text{DK}} = \delta \lambda \cos^2 \theta + \delta \gamma \frac{(r - M)^2 \sin^2 \theta}{\Delta}, \quad (3.22c)$$

$$b_{r\theta}^{\text{DK}} = (r - M) \cos \theta \sin \theta (\delta \gamma - \delta \lambda), \quad (3.22d)$$

$$b_{\theta\theta}^{\text{DK}} = \delta \lambda \sin^2 \theta (r - M)^2 + \delta \gamma \cos^2 \theta \Delta, \quad (3.22e)$$

$$b_{\phi\phi}^{\text{DK}} = \frac{\sin^2 \theta}{\Sigma - 2Mr} \left\{ 4aMr \delta q - \left[(r^2 + a^2)^2 - a^2 \sin^2 \theta \Delta \right] \delta V \right\}, \quad (3.22f)$$

and all other components vanish.

As is clear from the above expressions, the most general perturbation to a stationary, axisymmetric metric yields five non-vanishing metric components that depend still only on four arbitrary functions $(\delta V, \delta q, \delta \gamma, \delta \lambda)$ of the coordinates r and θ . This is unlike the standard bumpy formalism that introduces six non-vanishing metric

components that depend on four arbitrary functions (courtesy of the Newman-Janis algorithm applied to a non-Kerr metric). Furthermore, this analysis shows that two of the six arbitrary functions introduced in the generalized bumpy scheme of the previous section must not be independent, as argued earlier.

Following the insight from the previous section, we will henceforth allow these five metric components $(b_{tt}^{\text{DK}}, b_{rr}^{\text{DK}}, b_{r\theta}^{\text{DK}}, b_{\theta\theta}^{\text{DK}}, b_{\phi\phi}^{\text{DK}})$ to be arbitrary functions of r and θ , although technically there are only four independent degrees of freedom. We do this because it eases the analytic calculations to come when one investigates which conditions $b_{\alpha\beta}^{\text{DK}}$ must satisfy for there to exist an approximate second-order Killing tensor. Moreover, it allows us to relax the undesirable requirement, implicit in Eq. (3.22), that when $\delta V \neq 0$, then both b_{tt} and $b_{\phi\phi}$ must be nonzero in the $a \rightarrow 0$ limit.

3.3.2 Existence conditions for the Carter constant

Let us now follow the same methodology of Sec. 3.2.2 to determine what conditions the arbitrary functions must satisfy in order for the spacetime to have a second-order Killing tensor. We begin by parameterizing the Killing tensor as in Eq. (3.4), with the expansion of the null vectors as in Eq. (3.5) and the replacement of $BK \rightarrow DK$ everywhere. With this at hand, the Killing equation acquires the same structure as Eq. (3.8).

We have solved the Killing equations with MAPLE and the GRTENSORII package to find that the null vectors must satisfy:

$$\delta k_{\text{DK}}^\alpha = \left[\frac{r^2 + a^2}{\Delta} (\delta l_{\text{DK}}^r + \gamma_1) + \gamma_4, \delta l_{\text{DK}}^r + \gamma_1, -\frac{b_{r\theta}^{\text{DK}}}{\Sigma}, \frac{a}{\Delta} (\delta l_{\text{DK}}^r + \gamma_1) + \gamma_3 \right], \quad (3.23a)$$

$$\delta l_{\text{DK}}^\alpha = \left[-\frac{r^2 + a^2}{\Delta} \delta l_{\text{DK}}^r + \gamma_4, \delta l_{\text{DK}}^r, \frac{b_{r\theta}^{\text{DK}}}{\Sigma}, -\frac{a}{\Delta} \delta l_{\text{DK}}^r + \gamma_3 \right], \quad (3.23b)$$

where $\gamma_i \equiv \gamma_i(r)$ are arbitrary functions of radius, and δl_{DK}^r and $b_{r\theta}^{\text{DK}}$ are arbitrary functions of both r and θ . As before with δk_{BK}^r , we find below that the function δl_{DK}^r does not enter the metric perturbation, so we can set it to zero. The functions γ_i are

completely determined by the metric perturbation:

$$\begin{aligned}
b_{tt}^{\text{DK}} &= -\frac{a}{M} \frac{P_2^{\text{DK}}}{P_1^{\text{DK}}} b_{t\phi}^{\text{DK}} - \frac{a}{2M} \frac{\Sigma^2 \Delta}{P_1^{\text{DK}}} \frac{\partial b_{t\phi}^{\text{DK}}}{\partial r} - \frac{2a^2 r (r^2 + a^2) \Delta \sin \theta \cos \theta}{\Sigma P_1^{\text{DK}}} b_{r\theta}^{\text{DK}} \\
&+ \frac{(r^2 + a^2) \bar{\Sigma} \Delta}{\Sigma P_1^{\text{DK}}} \mathcal{I} + \frac{2a^2 r^2 \Delta \sin^2 \theta}{P_1^{\text{DK}}} \gamma_1 + \frac{\bar{\Sigma} (r^2 + a^2) \Delta}{\Sigma P_1^{\text{DK}}} \Theta_3 \\
&- \frac{a}{M} \frac{\Delta \sin^2 \theta}{\Sigma} \frac{P_3^{\text{DK}}}{P_1^{\text{DK}}} \gamma_3 + \frac{2\Delta}{\Sigma} \frac{P_4^{\text{DK}}}{P_1^{\text{DK}}} \gamma_4 - \frac{a^2}{2M} \frac{\Sigma \Delta^2 \sin^2 \theta}{P_1^{\text{DK}}} \frac{d\gamma_1}{dr} \\
&- \frac{a}{2M} \frac{\Delta^2 \left[(r^2 + a^2)^2 - a^2 \sin^2 \theta (r^2 - 4Mr + a^2) \right] \sin^2 \theta}{P_1^{\text{DK}}} \frac{d\gamma_3}{dr} \\
&- \frac{a^2}{2M} \frac{\Delta^2 (\Sigma - 4Mr) \sin^2 \theta}{P_1^{\text{DK}}} \frac{d\gamma_4}{dr}, \tag{3.24a}
\end{aligned}$$

$$b_{rr}^{\text{DK}} = -\frac{1}{\Delta} \mathcal{I} - \frac{1}{\Delta} \Theta_3, \tag{3.24b}$$

$$\begin{aligned}
b_{\phi\phi}^{\text{DK}} &= -\frac{(r^2 + a^2)^2}{a^2} b_{tt}^{\text{DK}} + \frac{\Delta}{a^2} \mathcal{I} - \frac{2(r^2 + a^2)}{a} b_{t\phi}^{\text{DK}} + \frac{\Delta}{a^2} \Theta_3 \\
&- \frac{2\Delta^2 \sin^2 \theta}{a} \gamma_3 + \frac{2\Delta^2}{a^2} \gamma_4, \tag{3.24c}
\end{aligned}$$

$$\frac{\partial b_{\theta\theta}^{\text{DK}}}{\partial r} = \frac{2r}{\Sigma} b_{\theta\theta}^{\text{DK}} + \frac{2a^2 \sin \theta \cos \theta}{\Sigma} b_{r\theta}^{\text{DK}} + 2 \frac{\partial b_{r\theta}^{\text{DK}}}{\partial \theta} + \frac{2r}{\Sigma} \mathcal{I} - 2r \gamma_1 + \frac{2r}{\Sigma} \Theta_3, \tag{3.24d}$$

$$\begin{aligned}
\frac{\partial^2 b_{t\phi}^{\text{DK}}}{\partial r^2} &= \frac{8aM \sin \theta \cos \theta}{\Sigma^4} \frac{P_5^{\text{DK}}}{P_1^{\text{DK}}} b_{r\theta}^{\text{DK}} - \frac{4aMr (r^2 + a^2) \sin \theta \cos \theta}{\Sigma^3} \frac{\partial b_{r\theta}^{\text{DK}}}{\partial r} \\
&+ \frac{2a^2 \sin^2 \theta}{\Sigma^2} \frac{P_6^{\text{DK}}}{P_1^{\text{DK}}} b_{t\phi}^{\text{DK}} - \frac{2r}{\Sigma} \frac{P_7^{\text{DK}}}{P_1^{\text{DK}}} b_{t\phi}^{\text{DK}} + \frac{4aMr \sin^2 \theta}{\Sigma^2} \frac{P_{15}^{\text{DK}}}{P_{16}^{\text{DK}}} \mathcal{I} \\
&- \frac{4aMr \sin^2 \theta}{\Sigma^2} \frac{P_8^{\text{DK}}}{P_1^{\text{DK}}} \gamma_1 + \frac{4aMr}{\Sigma^2} \frac{P_9^{\text{DK}}}{P_1^{\text{DK}}} \Theta_3 + \frac{2 \sin^2 \theta}{\Sigma^2} \frac{P_{10}^{\text{DK}}}{P_1^{\text{DK}}} \gamma_3 \\
&- \frac{16aM \sin^2 \theta}{\rho^4} \frac{P_{11}^{\text{DK}}}{P_1^{\text{DK}}} \gamma_4 - \frac{2a}{\Sigma^2} \frac{P_{12}^{\text{DK}}}{P_1^{\text{DK}}} \frac{d\gamma_1}{dr} - \frac{2 \sin^2 \theta}{\Sigma^2} \frac{P_{13}^{\text{DK}}}{P_1^{\text{DK}}} \frac{d\gamma_3}{dr} \\
&- \frac{2a \sin^2 \theta}{\Sigma^2} \frac{P_{14}^{\text{DK}}}{P_1^{\text{DK}}} \frac{d\gamma_4}{dr} - \frac{a\Delta \sin^2 \theta}{\Sigma} \frac{d^2 \gamma_1}{dr^2} \\
&- \frac{\Delta \sin^2 \theta}{\Sigma^2} \left[(r^2 + a^2)^2 - a^2 \sin^2 \theta (r^2 - 4Mr + a^2) \right] \frac{d^2 \gamma_3}{dr^2} \\
&- \frac{a\Delta (\Sigma - 4Mr) \sin^2 \theta}{\Sigma^2} \frac{d^2 \gamma_4}{dr^2}, \tag{3.24e}
\end{aligned}$$

where $\bar{\Sigma} \equiv r^2 - a^2 \cos^2 \theta$, $\Theta_r = \Theta_r(\theta)$ is an arbitrary function of polar angle, and P_i^{DK} are polynomials in r and $\cos \theta$, given explicitly in Appendix C [Eqs. (C.16) – (C.30)].

Notice that many of these relations are integro-differential, as \mathcal{I} is defined as

$$\mathcal{I} = \int dr \left[\frac{2a^2 \sin \theta \cos \theta}{\Sigma} b_{r\theta}^{\text{DK}} + 2r \gamma_1 + \Sigma \frac{d\gamma_1}{dr} \right]. \quad (3.25)$$

Notice also that the component $b_{r\theta}^{\text{DK}}$ is free and thus there are here truly only four independent metric components.

Any metric perturbation $b_{\alpha\beta}^{\text{DK}}$ that satisfies Eq. (3.24) will possess a Carter constant. If given a specific non-Kerr metric, one can then use these equations to reconstruct the γ_i and Θ_2 functions to automatically obtain the perturbative second-order Killing tensor associated with this spacetime.

Non-rotating limit

Let us now take the non-rotating limit, i.e. $a \rightarrow 0$, of the DK Carter conditions. As before, we expand all arbitrary functions as in Eqs. (3.11) and (3.12). Imposing the constraints

$$\Theta_{3,0} = 0, \quad (3.26a)$$

$$\gamma_{1,0} = -b_{rr,0}^{\text{DK}} f, \quad (3.26b)$$

$$\gamma_{3,0} = 0, \quad (3.26c)$$

$$\gamma_{3,1} = \frac{b_{rr,0}^{\text{DK}}}{2r^2} - \frac{r - 4M}{2r^3 f^2} b_{tt,0}^{\text{DK}}, \quad (3.26d)$$

$$\gamma_{4,0} = \frac{b_{tt,0}^{\text{DK}}}{2f^2} + \frac{b_{rr,0}^{\text{DK}}}{2}, \quad (3.26e)$$

where $f \equiv 1 - 2M/r$, forces the metric components to take the form

$$b_{tt}^{\text{DK}} = b_{tt,0}^{\text{DK}}, \quad (3.27a)$$

$$b_{rr}^{\text{DK}} = b_{rr,0}^{\text{DK}}, \quad (3.27b)$$

$$b_{\phi\phi}^{\text{DK}} = 0. \quad (3.27c)$$

All other pieces of $\mathcal{O}(a^0)$ in the remaining metric components can be set to zero by setting $(b_{r\theta}^{\text{DK}}, b_{\theta\theta}^{\text{DK}}, b_{t\phi}^{\text{DK}})$ to zero. With these choices, the differential conditions are

automatically satisfied, where we have set all integration constants to zero. The Killing tensor is then given by Eq. (3.4), with the perturbed null vector components

$$\delta k_{\text{DK}}^\alpha = \left[-\frac{b_{rr,0}^{\text{DK}}}{2} + \frac{b_{tt,0}^{\text{DK}}}{2f^2}, -b_{rr,0}^{\text{DK}}f, 0, \mathcal{O}(a) \right], \quad (3.28a)$$

$$\delta l_{\text{DK}}^\alpha = \left[\frac{b_{rr,0}^{\text{DK}}}{2} + \frac{b_{tt,0}^{\text{DK}}}{2f^2}, 0, 0, \mathcal{O}(a) \right], \quad (3.28b)$$

where here we have set $\delta l_{\text{DK}}^r = 0$. As before, the Killing tensor reduces exactly to that of the Schwarzschild spacetime.

3.4 Relating parameterizations

3.4.1 To each other

In the previous sections, we proposed two different parameterizations of deformed spacetimes suitable for modeling alternative theory predictions. These parameterizations are related via a gauge transformation. Under a general diffeomorphism, the metric transforms according to $b_{\mu\nu}^{\text{DK}} \rightarrow b_{\mu\nu}^{\text{DK}'} \equiv b_{\mu\nu}^{\text{DK}} + \nabla_{(\mu}\xi_{\nu)}$, where we parameterize the generating vectors as

$$\xi = [\xi_0(r), \xi_1(r, \theta), \xi_2(r, \theta), \xi_3(r)]. \quad (3.29)$$

The question is whether a generating vector exists that could take a generic $b_{\mu\nu}^{\text{DK}}$ metric perturbation to one of $b_{\mu\nu}^{\text{BK}}$ form. The DK parameterization has an (r, θ) component that is absent in the BK one, while the BK one has (t, r) and (r, ϕ) components that are absent in the DK parameterization.

Let us assume that we have a certain metric in DK form. The first task is to remove the (r, θ) component, i.e. to find a diffeomorphism such that $b_{r\theta}^{\text{DK}'} = 0$. This can be achieved by requiring that

$$b_{r\theta}^{\text{DK}} + \frac{1}{2}\Sigma \left[\frac{1}{\Delta} \frac{\partial \xi_1}{\partial \theta} + \frac{\partial \xi_2}{\partial r} \right] = 0, \quad (3.30)$$

whose solution is

$$\xi_1 = F_1(r) - \Delta \int \left(\frac{\partial \xi_2}{\partial r} + \frac{2b_{r\theta}^{\text{DK}}}{\Sigma} \right) d\theta, \quad (3.31)$$

where $F_1(r)$ is a free integration function and $\xi_2(r, \theta)$ is free.

The generating vector of Eq. (3.29) with the condition in Eq. (3.31) not only guarantees that $b_{r\theta}^{\text{DK}'} = 0$, but also ensures that the only non-vanishing components of the gauge-transformed metrics are the g_{tt} , g_{tr} , $g_{t\phi}$, g_{rr} , $g_{r\phi}$, $g_{\theta\theta}$ and $g_{\phi\phi}$ components, exactly the same nonzero components as in the BK metric. The new components are

$$b_{tt}^{\text{DK}'} = b_{tt}^{\text{DK}} - \frac{M\bar{\Sigma}}{\Sigma^2} \xi_1 + \frac{2a^2 Mr \sin \theta \cos \theta}{\Sigma^2} \xi_2, \quad (3.32a)$$

$$b_{tr}^{\text{DK}'} = -\frac{1}{2} \left(1 - \frac{2Mr}{\Sigma} \right) \frac{d\xi_0}{dr} - \frac{aMr \sin^2 \theta}{\Sigma} \frac{d\xi_3}{dr}, \quad (3.32b)$$

$$b_{t\phi}^{\text{DK}'} = b_{t\phi}^{\text{DK}} + \frac{aM\bar{\Sigma} \sin^2 \theta}{\Sigma^2} \xi_1 - \frac{2aMr(r^2 + a^2) \cos \theta \sin \theta}{\Sigma^2} \xi_2, \quad (3.32c)$$

$$b_{rr}^{\text{DK}'} = b_{rr}^{\text{DK}} + \frac{a^2 r}{\Delta^2} \xi_1 - \frac{a^2 \sin \theta \cos \theta}{\Delta} \xi_2 + \frac{\Sigma}{\Delta} \frac{\partial \xi_1}{\partial r}, \quad (3.32d)$$

$$b_{r\phi}^{\text{DK}'} = -\frac{\sin^2 \theta}{2\Sigma} \left\{ 2aMr \frac{d\xi_0}{dr} + \left[(r^2 + a^2)^2 + a^2 \Delta \sin^2 \theta \right] \frac{d\xi_3}{dr} \right\}, \quad (3.32e)$$

$$b_{\theta\theta}^{\text{DK}'} = b_{\theta\theta}^{\text{DK}} + r \xi_1 - a^2 \sin \theta \cos \theta \xi_2 + \Sigma \frac{\partial \xi_2}{\partial \theta}, \quad (3.32f)$$

$$b_{\phi\phi}^{\text{DK}'} = b_{\phi\phi}^{\text{DK}} + \frac{\sin^2 \theta}{\Sigma^2} \left[r^5 - a^2 Mr^2 + a^2 \cos^2 \theta (2r^3 + 2rM^2 + \Delta M) \right. \\ \left. + a^4 \cos^4 \theta (r - M) \right] \xi_1 + \sin \theta \cos \theta \left[\Delta + \frac{2Mr(r^2 + a^2)^2}{\Sigma^2} \right] \xi_2, \quad (3.32g)$$

where $\bar{\Sigma} \equiv r^2 - a^2 \cos^2 \theta$ and ξ_1 is given by Eq. (3.31).

The above result can be simplified somewhat by setting $\xi_2 = 0$ and $F_1(r) = 0$ in Eq. (3.31). Notice that g_{tr} and $g_{r\phi}$ are not modified by these vector components. The

modified components then become

$$b_{tt}^{\text{DK}'} = b_{tt}^{\text{DK}} - \frac{M\bar{\Sigma}}{\Sigma^2}\xi_1, \quad (3.33a)$$

$$b_{t\phi}^{\text{DK}'} = b_{t\phi}^{\text{DK}} + \frac{aM\bar{\Sigma}\sin^2\theta}{\Sigma^2}\xi_1, \quad (3.33b)$$

$$b_{rr}^{\text{DK}'} = b_{rr}^{\text{DK}} + \frac{a^2r}{\Delta^2}\xi_1 + \frac{\Sigma}{\Delta}\frac{\partial\xi_1}{\partial r}, \quad (3.33c)$$

$$b_{\theta\theta}^{\text{DK}'} = b_{\theta\theta}^{\text{DK}} + r\xi_1, \quad (3.33d)$$

$$b_{\phi\phi}^{\text{DK}'} = b_{\phi\phi}^{\text{DK}} + \frac{\sin^2\theta}{\Sigma^2}\left\{r^5 - a^2Mr^2 + a^2\cos^2\theta\left[2r(r^2 + M^2) + \Delta M\right] + a^4\cos^4\theta(r - M)\right\}\xi_1. \quad (3.33e)$$

We have therefore found a generic diffeomorphism that maps a DK metric to one that has the same nonzero components as a BK metric. Notice that ξ_0 and ξ_3 only enter to generate the g_{tr} and $g_{r\phi}$ components. If we know the form of the components that we are trying to map to, then we could solve for these two vector components. For example, let us assume that b_{tr}^{BK} and $b_{r\phi}^{\text{BK}}$ are given and we wish to find $\xi_{0,3}$ such that $b_{tr}^{\text{DK}'} = b_{tr}^{\text{BK}}$ and $b_{r\phi}^{\text{DK}'} = b_{r\phi}^{\text{BK}}$. This implies

$$0 = b_{tr}^{\text{BK}} + \frac{1}{2}\left(1 - \frac{2Mr}{\Sigma}\right)\frac{d\xi_0}{dr} - \frac{aMr\sin^2\theta}{\Sigma}\frac{d\xi_3}{dr}, \quad (3.34a)$$

$$0 = b_{r\phi}^{\text{BK}} + \frac{\sin^2\theta}{2\Sigma}\left\{2aMr\frac{d\xi_0}{dr} + \left[(r^2 + a^2)^2 + a^2\Delta\sin^2\theta\right]\frac{d\xi_3}{dr}\right\}. \quad (3.34b)$$

Let us, for one moment, allow $\xi_{0,3}$ to be arbitrary functions of (r, θ) . The solution to the above system is then

$$\begin{aligned} \xi_0 &= F_2(\theta) + \frac{2}{\Delta}\int\frac{dr}{\Sigma}\left[b_{tr}^{\text{BK}}\cos^2\theta(2a^2Mr - a^2r^2 - a^4) \right. \\ &\quad \left. - b_{tr}^{\text{BK}}(2a^2Mr + a^2r^2 + a^4) - 2aMr b_{r\phi}^{\text{BK}}\right], \end{aligned} \quad (3.35a)$$

$$\xi_3 = F_3(\theta) + \frac{2}{\Delta}\int dr\left[b_{r\phi}^{\text{BK}}\left(1 - \frac{2Mr}{\Sigma}\right) - \frac{2aMr\sin^2\theta}{\Sigma}b_{tr}^{\text{BK}}\right]. \quad (3.35b)$$

But of course, to avoid introducing other spurious components to the DK' metric, such as $b_{t\theta}^{\text{DK}}$, we must require that $\xi_{0,3}$ be functions of r only. This implies that the integrands must be themselves also functions of r only. Setting the integrands equal

to $F_2(r)$ and $F_3(r)$, we find the conditions

$$b_{tr}^{\text{BK}} = \left(1 - \frac{2Mr}{\Sigma}\right) F_2(r) + \frac{2aMr \sin^2 \theta}{\Sigma} F_3(r), \quad (3.36a)$$

$$b_{r\phi}^{\text{BK}} = \frac{2aMr \sin^2 \theta}{\Sigma} F_2(r) - \frac{[\Sigma^2 + a^4 (\Sigma + 2Mr)] \sin^2 \theta}{\Sigma} F_3(r). \quad (3.36b)$$

Provided that b_{tr}^{BK} and $b_{r\phi}^{\text{BK}}$ components can be written in the above form, the generating function becomes

$$\xi_0 = -2 \int F_2(r) dr, \quad (3.37a)$$

$$\xi_3 = -2 \int F_3(r) dr. \quad (3.37b)$$

3.4.2 To alternative theories

Dynamical Chern-Simons modified gravity

The BK and DK parameterizations can also be mapped to known alternative theory black hole metrics. In dynamical CS gravity [1], one can employ the slow-rotation approximation, where one assumes the black hole's spin angular momentum is small, $|S|/M^2 \ll 1$, and the small-coupling approximation, where one assumes the theory's corrections are small deformations away from GR to find an analytical black hole solution. Yunes and Pretorius [101] found that this solution is simply $g_{\mu\nu} = \hat{g}_{\mu\nu} + b_{\mu\nu}^{\text{CS}}$, where $\hat{g}_{\mu\nu}$ is the Kerr metric (expanded in the slow-rotation limit), while the only non-vanishing component of the deformation tensor in Boyer-Lindquist coordinates is

$$b_{t\phi}^{\text{CS}} = \frac{5}{8} \zeta_{\text{CS}} \frac{a}{M} \frac{M^5}{r^4} \sin^2 \theta \left(1 + \frac{12M}{7r} + \frac{27M^2}{10r^2}\right), \quad (3.38)$$

where a is the Kerr spin parameter, M is the black hole mass and ζ_{CS} is a dimensionless constant that depends on the CS couplings and is assumed to be small.

Such a non-GR black hole solution can be mapped to the generalized bumpy parameterization of Eqs. (3.1) and (3.10) via $\delta_2 = \delta g_\phi^{\text{CS}} = \delta_5$, and all other δ_i and Θ_i

vanish. The quantity $\delta g_\phi^{\text{CS}}$ is given by [87]

$$\delta g_\phi^{\text{CS}} = -\zeta_{\text{CS}} a M^4 \frac{70r^2 + 120Mr + 189M^2}{112r^8(1 - 2M/r)}. \quad (3.39)$$

With these choices, the null vectors become

$$k^\alpha = \left(\frac{r^2 + a^2}{\Delta}, 1, 0, \frac{a}{\Delta} + \delta g_\phi^{\text{CS}} \right), \quad (3.40a)$$

$$l^\alpha = \left(\frac{r^2 + a^2}{\Delta}, -1, 0, \frac{a}{\Delta} + \delta g_\phi^{\text{CS}} \right), \quad (3.40b)$$

which agrees with Eq. (35) of [87]. Moreover, with these choices all the metric components vanish except for $g_{t\phi}$, which must be equal to Eq. (3.38) for the differential constraint in Eq. (3.10) to be satisfied.

Similarly, we can map it to the DK parameterization of Eqs. (3.21) and (3.22) via $\gamma_3 = \delta g_\phi^{\text{CS}}$, and all other arbitrary functions vanish. We have checked that Eq. (3.38) satisfies the differential constraint found in Sec. 3.3.

Dynamical, Quadratic Gravity

We can similarly map the BK and DK parameterizations to the black hole solution found in dynamical quadratic gravity [103]. Treating GR corrections as small deformations (i.e. working in the small-coupling limit), Yunes and Stein [103] found that the unique non-spinning black hole solution is $g_{\mu\nu} = \hat{g}_{\mu\nu} + b_{\mu\nu}^{\text{QG}}$, where $\hat{g}_{\mu\nu}$ is the Schwarzschild metric, while $b_{\mu\nu}^{\text{QG}}$ in Schwarzschild coordinates is given by [103]

$$b_{tt}^{\text{QG}} = -\frac{\zeta_{\text{QG}} M^3}{3 r^3} \left(1 + \frac{26M}{r} + \frac{66 M^2}{5 r^2} + \frac{96 M^3}{5 r^3} - \frac{80M^4}{r^4} \right), \quad (3.41a)$$

$$b_{rr}^{\text{QG}} = -\frac{\zeta_{\text{QG}} M^2}{f^2 r^2} \left(1 + \frac{M}{r} + \frac{52 M^2}{3 r^2} + \frac{2M^3}{r^3} + \frac{16 M^4}{5 r^4} - \frac{368 M^5}{3 r^5} \right), \quad (3.41b)$$

where M is the mass of the Schwarzschild black hole and ζ_{QG} is a dimensionless constant that depends on the couplings of the theory and is assumed to be small

For a spherically symmetric background, one can easily show that the Schwarzschild Killing tensor (i.e., one whose only non-vanishing components are $\xi_{\theta\theta} = r^4$ and $\xi_{\phi\phi} =$

$r^4 \sin^2 \theta$) satisfies the Killing equation regardless of the functional form of the g_{tt} and g_{rr} components of the metric. This means that the perturbed vectors δk^α and δl^α must adjust so that the above is true. We find that the following vector components do just that:

$$\delta k^t = \frac{\zeta_{\text{QG}} M^2 r^4}{2f r^6} \left(1 + \frac{8M}{3r} + \frac{14M^2}{r^2} + \frac{128M^3}{5r^3} + \frac{48M^4}{r^4} \right), \quad (3.42a)$$

$$\delta k^r = \frac{\zeta_{\text{QG}} M^2 r^4}{f r^6} \left(1 + \frac{M}{r} + \frac{52M^2}{3r^2} + \frac{2M^3}{r^3} + \frac{16M^4}{5r^4} - \frac{368M^5}{3r^5} \right), \quad (3.42b)$$

$$\delta l^t = -\frac{\zeta_{\text{QG}} M^2 r^4}{2f^2 r^6} \left(1 + \frac{4M}{3r} + \frac{26M^2}{r^2} + \frac{32M^3}{5r^3} + \frac{48M^4}{5r^4} - \frac{448M^5}{3r^5} \right), \quad (3.42c)$$

and all other components vanish. It must be the case that perturbed null vectors exist to reduce the Killing tensor to its Schwarzschild counterpart; as we have shown in Sec. 3.2.2 and 3.3.2 that in the nonrotating limit both the BK and DK parameterizations allow for generic g_{tt} and g_{rr} deformations.

Arbitrary perturbations: perturbation to γ_3 , perturbations to γ_1 and γ_4

We can understand the functions that parametrize the metric perturbation by considering perturbations where we allow only a few of the parametrizing functions to be nonzero. Consider a perturbation in the deformed Kerr parametrization of Eqs. (3.21) and (3.22) described by $\gamma_1 = \gamma_4 = \Theta_3 = 0$ and $b_{r\theta} = b_{\theta\theta} = 0$. In the small a limit, the only nonzero component of the metric is the (t, ϕ) component:

$$b_{t\phi} = -f [r^2 \sin^2 \theta \gamma_3(r) + C], \quad (3.43)$$

where $f \equiv 1 - 2M/r$ and C is a constant. Now consider a perturbation in the DK parametrization whose only nonzero parameters are γ_1 and γ_4 . In the small a limit,

this produces perturbations to the metric given by

$$b_{tt} = f \gamma_1(r) + 2f^2 \gamma_4(r), \quad (3.44a)$$

$$b_{rr} = -f^{-1} \gamma_1(r), \quad (3.44b)$$

$$b_{\phi\phi} = f^2 \sin^2 \theta \left[\frac{r^4}{2M} \frac{d\gamma_1}{dr} + 2r^2 \gamma_4(r) + \frac{r^3(r-4M)}{2M} \frac{d\gamma_4}{dr} \right]. \quad (3.44c)$$

We see that in the DK parameterization γ_3 controls modifications to frame-dragging (and thus the ergosphere), while γ_1 and γ_4 control modifications to the location of the event-horizon and the innermost-stable circular orbit.

3.5 Motion in alternative theories of gravity

Now we turn our attention to motion in the BK and DK spacetimes. The derivation of the equations of motion in Sec. 1.3 is fairly general. In particular, this derivation is independent of the metric used; in no place did we use that the spacetime was Kerr. We required the divergence of the test particle stress-energy tensor vanishes; this condition is always true in GR, because of a combination of local stress-energy conservation and the equivalence principle.

One might wonder whether the divergence-free condition of the stress-energy tensor holds in more general theories. In any metric GR deformation, the field equations will take the form

$$G_{\alpha\beta} + \mathcal{H}_{\alpha\beta} = T_{\alpha\beta} + T_{\alpha\beta}^{\mathcal{H}}, \quad (3.45)$$

where $G_{\alpha\beta}$ is the Einstein tensor, $\mathcal{H}_{\alpha\beta}$ is a tensorial deformation of the Einstein equations, and $T_{\alpha\beta}^{\mathcal{H}}$ is a possible stress-energy modification, associated with additional fields. The divergence of this equation then leads to

$$\nabla^\alpha \mathcal{H}_{\alpha\beta} = \nabla^\alpha T_{\alpha\beta} + \nabla^\alpha T_{\alpha\beta}^{\mathcal{H}}, \quad (3.46)$$

since the Bianchi identities force the divergence of the Einstein tensor to vanish. The Bianchi identities hold in alternative theories, as this is a geometric constraint and

not one that derives from the action. We see then that the divergence of the matter stress-energy tensor vanishes independently provided

$$\nabla^\alpha \mathcal{H}_{\alpha\beta} = \nabla^\alpha T_{\alpha\beta}^{\mathcal{H}}. \quad (3.47)$$

Whether this condition is satisfied depends somewhat on the theory of interest. Theories that include additional degrees of freedom that couple both to the geometry and have their own dynamics usually satisfy Eq. (3.47). This is because additional equations of motion arise upon variation of the action with respect to these additional degrees of freedom, and these additional equations reduce to Eq. (3.47). Such is the case, for example, in dynamical CS modified gravity [87]. If no additional degrees of freedom are introduced, whether Eq. (3.47) is satisfied depends on whether the divergence of the new tensor $\mathcal{H}_{\alpha\beta}$ vanishes, which need not in general be the case.

Recently, it was shown that the equations of motion are geodesic to leading order in the mass-ratio for any classical field theory that satisfies the following constraints [40]:

- It derives from a diffeomorphism-covariant Lagrangian, ensuring a Bianchi identity;
- It leads to second-order field equations.

The second condition seems somewhat too stringent, as we know of examples where third-order field equations still lead to geodesic motion, i.e. dynamical CS gravity [87]. Therefore, it seems reasonable to assume that this condition could be relaxed in the future. Based on this, we take the viewpoint that the equations of motion are geodesic even in the class of alternative theories we consider here.

The geodesic equations can be rewritten in first-order form provided that three constants of the motion exist. In Sec. 3.2.2, we showed that provided the generalized bumpy functions satisfy certain conditions, then an approximate, second-order Killing tensor and a conserved Carter constant exist. Furthermore, it is easy to see that the metric in Eqs. (3.1) and (3.2) remains stationary and axisymmetric, since the metric components b_{tt}^{BK} , b_{tr}^{BK} , $b_{t\phi}^{\text{BK}}$, b_{rr}^{BK} , $b_{r\phi}^{\text{BK}}$, $b_{\theta\theta}^{\text{BK}}$, and $b_{\phi\phi}^{\text{BK}}$ are functions of only r and θ .

The constants of the motion are

$$E = \hat{E} + \epsilon (b_{\mu\nu} t^\mu \hat{u}^\nu + \hat{g}_{\mu\nu} t^\mu \delta u^\nu), \quad (3.48)$$

$$L = \hat{L} + \epsilon (b_{\mu\nu} \phi^\mu \hat{u}^\nu + \hat{g}_{\mu\nu} \phi^\mu \delta u^\nu), \quad (3.49)$$

$$C = \hat{C} + \epsilon \left[\delta \xi_{\mu\nu} \hat{u}^\mu \hat{u}^\nu + 2 \hat{\xi}_{\mu\nu} \hat{u}^{(\mu} \delta u^{\nu)} \right], \quad (3.50)$$

while the normalization condition becomes

$$0 = b_{\mu\nu} \hat{u}^\mu \hat{u}^\nu + 2 \hat{g}_{\mu\nu} \hat{u}^\mu \delta u^\nu, \quad (3.51)$$

since by definition, $-1 = \hat{g}_{\mu\nu} \hat{u}^\mu \hat{u}^\nu$. In these equations, $\hat{u}^\mu = (\hat{t}, \hat{r}, \hat{\theta}, \hat{\phi})$ is the Kerr four-velocity, while δu^μ is a perturbation.

Equations (3.48) – (3.51) can be decoupled once we make a choice for (E, L, Q) . This choice affects whether the turning points in the orbit are kept the same as in GR or whether the constants of the motion are kept the same. Here we choose the latter by setting $E = \hat{E}$, $L = \hat{L}$ and $C = \hat{C}$, which then implies that δu^μ must be such that all terms in parenthesis in Eqs. (3.48) – (3.50) vanish. Using this condition and Eq. (3.51), we then find that

$$\Sigma^2 \left(\frac{dr}{d\tau} \right)^2 = R(r) + \delta R(r, \theta), \quad (3.52)$$

$$\Sigma^2 \left(\frac{d\theta}{d\tau} \right)^2 = \Theta(\theta) + \delta \Theta(r, \theta), \quad (3.53)$$

$$\Sigma \left(\frac{d\phi}{d\tau} \right) = \Phi(r, \theta) + \delta \Phi(r, \theta), \quad (3.54)$$

$$\Sigma \left(\frac{dt}{d\tau} \right) = T(r, \theta) + \delta T(r, \theta), \quad (3.55)$$

where $R(r)$, $\Theta(\theta)$, $\Phi(r, \theta)$, and $T(r, \theta)$ are defined in Eqs. (1.14) – (1.17). The per-

turbations to the potential functions $\delta T(r, \theta)$, $\delta R(r, \theta)$, $\delta \Theta(r, \theta)$, and $\delta \Phi(r, \theta)$ are

$$\delta T(r, \theta) = \left[\frac{(r^2 + a^2)^2}{\Delta} - a^2 \sin^2 \theta \right] b_{t\alpha} \hat{u}^\alpha + \frac{2aMr}{\Delta} b_{\phi\alpha} \hat{u}^\alpha, \quad (3.56)$$

$$\delta \Phi(r, \theta) = \frac{2aMr}{\Delta} b_{t\alpha} \hat{u}^\alpha - \frac{\Sigma - 2Mr}{\Delta \sin^2 \theta} b_{\phi\alpha} \hat{u}^\alpha, \quad (3.57)$$

$$\delta R(r, \theta) = \Delta [A(r, \theta) r^2 + B(r, \theta)], \quad (3.58)$$

$$\delta \Theta(r, \theta) = A(r, \theta) a^2 \cos^2 \theta - B(r, \theta), \quad (3.59)$$

where the functions $A(r, \theta)$ and $B(r, \theta)$ are proportional to the perturbation:

$$A(r, \theta) = 2 \left[b_{\alpha t} \hat{t} + b_{\alpha \phi} \hat{\phi} \right] \hat{u}^\alpha - b_{\alpha \beta} \hat{u}^\alpha \hat{u}^\beta, \quad (3.60a)$$

$$B(r, \theta) = 2 \left[\left(\hat{\xi}_{tt} \hat{t} + \hat{\xi}_{t\phi} \hat{\phi} \right) \delta \hat{t} + \left(\hat{\xi}_{t\phi} \hat{t} + \hat{\xi}_{\phi\phi} \hat{\phi} \right) \delta \hat{\phi} \right] + \delta \xi_{\alpha\beta} \hat{u}^\alpha \hat{u}^\beta. \quad (3.60b)$$

As before, we have dropped the superscript BK here. Interestingly, notice that the perturbation automatically couples the (r, θ) sector, so that the first-order equations are not necessarily separable. One can choose, however, the γ_i functions in such a way so that the equations remain separable, as will be shown elsewhere.

The perturbations to the potential functions result in changes to the orbital frequencies. In particular, for circular, equatorial orbits, the orbital frequency becomes

$$\begin{aligned} \Omega^\phi &= \hat{\Omega}^\phi - \frac{(rM)^{1/2}(r - 3M) + 2aM}{r^{5/4} (r^{3/2} + aM^{1/2})^2} \delta T(r) \\ &\quad + \frac{[r^{1/2}(r - 3M) + 2aM^{1/2}]^{1/2}}{r^{5/4} (r^{3/2} + aM^{1/2})} \delta \Phi(r), \end{aligned} \quad (3.61)$$

where $\hat{\Omega}^\phi$ is given in Eq. (1.52), δT and $\delta \Phi$ are given by Eq. (3.56) and (3.57), and we have used that $E = \hat{E}$ and $L = \hat{L}$. In the far field limit ($M/r \ll 1$), this becomes

$$\Omega \sim \hat{\Omega} + \frac{1}{r^2} \delta \Phi, \quad (3.62)$$

where for simplicity, we have assumed that $\delta \Phi$ and δT are both of order unity. Given any particular metric perturbation, one can easily recalculate such a correction to

Kepler’s law from Eq. (3.61). Clearly, a modification of this type in the Kepler relation modifies the dissipative dynamics when converting quantities that depend on the orbital frequency to radius and vice-versa.

3.6 Summary and future work

The detection of GWs from EMRIs should allow for the detailed mapping of the space-time metric on which the small compact objects move. Such a mapping allows for null tests of GR, as one would in principle be able to constrain deviations of the background spacetime from the Kerr metric. To carry out such tests, however, one requires a parameterization of the metric tensor that can handle model-independent, non-GR deviations. We have constructed two such parameterizations: one as a generalization of the bumpy black hole formalism (the BK scheme) and one as a generalized deformation of the Kerr metric (the DK scheme). The former promotes the non-vanishing components of the metric perturbation that contain bumps to arbitrary functions of radius and polar angle. The latter takes the most general stationary, axisymmetric line element without assuming Ricci-flatness and constructs a generic metric deformation from it. In both cases, we constrained the arbitrary functions they introduce by requiring that the spacetime has an approximate second-order Killing tensor.

These schemes differ from each other in the metric components that are assumed not to vanish. We have found a gauge transformation, however, that relates them. That is, we have shown that a generating vector exists such that the BK metric can be mapped to the DK one. We have also mapped both parameterizations to known analytical non-GR solutions, thus automatically finding their respective Killing tensors and Carter constants.

The perturbative nature of our approach puts some limitation on the generality of the deformation. Throughout this chapter, we restricted the metric deformation to be a small deviation away from the GR solution. But due to the structure of the perturbation, there can be regions in spacetime where this deformation dominates over the GR background. For example, the full metric tensor might lose Lorentzian

signature if the metric perturbation dominates over the Kerr background and it possesses a certain definite sign, i.e., the metric will no longer have $\det(g) < 0$. Clearly, such regions are unphysical, and the coupling constants that control the magnitude of the perturbation should be adjusted appropriately to ensure that if they exist, they are hidden inside the horizon.

We should emphasize that we were guided by two principles in the construction of the parameterized schemes proposed here. First, we wanted to ensure that the parameterizations would easily map to known analytic solutions. Second, we wished to retain a smooth Kerr limit, such that when the deformation parameters are taken to zero, the deformed metric goes smoothly to Kerr. This in turn guaranteed that certain properties of the Kerr background were retained, such as the existence of a horizon. We additionally required that the metric tensors allowed a second-order perturbative Killing tensor, so that there exists a perturbative Carter constant. This latter requirement is not strictly necessary to perform null tests, as one could build GWs from the evolution of the full second-order equations of motion without rewriting them in first-order form.

An interesting avenue of future research would be to investigate the Petrov type [69] of the BK and DK metrics. Brink has shown that GR spacetimes that admit a Carter constant must also be of Type D [15]. In alternative theories of gravity, however, a formal mathematical proof of the previous statement is lacking. We have here found Ricci-curved metrics that admit a Carter constant. One could now attempt to prove that the perturbative Carter existence conditions found in this chapter also automatically imply that the spacetime is approximately Petrov Type D. This is a purely mathematical result that is beyond the scope of this chapter.

An interesting physical question that could now be answered with either the DK or BK frameworks is whether LISA could place interesting constraints on non-GR Kerr deformations. To answer this question, one would have to evolve geodesics in either the BK or DK framework and construct the associated GWs. One could then use a Fisher analysis to determine how well the deviation from Kerr could be measured or constrained by LISA. We will investigate this problem in a forthcoming publication.

Chapter 4

Spin-curvature coupling

The work in this chapter will be submitted to *Physical Review D* for publication at a future date and was done in collaboration with Scott A. Hughes.

4.1 Introduction

Extreme mass-ratio inspirals (EMRIs), in which a small compact object of $\sim 1 - 100 M_\odot$ falls into a massive black hole (MBH) of $\sim 10^6 M_\odot$, are a particularly interesting source of low-frequency GWs. As the small body spirals slowly into the MBH, it probes the structure of the surrounding spacetime and the information is encoded into the emitted GWs. Another motivation for studying the evolution of EMRIs is the fact that the large mass ratio of the two bodies allows us to do many of the calculations analytically or quasi-analytically instead of relying entirely on numerical simulations. These analytic (or semi-analytic) results can help us gain insight into the orbital dynamics of more general systems. For example, we can use results from black hole perturbation theory to extend the ability of the effective one-body approach to accurately model the dynamics of coalescing binary systems [100, 9].

To zeroth order in the mass ratio, the small body moves on a geodesic of the background spacetime, which is curved because of the presence of the large body, i.e.,

$$\frac{Dp^\alpha}{d\tau} = 0, \tag{4.1}$$

where the derivative operator $D/d\tau$ is a covariant derivative along the small body's trajectory. Higher order effects perturb the orbit of the small body away from a geodesic:

$$\frac{Dp^\alpha}{d\tau} = F^\alpha, \quad (4.2)$$

where the force F^α can arise from a number of physical effects. One interesting example is the gravitational self-force F_{sf}^α , which comes from the fact that the small body also curves spacetime. This can be broken into two contributions: $F_{\text{sf}}^\alpha = F_{\text{diss}}^\alpha + F_{\text{cons}}^\alpha$, where the dissipative portion F_{diss}^α is time-reversal asymmetric and describes the loss of energy and angular momentum due to the emission of GWs, and the conservative portion F_{cons}^α is time-reversal symmetric and describes a shift to the gravitational field due to the curvature of the small body. Many groups have put considerable effort into computing the gravitational self-force; see Ref. [71] for a very detailed overview and discussion of the self-force problem in general relativity, and Refs. [7, 95] for examples of recent progress in the field. They have found that for a small body of mass μ , the gravitational self-force scales as μ^2 .

Other forces arise when we consider that the small body is not a point mass, but instead has internal structure. In particular, if the small body has spin (as all known astrophysical bodies do), the spin of the small body couples to the curvature of the background spacetime, modifying the trajectory of the smaller body according to the Papapetrou equations [68, 29]:

$$\frac{Dp^\alpha}{d\tau} = -\frac{1}{2}S^{\lambda\mu}u^\nu R^\alpha{}_{\nu\lambda\mu}, \quad (4.3)$$

$$\frac{DS^{\mu\nu}}{d\tau} = p^\mu u^\nu - p^\nu u^\mu. \quad (4.4)$$

The vector $u^\mu \equiv dx^\mu/d\tau$ is the particle's four-velocity, and p^μ is the particle's four-momentum. For a spinning body, p^μ and u^μ are not exactly parallel to one another, although they are parallel at leading order in the small body's spin:

$$p^\alpha = \mu u^\alpha + \mathcal{O}(s^2). \quad (4.5)$$

We discuss these points further in Sec. 4.2, where we derive these equations. The tensors $S^{\alpha\beta}$ describes the spin of the small body:

$$S^{\alpha\beta} = 2 \int_{\Sigma} (x^{[\alpha} - z^{[\alpha}) T^{\beta]\gamma} d\Sigma_{\gamma}, \quad (4.6)$$

where Σ is an arbitrary spacelike hypersurface. The tensor $R^{\alpha}{}_{\nu\lambda\mu}$ is the Riemann curvature tensor of the spacetime, and it describes how nearby trajectories diverge from one another due to gravitational tidal effects. If the small body is nonspinning, Eq. (4.3) reduces to the geodesic equation [Eq. (4.1)]; otherwise the right-hand side of Eq. (4.3) acts like a force acting on the small body. For a small body of mass μ and dimensionless spin s , the spin force scales as $\mu^2 s$, which is the same scaling with μ as the gravitational self-force. This suggests that if we include the gravitational self-force we also need to take into account the spin force.

So far, the effect of the spin of the small body on the orbital trajectory has not been studied in great detail. Previous work taking into account the spin of the small body has relied on simplified waveforms (for example, “kludge” waveforms that use post-Newtonian approximation extended beyond its region of validity) [6, 8] or been limited to an analysis of circular, equatorial orbits with the spin of the small body parallel or nearly parallel to the spin of the large black hole [8, 20, 41, 47]. These studies have shown that including spin effects can change the GW phase by several to several tens of radians in one year of observations. This is enough of a phase difference that GW measurements that do not take into account spin effects are likely to be biased by some (currently unknown) systematic offset.

As a first step to building waveforms that incorporate the spin of the small body, in this chapter we compute the spin force along a geodesic for generic orbits and spin orientations. Our approach is to treat the effect of the spin of the small body perturbatively; i.e., we identify the spin tensor as order s , and we expand the four-momentum as $p^{\mu} = p_{\text{geod}}^{\mu} + \Delta p^{\mu}$, where p_{geod}^{μ} is a geodesic trajectory and Δp^{μ} is of

order s . Then the equation of motion of Δp^μ is given by

$$\begin{aligned} \frac{D(\Delta p^\alpha)}{d\tau} &= -\frac{1}{2\mu} S^{\lambda\mu} p_{\text{geod}}^\nu R^\alpha{}_{\nu\lambda\mu} + \mathcal{O}(s^2) \\ &\equiv F_{\text{spin}}^\alpha, \end{aligned} \quad (4.7)$$

$$\frac{DS^{\alpha\beta}}{d\tau} = \mathcal{O}(s^2), \quad (4.8)$$

where we have defined the spin force as the right-hand side of Eq. (4.7). Notice that the spin force is purely conservative and does not dissipate energy or angular momentum. As mentioned in Eq. (4.5), p^α and u^α are parallel to linear order in s , so in Eq. (4.7) we can treat them as parallel. Since we are treating the effect of the spin perturbatively, Eqs. (4.7) and (4.8) are evaluated along the geodesic trajectory. We also need to choose a spin supplementary condition; we choose to let

$$S^{\alpha\beta} u_\alpha = 0, \quad (4.9)$$

which fixes the small body's center of mass. We can relate the spin tensor to the spin vector according to

$$S^{\alpha\beta} = \epsilon^{\alpha\beta\mu\nu} u_\mu S_\nu. \quad (4.10)$$

Defining the spin vector in this way means that the spin tensor automatically satisfies the spin supplementary condition in Eq. (4.9). Then the evolution equation for S^α is simply

$$\frac{DS^\alpha}{d\tau} = \mathcal{O}(s^2); \quad (4.11)$$

i.e., the spin vector is parallel-transported along the orbit to linear order in the spin.

This chapter is organized as follows. In Sec. 4.2 we derive the Papapetrou equations following the approach of Papapetrou [68]. In Sec. 4.3 we compute the evolution of the spin vector and the change in the orbital trajectory for orbits in the Schwarzschild spacetime, and we compare the magnitudes of the gravitational self-force and the conservative portion of the spin force. We find that the effect of the spin, although not as large as the gravitational self-force, is not negligible compared

to the self-force. In Sec. 4.4 we discuss spin evolution and the change in the orbital trajectory for generic orbits in the Kerr spacetime. Section 4.5 summarizes our analysis and discusses future work.

4.2 Derivation of the Papapetrou equations

4.2.1 Overview

Here we derive the equations of motion for a spinning body. Our approach is based upon the approach of Papapetrou [68]. We begin with the dynamical equation

$$\nabla_\nu T^{\mu\nu} = 0, \quad (4.12)$$

where $T^{\mu\nu}$ is the stress-energy tensor of the particle. Expanding the covariant derivative gives

$$\partial_\nu T^{\mu\nu} + \Gamma^\mu_{\nu\lambda} T^{\nu\lambda} + \Gamma^\nu_{\nu\lambda} T^{\mu\lambda} = 0. \quad (4.13)$$

The Christoffel symbol $\Gamma^\nu_{\nu\lambda}$ can be written as

$$\Gamma^\nu_{\nu\lambda} = \frac{1}{\sqrt{|g|}} \partial_\lambda \sqrt{|g|}, \quad (4.14)$$

where $g \equiv \det(g_{\mu\nu})$. We can use this to rewrite Eq. (4.13) as

$$\partial_\nu \mathcal{T}^{\mu\nu} + \Gamma^\mu_{\nu\lambda} \mathcal{T}^{\nu\lambda} = 0, \quad (4.15)$$

where $\mathcal{T}^{\mu\nu}$ is defined by

$$\mathcal{T}^{\mu\nu} \equiv \sqrt{|g|} T^{\mu\nu}. \quad (4.16)$$

The next step is to define a single-pole and pole-dipole body in terms of $\mathcal{T}^{\mu\nu}$. Let X^α denote the position of the body and x^α be some coordinate in spacetime. We define δx^α as

$$\delta x^\alpha \equiv x^\alpha - X^\alpha, \quad (4.17)$$

A single-pole body is one for which

$$\int \mathcal{T}^{\mu\nu} dV \neq 0 \quad (4.18)$$

for some values of μ and ν , and

$$\int \delta x^{\rho_1} \dots \delta x^{\rho_n} \mathcal{T}^{\mu\nu} dV = 0 \quad (4.19)$$

for $n \geq 1$. In these integrals, dV indicates an integral over the three-dimensional space with constant t . A pole-dipole body is one for which

$$\int \mathcal{T}^{\mu\nu} dV \neq 0, \quad (4.20a)$$

$$\int \delta x^\rho \mathcal{T}^{\mu\nu} dV \neq 0, \quad (4.20b)$$

for some values of μ , ν , and ρ , and

$$\int \delta x^{\rho_1} \dots \delta x^{\rho_n} \mathcal{T}^{\mu\nu} dV = 0 \quad (4.21)$$

for $n \geq 2$.

Now we are ready to derive the equations of motion. The derivation proceeds as follows. We take the dynamical equation $\nabla_\nu T^{\mu\nu} = 0$ and its derivatives, and we integrate these relationships over a spatial volume. We expand the Christoffel symbols in the covariant derivative, i.e.,

$$\Gamma = \Gamma_0 + \delta x \partial\Gamma + \frac{1}{2}\delta x^2 \partial^2\Gamma + \dots, \quad (4.22)$$

where Γ_0 , $\partial\Gamma$, and $\partial^2\Gamma$ are all evaluated at the position of the orbiting body. When we insert this into the dynamical equation and its derivatives, we end up with terms that look like $\int \mathcal{T} dV$, $\int \mathcal{T} \delta x dV$, $\int \mathcal{T} \delta x^2 dV$, and so on. If the body is a pure monopole, then we can set all terms involving integrals of \mathcal{T} and factors of δx to zero, and we recover the geodesic equation. If the body has a nonzero dipole, then

we must keep terms that look like $\int \mathcal{T} \delta x dV$, and the equations of motion include additional terms that couple the body's spin to derivatives of the Christoffel symbols.

4.2.2 Motion of a single-pole body

We start with the case of a single-pole body, which we show moves along a geodesic. Once we have this simpler result, it will be easier to understand the more complicated motion of a pole-dipole body. We use the dynamical equation given in Eq. (4.15), and the expression

$$\partial_\gamma (x^\alpha \mathcal{T}^{\beta\gamma}) = \mathcal{T}^{\alpha\beta} - x^\alpha \Gamma^\beta_{\mu\nu} \mathcal{T}^{\mu\nu}, \quad (4.23)$$

which follows directly from Eq. (4.15). Integrating Eqs. (4.15) and (4.23) over a three-dimensional volume of constant t gives

$$\frac{d}{dt} \int \mathcal{T}^{\mu 0} dV = - \int \Gamma^\mu_{\nu\lambda} \mathcal{T}^{\nu\lambda} dV, \quad (4.24)$$

$$\frac{d}{dt} \int x^\alpha \mathcal{T}^{\beta 0} dV = \int \mathcal{T}^{\alpha\beta} dV - \int x^\alpha \Gamma^\beta_{\nu\lambda} \mathcal{T}^{\nu\lambda} dV. \quad (4.25)$$

Since the size of the body is small, we can expand the Christoffel symbols as

$$\Gamma^\alpha_{\mu\nu} = \Gamma^\alpha_{\mu\nu}|_X + \partial_\sigma \Gamma^\alpha_{\mu\nu}|_X \delta x^\sigma + \dots, \quad (4.26)$$

where the subscript X indicates that we evaluate the quantity at the location of the body X^α . Substituting this expansion into Eq. (4.24), and using the fact that this is a single-pole body to eliminate integrals containing $\delta x^\sigma \mathcal{T}^{\mu\nu}$, we get

$$\frac{d}{dt} \int \mathcal{T}^{\mu 0} dV = -\Gamma^\mu_{\nu\lambda} \int \mathcal{T}^{\nu\lambda} dV. \quad (4.27)$$

(For the sake of brevity, we have dropped the subscript X .) Equation (4.25) becomes

$$\frac{d}{dt} \left(X^\alpha \int \mathcal{T}^{\beta 0} dV \right) = \int \mathcal{T}^{\alpha\beta} dV - X^\alpha \Gamma^\beta_{\nu\lambda} \int \mathcal{T}^{\nu\lambda} dV. \quad (4.28)$$

We can simplify this further using Eq. (4.27):

$$\frac{dX^\alpha}{dt} \int \mathcal{T}^{\beta 0} dV = \int \mathcal{T}^{\alpha\beta} dV. \quad (4.29)$$

We introduce the quantity $M^{\alpha\beta}$ according to

$$M^{\alpha\beta} = u^0 \int \mathcal{T}^{\alpha\beta} dV, \quad (4.30)$$

where $u^0 \equiv dt/d\tau$ and τ is the proper time. Substituting Eq. (4.30) into Eqs. (4.27) and (4.29) gives

$$\frac{d}{d\tau} \left(\frac{M^{\alpha 0}}{u^0} \right) = -\Gamma^\alpha_{\mu\nu} M^{\mu\nu}, \quad (4.31)$$

$$M^{\alpha\beta} = \frac{u^\alpha}{u^0} M^{\beta 0}, \quad (4.32)$$

where $u^\alpha \equiv dX^\alpha/d\tau$. If we plug $\beta = 0$ into Eq. (4.32), we get

$$M^{\alpha 0} = \frac{u^\alpha}{u^0} M^{00}. \quad (4.33)$$

Substituting Eq. (4.33) into Eq. (4.32) allows us to write $M^{\alpha\beta}$ as

$$M^{\alpha\beta} = m u^\alpha u^\beta, \quad (4.34)$$

where the parameter m is defined as

$$m \equiv \frac{M^{00}}{(u^0)^2}. \quad (4.35)$$

Plugging Eq. (4.34) into Eq. (4.31) gives the equation of motion,

$$\frac{d}{d\tau} (m u^\alpha) + \Gamma^\alpha_{\mu\nu} m u^\mu u^\nu = 0. \quad (4.36)$$

Notice the τ derivative contains both u^α and m . We can separate it by multiplying

Eq. (4.36) by u^α . Some mathematical manipulation reveals that

$$\frac{dm}{d\tau} = 0; \quad (4.37)$$

as we might have expected, m is the body's rest mass. This lets us write the equation of motion as

$$\frac{du^\alpha}{d\tau} + \Gamma^\alpha_{\mu\nu} u^\mu u^\nu = 0, \quad (4.38)$$

which we recognize as the geodesic equation.

4.2.3 Motion of a pole-dipole body

Now we consider the motion of a pole-dipole body. As for a single-pole body, we begin with Eqs. (4.15) and (4.23). We also consider the expression

$$\partial_\delta (x^\alpha x^\beta \mathcal{T}^{\gamma\delta}) = x^\alpha \mathcal{T}^{\beta\gamma} + x^\beta \mathcal{T}^{\alpha\gamma} - x^\alpha x^\beta \Gamma^\gamma_{\mu\nu} \mathcal{T}^{\mu\nu}, \quad (4.39)$$

which follows from Eq. (4.15). We integrate these equations over a three-dimensional volume of constant t to obtain Eqs. (4.24), (4.25), and

$$\frac{d}{dt} \int x^\alpha x^\beta \mathcal{T}^{\gamma 0} dV = \int x^\alpha \mathcal{T}^{\beta\gamma} dV + \int x^\beta \mathcal{T}^{\alpha\gamma} dV - \int x^\alpha x^\beta \Gamma^\gamma_{\mu\nu} \mathcal{T}^{\mu\nu} dV. \quad (4.40)$$

As before, we expand the Christoffel symbols around X^α as described in Eq. (4.26). However, because the body is a pole-dipole, we cannot eliminate integrals containing $\delta x^\sigma \mathcal{T}^{\mu\nu}$. For a pole-dipole body, we keep those terms and eliminate integrals containing $\delta x^\sigma \delta x^\rho \mathcal{T}^{\mu\nu}$. Then Eq. (4.24) becomes

$$\frac{d}{dt} \int \mathcal{T}^{\alpha 0} dV = -\Gamma^\alpha_{\mu\nu} \int \mathcal{T}^{\mu\nu} dV - \partial_\sigma \Gamma^\alpha_{\mu\nu} \int \delta x^\sigma \mathcal{T}^{\mu\nu} dV. \quad (4.41)$$

Expanding the Christoffel symbols and using the relationship in Eq. (4.41) allows us to write Eq. (4.25) as

$$\frac{d}{dt} \int \delta x^\alpha \mathcal{T}^{\beta 0} dV + \frac{dX^\alpha}{dt} \int \mathcal{T}^{\beta 0} dV = \int \mathcal{T}^{\alpha\beta} dV - \Gamma^\beta_{\mu\nu} \int \delta x^\alpha \mathcal{T}^{\mu\nu} dV. \quad (4.42)$$

Finally, we expand the Christoffel symbols and use Eqs. (4.41) and (4.42) to write Eq. (4.40) as

$$\frac{dX^\alpha}{dt} \int \delta x^\beta \mathcal{T}^{\gamma 0} dV + \frac{dX^\beta}{dt} \int \delta x^\alpha \mathcal{T}^{\gamma 0} dV = \int \delta x^\alpha \mathcal{T}^{\beta\gamma} dV + \int \delta x^\beta \mathcal{T}^{\alpha\gamma} dV. \quad (4.43)$$

We introduce the following definitions:

$$M^{\lambda\mu\nu} = -u^0 \int \delta x^\lambda \mathcal{T}^{\mu\nu} dV, \quad (4.44)$$

$$S^{\alpha\beta} = -\frac{1}{u^0} (M^{\alpha\beta 0} - M^{\beta\alpha 0}). \quad (4.45)$$

Notice that the definition of $M^{\lambda\mu\nu}$ implies that $M^{0\mu\nu} = 0$ since we are integrating over a surface of constant t so $\delta x^0 = 0$. We use these definitions of $M^{\lambda\mu\nu}$ and $S^{\alpha\beta}$ and the definition of $M^{\alpha\beta}$ given in Eq. (4.30) to rewrite Eqs. (4.41), (4.42), and (4.50). It is simple to show that Eq. (4.50) becomes

$$u^0 (M^{\alpha\beta 0} + M^{\beta\alpha 0}) = u^\alpha M^{\beta\gamma 0} + u^\beta M^{\alpha\gamma 0}. \quad (4.46)$$

We use this relationship to relate $M^{\lambda\mu\nu}$ to u^α and $S^{\mu\nu}$:

$$M^{\alpha\beta\gamma} = -\frac{1}{2} (S^{\alpha\beta} u^\gamma + S^{\alpha\gamma} u^\beta) + \frac{1}{2} \frac{u^\alpha}{u^0} (S^{0\beta} u^\gamma + S^{0\gamma} u^\beta). \quad (4.47)$$

Now we look at Eq. (4.42). Substituting the definitions for $M^{\lambda\mu\nu}$ and $M^{\alpha\beta}$ into Eq. (4.42) gives

$$M^{\alpha\beta} = \frac{u^\alpha}{u^0} M^{\beta 0} - \frac{d}{d\tau} \left(\frac{M^{\alpha\beta 0}}{u^0} \right) - \Gamma^\beta_{\mu\nu} M^{\alpha\mu\nu}. \quad (4.48)$$

From the definition of $M^{\alpha\beta}$ in Eq. (4.34), we know that $M^{\alpha\beta}$ is symmetric under the

exchange of the indices α and β , i.e., $M^{\alpha\beta} = M^{\beta\alpha}$. Enforcing this condition gives

$$\frac{dS^{\alpha\beta}}{d\tau} = -\frac{u^\alpha}{u^0}M^{\beta 0} + \frac{u^\beta}{u^0}M^{\alpha 0} - \Gamma^\alpha_{\mu\nu} M^{\beta\mu\nu} + \Gamma^\beta_{\mu\nu} M^{\alpha\mu\nu}. \quad (4.49)$$

With a bit more manipulation, we can rewrite Eq. (4.49) as

$$\begin{aligned} \frac{dS^{\alpha\beta}}{d\tau} + \frac{u^\alpha}{u^0} \frac{dS^{\beta 0}}{d\tau} - \frac{u^\beta}{u^0} \frac{dS^{\alpha 0}}{d\tau} &= M^{\alpha\mu\nu} \left(\Gamma^\beta_{\mu\nu} - \frac{u^\beta}{u^0} \Gamma^0_{\mu\nu} \right) \\ &\quad - M^{\beta\mu\nu} \left(\Gamma^\alpha_{\mu\nu} - \frac{u^\alpha}{u^0} \Gamma^0_{\mu\nu} \right). \end{aligned} \quad (4.50)$$

Substituting the definition of $M^{\alpha\beta\gamma}$ from Eq. (4.47) allows us to write Eq. (4.50) in terms of covariant derivatives of $S^{\alpha\beta}$:

$$\frac{DS^{\alpha\beta}}{d\tau} + \frac{u^\alpha}{u^0} \frac{DS^{\beta 0}}{d\tau} - \frac{u^\beta}{u^0} \frac{DS^{\alpha 0}}{d\tau} = 0. \quad (4.51)$$

Multiplying Eq. (4.51) by u_β gives¹

$$\frac{1}{u^0} \frac{DS^{\alpha 0}}{d\tau} + u_\beta \frac{DS^{\alpha\beta}}{d\tau} + u_\beta \frac{u^\alpha}{u^0} \frac{DS^{\beta 0}}{d\tau} = 0. \quad (4.52)$$

Finally, we substitute this expression into Eq. (4.51) and get

$$\frac{DS^{\alpha\beta}}{d\tau} - u^\alpha u_\mu \frac{DS^{\beta\mu}}{d\tau} + u^\beta u_\mu \frac{DS^{\alpha\mu}}{d\tau} = 0. \quad (4.53)$$

Equation (4.53) describes the evolution of the spin tensor $S^{\alpha\beta}$. We put this in the same form as Eq. (4.4) further below after defining the four-momentum for a spinning body.

Finally, we look at Eq. (4.41). It is simple to show that when we use $M^{\alpha\beta}$ and $M^{\alpha\beta\gamma}$, Eq. (4.41) becomes

$$\frac{d}{d\tau} \left(\frac{M^{\alpha 0}}{u^0} \right) = -\Gamma^\alpha_{\mu\nu} M^{\mu\nu} + \partial_\sigma \Gamma^\alpha_{\mu\nu} M^{\sigma\mu\nu}. \quad (4.54)$$

¹Our result here differs from Papapetrou's. In his paper, the metric has signature $(+, -, -, -)$, so $u^\alpha u_\alpha = 1$. In this thesis we use metric signature $(-, +, +, +)$, so $u^\alpha u_\alpha = -1$.

We can use the definitions of $S^{\alpha\beta}$ and $M^{\alpha\beta}$ given in Eqs (4.45) and (4.48), respectively, to write $M^{\alpha 0}$ as

$$M^{\alpha 0} + \Gamma^{\alpha}_{\mu\nu} S^{\mu 0} u^{\nu} = \frac{u^{\alpha}}{u^0} (M^{00} + \Gamma^0_{\mu\nu} S^{\mu 0} u^{\nu}) + \frac{DS^{\alpha 0}}{d\tau}. \quad (4.55)$$

We introduce the quantity m defined by

$$m = -\frac{1}{u^0} (M^{\alpha 0} + \Gamma^{\alpha}_{\mu\nu} S^{\mu 0} u^{\nu}) u_{\alpha}. \quad (4.56)$$

Multiplying Eq. (4.55) by u_{α}/u^0 lets us write m as

$$m = \frac{1}{(u^0)^2} (M^{00} + \Gamma^0_{\mu\nu} S^{\mu 0} u^{\nu}) - \frac{u_{\alpha}}{u^0} \frac{DS^{\alpha 0}}{d\tau}. \quad (4.57)$$

Then, when we combine Eqs. (4.52), (4.55), and (4.57) we get

$$\frac{1}{u^0} M^{\alpha 0} = m u^{\alpha} - \Gamma^{\alpha}_{\mu\nu} S^{\mu 0} \frac{u^{\nu}}{u^0} - u_{\beta} \frac{DS^{\alpha\beta}}{d\tau}. \quad (4.58)$$

We insert this expression for $M^{\alpha 0}$ into Eq. (4.54), and with some mathematical manipulation we get the equation of motion for the body,

$$\frac{D}{d\tau} \left(m u^{\alpha} - u_{\beta} \frac{DS^{\alpha\beta}}{d\tau} \right) + \frac{1}{2} S^{\mu\nu} u^{\sigma} R^{\alpha}_{\nu\sigma\mu} = 0, \quad (4.59)$$

where $R^{\alpha}_{\nu\sigma\mu}$ is the Riemann curvature tensor,

$$R^{\alpha}_{\nu\sigma\mu} = \partial_{\mu} \Gamma^{\alpha}_{\nu\sigma} - \partial_{\nu} \Gamma^{\alpha}_{\mu\sigma} + \Gamma^{\alpha}_{\mu\rho} \Gamma^{\rho}_{\nu\sigma} - \Gamma^{\alpha}_{\nu\rho} \Gamma^{\rho}_{\mu\sigma}. \quad (4.60)$$

The form of Eq. (4.59) inspires us to define the momentum p^{α} as

$$p^{\alpha} = m u^{\alpha} - u_{\beta} \frac{DS^{\alpha\beta}}{d\tau}. \quad (4.61)$$

Notice that for a spinning body, the body's momentum p^{α} is no longer parallel to its

four-velocity u^α . Then the equation of motion of the body is given by

$$\frac{Dp^\alpha}{d\tau} = -\frac{1}{2}S^{\mu\nu}u^\sigma R^\alpha{}_{\nu\sigma\mu}. \quad (4.62)$$

Inserting the definition of the momentum vector given in Eq. (4.61) into Eq. (4.53) allows us to write the evolution of the spin as

$$\frac{DS^{\alpha\beta}}{d\tau} = p^\alpha u^\beta - p^\beta u^\alpha. \quad (4.63)$$

Equations (4.59) and (4.63) are in the same form as the equations of motion we gave in the introduction [Eqs. (4.3) and (4.4)]. Notice that the right-hand side of Eq. (4.63) is $\mathcal{O}(s^2)$, and so by the definition of p^α in Eq. (4.61), p^α and u^α are parallel to order $\mathcal{O}(s)$, as we stated in Eq. (4.5).

For further discussion of this derivation, including a discussion of the transformation properties of $M^{\alpha\beta\gamma}$, $M^{\mu\nu}$, and $S^{\alpha\beta}$, see Papapetrou's 1951 paper [68]. It is also worth noting that we can use this technique to define the equations of motion for bodies with higher-order multipoles (see, e.g., [90]). For the purposes of this thesis, there is no need to go beyond the equations of motion of a pole-dipole body.

4.3 Results: Orbits in Schwarzschild

For the Schwarzschild spacetime, we can always choose our coordinates so the background orbit lies in the equatorial plane. Then the spin force reduces to

$$F_{\text{spin}}^t = -\frac{3M}{rf} \frac{dr}{d\tau} \frac{d\phi}{d\tau} S^\theta, \quad (4.64)$$

$$F_{\text{spin}}^r = -\frac{3Mf}{r} \frac{dt}{d\tau} \frac{d\phi}{d\tau} S^\theta, \quad (4.65)$$

$$F_{\text{spin}}^\theta = \frac{3M}{r^3} \frac{d\phi}{d\tau} \left(\frac{dr}{d\tau} S^t - \frac{dt}{d\tau} S^r \right), \quad (4.66)$$

$$F_{\text{spin}}^\phi = 0, \quad (4.67)$$

where $f \equiv 1 - 2M/r$. The component F^t is related to the work done over a cycle while F^r describes a change to the normal gravitational force. Notice that F^t averages to zero over an orbit; on average, the spin force conserves energy.

The evolution of the spin vector is given by

$$\frac{dS^t}{d\tau} = -\frac{M}{r^2 f} \left(\frac{dr}{d\tau} S^t + \frac{dt}{d\tau} S^r \right), \quad (4.68)$$

$$\frac{dS^r}{d\tau} = -\frac{Mf}{r^2} \frac{dt}{d\tau} S^t + \frac{M}{r^2 f} \frac{dr}{d\tau} S^r + rf \frac{d\phi}{d\tau} S^\phi, \quad (4.69)$$

$$\frac{dS^\theta}{d\tau} = -\frac{1}{r} \frac{dr}{d\tau} S^\theta, \quad (4.70)$$

$$\frac{dS^\phi}{d\tau} = -\frac{1}{r} \left(\frac{d\phi}{d\tau} S^r + \frac{dr}{d\tau} S^\phi \right). \quad (4.71)$$

Notice that Eqs. (4.68), (4.69), and (4.71) are coupled while Eq. (4.70) is independent of the others. The components S^t , S^r , and S^ϕ precess, but the component S^θ , which is perpendicular to the orbital plane, does not. The component S^θ can be calculated analytically by solving Eq. (4.70):

$$S^\theta = \frac{c^\theta}{r}, \quad (4.72)$$

where c^θ is a constant. The factor of $1/r$ arises because we are using Boyer-Lindquist coordinates (t, r, θ, ϕ) which are not orthonormal. It is simple to transform to orthonormal coordinates for the Schwarzschild metric; vector components in orthonormal coordinates are related to the components in Boyer-Lindquist coordinates by

$$S^{\hat{t}} = \left(1 - \frac{2M}{r} \right)^{1/2} S^t, \quad (4.73a)$$

$$S^{\hat{r}} = \left(1 - \frac{2M}{r} \right)^{-1/2} S^r, \quad (4.73b)$$

$$S^{\hat{\theta}} = r S^\theta, \quad (4.73c)$$

$$S^{\hat{\phi}} = r \sin \theta S^\phi. \quad (4.73d)$$

Applying this transformation, we see that the $\hat{\theta}$ -component of the spin vector is

constant,

$$S^{\hat{\theta}} = c^{\theta}. \quad (4.74)$$

The components S^t , S^r , and S^ϕ must be calculated by numerically solving Eqs. (4.68), (4.69), and (4.71). From the evolution equations, we see that the magnitude of the spin vector $|\vec{S}| \equiv \sqrt{S^\alpha S_\alpha}$ remains constant along the orbit. We use this fact to limit our attention to the spatial components of the spin vector since we can solve for S^t from $|\vec{S}|$ and the spatial components.

4.3.1 Case 1: Initial spin $\vec{S}_0 = \mu^2 \hat{\theta}$

We begin by considering the case where the spin vector is perpendicular to the orbital plane, i.e., $S^{\hat{\theta}}$ is the only nonzero component of the spin vector. We define the constant c^θ in Eq. (4.74) by choosing the magnitude of the spin vector to be $|\vec{S}| = \mu^2$; this sets $c^\theta = \mu^2$. For this spin orientation, the only nonzero components of the spin force are F^t and F^r .

Figure 4-1 compares the trajectory of a body with mass $\mu = 10^{-5}M$ and initial spin vector $\vec{S}_0 = \mu^2 \hat{\theta}$ and a geodesic. The background geodesic is an equatorial orbit around a Schwarzschild black hole with orbital parameters $p = 10M$ and $e = 0.3$. The spin of the small body causes a decrease in the radial period, which leads to a phase difference between the radial trajectory and the background geodesic. Since $F^\theta = 0$ for this configuration, the orbit remains equatorial. There is also an accumulated phase difference in the ϕ coordinate; for the case of a black hole of mass $10 M_\odot$ orbiting a MBH of mass $10^6 M_\odot$, this amounts to $\Delta\phi \sim 1$ rad/yr.

Since both the spin force and the gravitational self-force scale like μ^2 , it is interesting to see how they compare to one another. In Fig. 4-2 we compare the spin force to the conservative contribution of the gravitational self-force [7]. For this set of orbital parameters, the spin force is about an order of magnitude smaller, indicating that the effect of the spin force is small compared to the effect of the gravitational self-force but not negligible.

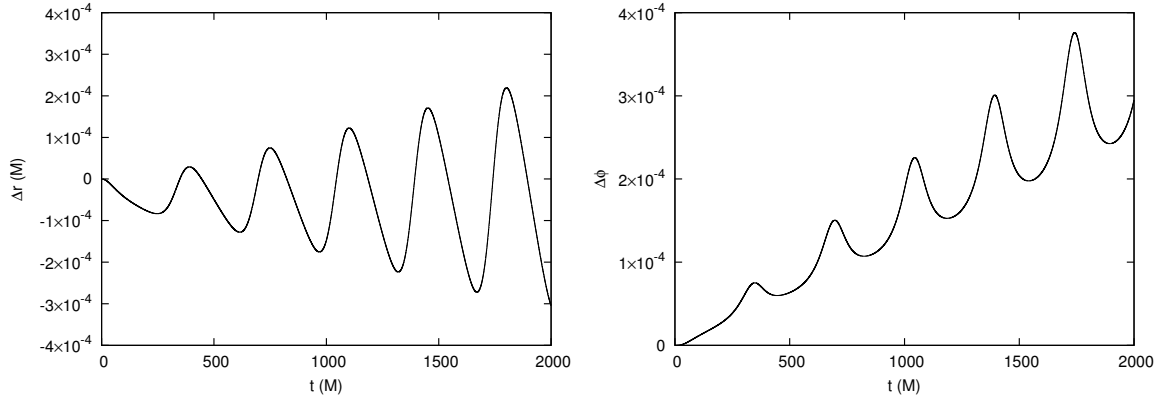


Figure 4-1: Comparison between the trajectory of a body with mass $\mu = 10^{-5}M$ and initial spin vector $\vec{S}_0 = \mu^2 \hat{\theta}$ and a geodesic. The background geodesic is an equatorial orbit around a Schwarzschild black hole with orbital parameters $p = 10M$ and $e = 0.3$. The spin of the small body produces a phase difference between the geodesic and perturbed trajectories, which causes Δr to grow. There is also an accumulated phase difference in the ϕ coordinate.

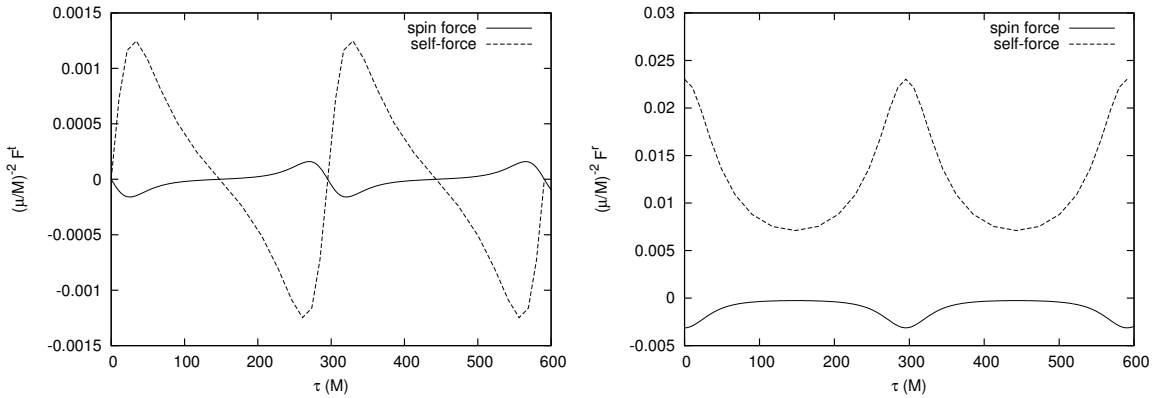


Figure 4-2: Comparison between the spin force and the conservative part of the gravitational self-force for an equatorial orbit around a Schwarzschild black hole with orbital parameters $p = 10M$ and $e = 0.3$. The initial spin vector is $\vec{S}_0 = \mu^2 \hat{\theta}$. The spin force is smaller than the gravitational self-force by about an order of magnitude, indicating that influence of the spin of the small body is not negligible compared to the gravitational self-force.

4.3.2 Case 2: Initial spin $\vec{S}_0 = \mu^2 \hat{\phi}$

Now we consider a case where the spin vector precesses. Let the initial condition of the spin vector be

$$\vec{S}_0 = \mu^2 \hat{\phi}. \quad (4.75)$$

This choice sets the magnitude of the spin vector to be $|\vec{S}| = \mu^2$, as in the previous case. We describe the precession of the spin vector as follows. First we transform the spin vector from orthonormal coordinates $(\hat{r}, \hat{\theta}, \hat{\phi})$ to Cartesian coordinates (x, y, z) using a rotation matrix:

$$\begin{pmatrix} S_x \\ S_y \\ S_z \end{pmatrix} = \begin{pmatrix} \sin \theta \cos \phi & \cos \theta \cos \phi & -\sin \phi \\ \sin \theta \sin \phi & \cos \theta \sin \phi & \cos \phi \\ \cos \theta & \sin \theta & 0 \end{pmatrix} \begin{pmatrix} S^{\hat{r}} \\ S^{\hat{\theta}} \\ S^{\hat{\phi}} \end{pmatrix}. \quad (4.76)$$

Then we describe the spin vector in terms of the angles α , the angle between the spin vector and the z -axis, and β , the angle between the spin vector and the x -axis:

$$\tan \alpha = \frac{\sqrt{S_x^2 + S_y^2}}{S_z}, \quad (4.77)$$

$$\tan \beta = \frac{S_y}{S_x}. \quad (4.78)$$

We also introduce the magnitude of the spatial portion of the spin vector $|S^i|$,

$$|S^i| = \sqrt{S_x^2 + S_y^2 + S_z^2}. \quad (4.79)$$

Figure 4-3 plots the evolution of the angles α and β and the magnitude $|S^i|$ for an equatorial orbit with orbital parameters $p = 10M$, $e = 0.3$. The component $S^{\hat{\theta}}$ remains zero along the orbit, which corresponds to $\alpha = \pi/2$. The variation in the angle β corresponds to a spin vector rotating in the equatorial plane. The oscillations in $|S^i|$ are due to variations in the small body's orbiting speed around the black hole, and are similar to the effects of Thomas precession, which describes the change in a body's angular momentum under a Lorentz transformation. Note that although the

magnitude of the three-vector S^i varies, the magnitude of the four-vector S^α remains constant.

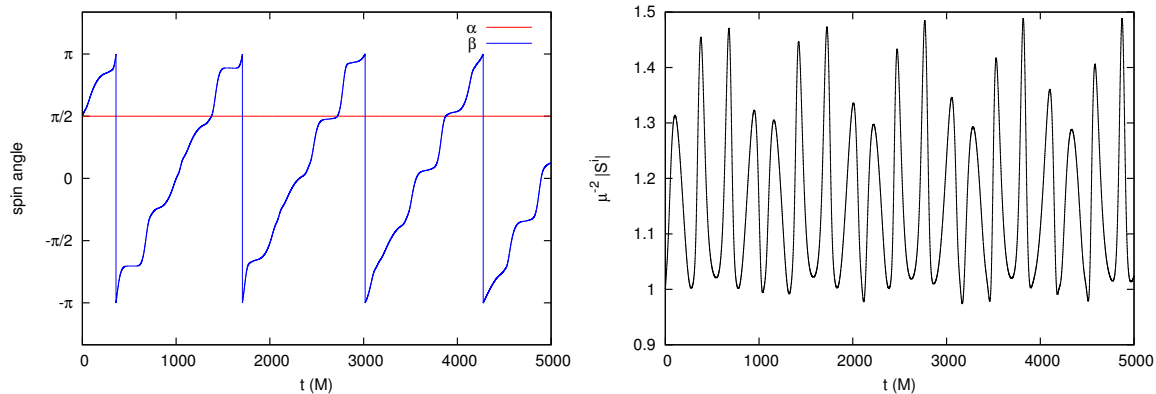


Figure 4-3: Evolution of the spin vector along an equatorial orbit around a Schwarzschild black hole with orbital parameters $p = 10M$ and $e = 0.3$. The initial spin vector is $\vec{S}_0 = \mu^2 \hat{\phi}$. The spin precession is described by the spin angles α and β , defined in Eq. (4.77) and (4.78), and the magnitude of the spatial part of the spin vector, defined in Eq. (4.79). The angles $\alpha = \pi/2$ and β describe a spin vector rotating in the equatorial plane.

For this configuration, the only nonzero component of the spin force is F^θ . We do not compare the spin force with the magnitude of the gravitational self-force because by symmetry, the θ -component of the gravitational self-force is exactly zero. The fact that F^θ is nonzero means that the spin of the small body causes the orbit to oscillate around the equatorial plane. Figure 4-4 shows the difference between the trajectory of a body with mass $\mu = 10^{-5}M$ and the background geodesic that is equatorial with orbital parameters $p = 10M$ and $e = 0.3$. The primary effect of the small body's spin is to make the orbit to oscillate around the equatorial plane by an amount $\Delta\theta$. There are also small changes to the r and ϕ motions.

4.4 Results: Orbits in Kerr

Orbits in the Kerr spacetime are much more complicated than in Schwarzschild. Unlike in the Schwarzschild case, we cannot map every orbit to an equatorial orbit via a coordinate transformation. In general, both the r and θ motions are periodic, and they are described by coupled differential equations.

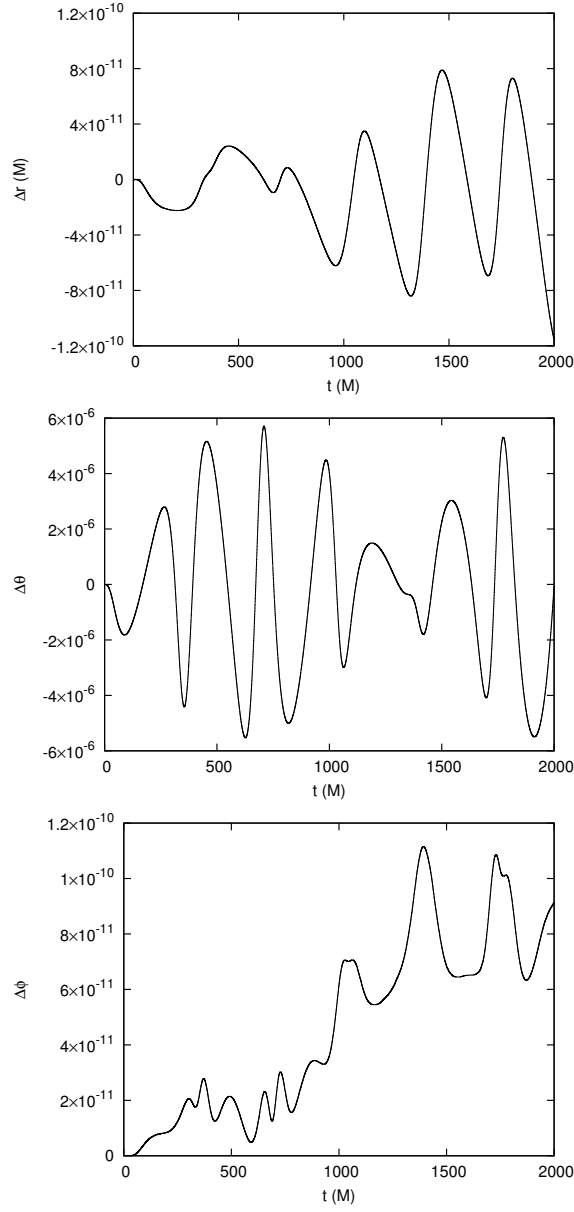


Figure 4-4: Comparison between the trajectory of a body with mass $\mu = 10^{-5}M$ and initial spin vector $\vec{S}_0 = \mu^2 \hat{\phi}$ and a geodesic. The background geodesic is an equatorial orbit around a Schwarzschild black hole with orbital parameters $p = 10M$ and $e = 0.3$. The spin of the small body causes the orbit to oscillate around the equatorial plane by an amount $\Delta\theta$. There are also slight differences in the r and ϕ motions.

Additionally, in order to describe the spin vector as in Sec. 4.3, we need to be able to describe the spin vector in orthonormal coordinates $(\hat{t}, \hat{r}, \hat{\theta}, \hat{\phi})$, which is more complicated than in the Schwarzschild case since the Kerr metric is not diagonal. We introduce an orthonormal basis,

$$v^{\hat{t}} = \sqrt{\frac{\Delta}{\Sigma}} (dt + a \sin^2 \theta d\phi) , \quad (4.80a)$$

$$v^{\hat{r}} = \sqrt{\frac{\Sigma}{\Delta}} dr , \quad (4.80b)$$

$$v^{\hat{\theta}} = \sqrt{\Sigma} d\theta , \quad (4.80c)$$

$$v^{\hat{\phi}} = \frac{\sin \theta}{\sqrt{\Sigma}} [a dt + (r^2 + a^2) d\phi] , \quad (4.80d)$$

where $\Delta \equiv r^2 - 2Mr + a^2$ and $\Sigma \equiv r^2 + a^2 \cos^2 \theta$, as given in Eq. (1.2). The spin components in this orthonormal basis are related to the components in Boyer-Lindquist coordinates by

$$S^{\hat{t}} = \sqrt{\frac{\Delta}{\Sigma}} S^t + \frac{a \sin \theta}{\sqrt{\Sigma}} S^\phi , \quad (4.81a)$$

$$S^{\hat{r}} = \sqrt{\frac{\Sigma}{\Delta}} S^r , \quad (4.81b)$$

$$S^{\hat{\theta}} = \sqrt{\Sigma} S^\theta , \quad (4.81c)$$

$$S^{\hat{\phi}} = a \sin^2 \theta \sqrt{\frac{\Delta}{\Sigma}} S^t + \frac{(r^2 + a^2) \sin \theta}{\sqrt{\Sigma}} S^\phi . \quad (4.81d)$$

Then we relate the spin components in coordinates $(\hat{t}, \hat{r}, \hat{\theta}, \hat{\phi})$ to Cartesian coordinates (x, y, z) as given in Eq. (4.76), and we define the spin angles α and β as in Eqs. (4.77) and (4.78) and the magnitude of the spatial portion of the spin vector $|S^i|$ as in Eq. (4.79). Note that this rotation to Cartesian coordinates is not strictly correct since the Kerr spacetime is not spherically symmetric; however, it is sufficient to describe the precession of the spin vector.

Now we are ready to compute the effect of spin on Kerr orbits. Below we compute the spin vector and trajectory for several different initial spin orientations and background geodesics.

4.4.1 Case 1: Equatorial orbit, initial spin $\vec{S}_0 = \mu^2 \hat{\theta}$

We begin by considering the case where the background geodesic is an equatorial orbit, and the initial spin vector is aligned with the spin of the MBH. We choose to let $\vec{S}_0 = \mu^2 \hat{\theta}$ so the magnitude of the spin vector is $|\vec{S}| = \mu^2$. Since the spin of the orbiting body, the spin of the MBH, and the orbital angular momentum are all aligned, the spin remains constant along the orbit. We show the deviation of the trajectory from the background geodesic in Fig. 4-5, where the background spacetime is the Kerr metric with spin $a = 0.5M$, the mass of the orbiting body is $\mu = 10^{-5}M$, and the background geodesic has orbital parameters $p = 10M$ and $e = 0.3$. These results are very similar to what we found for an equatorial orbit around a Schwarzschild black hole with the same orbital parameters. The spin of the orbiting body produces a phase difference between the small body's r and ϕ motion and the background geodesic. The θ -component of the spin force is zero, so the trajectory remains in the equatorial plane.

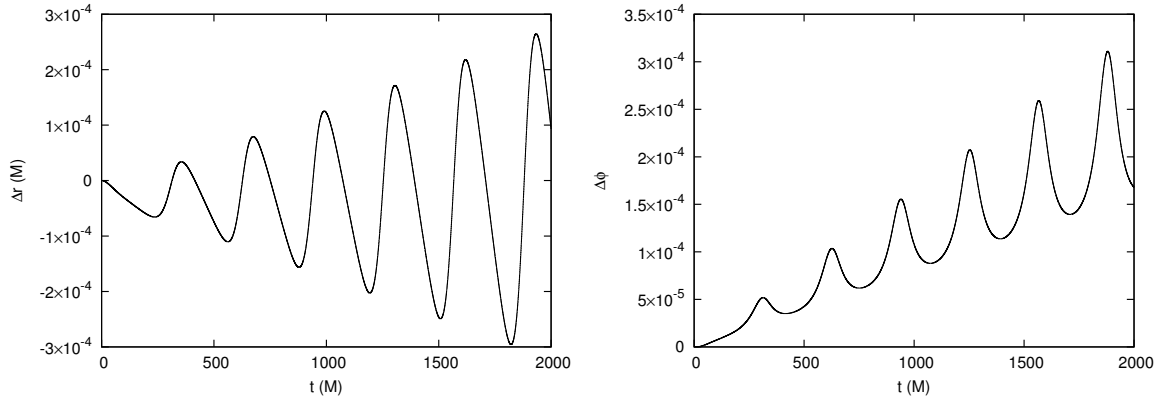


Figure 4-5: Comparison between the trajectory of a body with mass $\mu = 10^{-5}M$ and initial spin vector $\vec{S}_0 = \mu^2 \hat{\theta}$ and a geodesic. The background geodesic is an equatorial orbit around a Kerr black hole with spin $a = 0.5M$ and orbital parameters $p = 10 M$ and $e = 0.3$. The spin of the small body produces a phase difference between the geodesic and perturbed trajectories, which causes Δr to grow. There is also an accumulated phase difference in the ϕ coordinate.

4.4.2 Case 2: Inclined orbit, initial spin $\vec{S}_0 = \mu^2 \hat{\theta}$

Now we consider the motion of a small body with initial spin vector $\vec{S}_0 = \mu^2 \hat{\theta}$ along on inclined orbit. We choose a background geodesic around a Kerr black hole with $a = 0.5M$ and orbital parameters $p = 10M$, $e = 0.3$, and $\theta_{\min} = \pi/3$. Since the orbital angular momentum and spin of the small body are not aligned, the spin vector precesses along the orbit. We plot the evolution of the spin vector in Fig. 4-6. The spin angles α and β , defined in Eq. (4.77) and (4.78), respectively, describe precession of the spin vector. As the small body orbits the black hole, the spin of the small body slowly rotates in the equatorial plane. The component aligned with the spin of the black hole remains nearly constant, with small, rapid oscillations around the average value. We plot the change in the trajectory due to the spin of the small body for an orbiting body with mass $\mu = 10^{-5}M$ in Fig. 4-7. For this configuration, the new r and θ motions are out of phase with the background geodesic. There is also an accumulated phase difference in the ϕ direction.

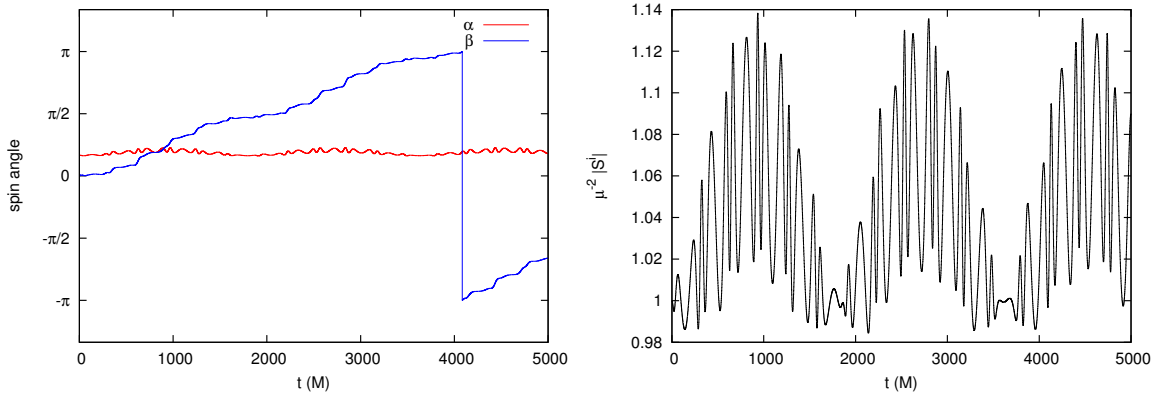


Figure 4-6: Evolution of the spin vector along an equatorial orbit around a Kerr black hole of spin $a = 0.5M$ with orbital parameters $p = 10M$, $e = 0.3$, and $\theta_{\min} = \pi/3$. The initial spin vector is $\vec{S}_0 = \mu^2 \hat{\theta}$. The spin angles α and β describe the orientation of the spin vector, as defined in Eq. (4.77) and (4.78), respectively. The quantity $|S^i|$ is the magnitude of the spatial part of the spin vector [Eq. (4.79)].

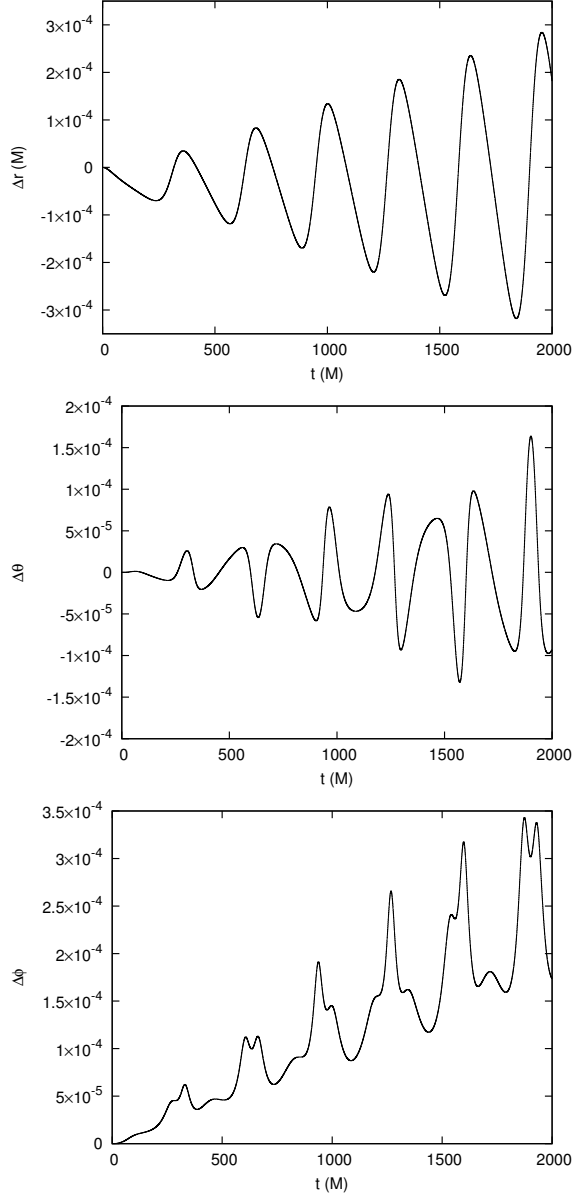


Figure 4-7: Comparison between the trajectory of a body with mass $\mu = 10^{-5}M$ and initial spin vector $\vec{S}_0 = \mu^2 \hat{\theta}$ and a geodesic. The background geodesic is an inclined orbit around a Kerr black hole with spin $a = 0.5M$ and orbital parameters $p = 10M$, $e = 0.3$, and $\theta_{\min} = \pi/3$. The spin of the small body perturbs the motion. There is an accumulated phase difference between the trajectory and the background geodesic in the r , θ , and ϕ coordinates.

4.4.3 Case 3: Inclined orbit, initial spin $\vec{S}_0 = \mu^2 \hat{\phi}$

We conclude with the case where the initial spin vector has the form $\vec{S}_0 = \mu^2 \hat{\phi}$ and magnitude $|\vec{S}| = \mu^2$. We look at a background geodesic of a Kerr black hole with spin $a = 0.5M$ and orbital parameters $\mu = 10^{-5}M$, $p = 10M$, $e = 0.3$, and $\theta_{\min} = \pi/3$. Figure 4-8 plots the evolution of the spin vector, and Fig. 4-8 shows the deviation of the trajectory from the background geodesic. For this configuration, the spin rotates more rapidly in the equatorial plane than for the configuration in Sec. 4.4.2. The initial spin vector lies in the equatorial plane, and as the small body orbits, the spin oscillates rapidly around the equatorial plane. We plot the change in the trajectory in Fig. 4-9. The results are similar to what we found in Sec. 4.3.2 for a particle with initial spin vector $\vec{S}_0 = \mu^2 \hat{\phi}$ around a Schwarzschild black hole. The perturbations to the trajectory in the r , θ , and ϕ directions average to zero over long times, indicating that there is no accumulated phase difference between the trajectory and the background geodesic. However, the spin of the small body does produce instantaneous perturbations to the trajectory.

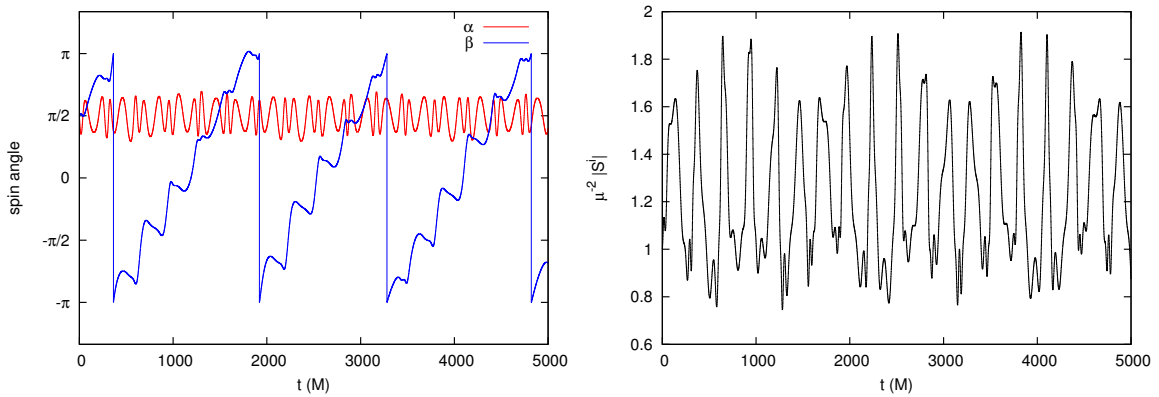


Figure 4-8: Evolution of the spin vector along an equatorial orbit around a Kerr black hole of spin $a = 0.5M$ with orbital parameters $p = 10M$, $e = 0.3$, and $\theta_{\min} = \pi/3$. The initial spin vector is $\vec{S}_0 = \mu^2 \hat{\phi}$. The spin precession is described by the spin angles α and β , defined in Eq. (4.77) and (4.78), and the magnitude of the spatial part of the spin vector, defined in Eq. (4.79).

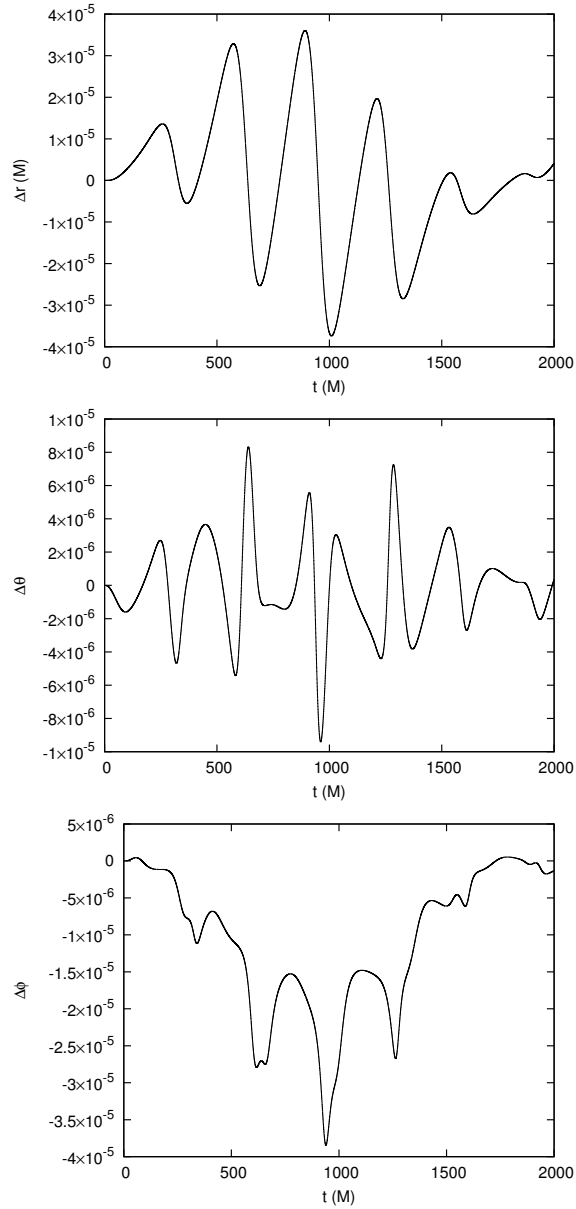


Figure 4-9: Comparison between the trajectory of a body with mass $\mu = 10^{-5}M$ and initial spin vector $\vec{S}_0 = \mu^2 \hat{\phi}$ and a geodesic. The background geodesic is an orbit around a Kerr black hole with orbital parameters $p = 10M$, $e = 0.3$, and $\theta_{\min} = \pi/3$. The spin of the small body causes the orbit to oscillate around the equatorial plane by an amount $\Delta\theta$. There are also perturbations to the r and ϕ coordinates, but there is no accumulated phase difference in r or ϕ .

4.5 Summary and future work

This chapter presents a first analysis of the effect of spin-curvature coupling on the motion of a small body orbiting a massive black hole. We begin by deriving the equation of motion for the small body and the spin evolution equation in Sec. 4.2, following the approach of Papapetrou [68]. We show that the equations of motion follow from the dynamical equation $\nabla_\mu T^{\mu\nu} = 0$ and the definition of a pole-dipole particle. We compute the effects of the spin of the small body in Secs. 4.3 and 4.4. We begin by considering orbits in the Schwarzschild spacetime in Sec. 4.3. We compute the change in the trajectory and evolution of the spin vector for different initial values of the spin vector. We also compare the spin force to the conservative part of the gravitational self-force, as calculated by Barack and Sago [7]. We find that the magnitude of the spin force is within about an order of magnitude of the gravitation self-force, indicating that the effect of the spin force is not negligible compared to the gravitational self-force. In Sec. 4.4 we calculate the change in the trajectory and evolution of the spin vector for orbits in the Kerr spacetime.

Now that we have laid the groundwork for describing the motion of spinning particles in the Kerr spacetime, it would be interesting to look for observational effects of the spin force. Spin effects could have an effect on the motion of a pulsar around a MBH. There are currently efforts underway to find a pulsar orbiting the galactic center with the goal of using pulsar timing to map the spacetime around Sgr A* [57]. Spin-curvature coupling will also change the GWs emitted by an EMRI. Since the detection of low-frequency GWs relies upon having very accurate waveform models for matched filtering, it would be interesting to see how much the spin of the small body affects the waveform.

Since we can expand any function evaluated along a Kerr geodesic in harmonics of the orbital frequencies Ω_r , Ω_θ , and Ω_ϕ (cf. Ref. [32]), we can simplify our calculations by working in the frequency domain. Furthermore, the results we obtained in the time domain show that the spin precession and spin force vary smoothly in a harmonic fashion, indicating that they can be described well by a Fourier expansion. This would

speed up calculations since instead of having to do a full numerical evolution of the trajectory, we would only need to perform a few numerical integrals to determine the Fourier coefficients. Also, having a description of the spin force in the frequency domain would allow us to use existing frequency-domain codes to compute the GW emission. We are currently in the process of calculating the spin force in the frequency domain.

Appendix A

Averaging functions along black hole orbits

In this appendix, we describe how to average functions along geodesics of Kerr using a technique developed by Drasco and Hughes [32]. A key element of this technique is the separation of the r and θ motion by introducing a new time coordinate. In Boyer-Lindquist coordinates, the r and θ equations of motion [Eqs. (1.14) and (1.15)] remain coupled due to the factors of $\Sigma \equiv r^2 + a^2 \cos^2 \theta$ that appear on the left-hand side of these equations. We can eliminate the residual coupling between r and θ by parametrizing the orbits in terms of the time coordinate λ , which is defined by $d\lambda = d\tau/\Sigma$. Then the equations of motion become

$$\left(\frac{dr}{d\lambda}\right)^2 = R(r), \tag{A.1}$$

$$\left(\frac{d\theta}{d\lambda}\right)^2 = \Theta(\theta), \tag{A.2}$$

$$\frac{d\phi}{d\lambda} = \Phi(r, \theta), \tag{A.3}$$

$$\frac{dt}{d\lambda} = T(r, \theta), \tag{A.4}$$

where $R(r)$, $\Theta(\theta)$, $\Phi(r, \theta)$, and $T(r, \theta)$ are defined in Eqs. (1.14) – (1.17).

Since this choice explicitly separates the r and θ motion, we can construct $r(\lambda)$

and $\theta(\lambda)$ simply by integrating Eq. (A.1) and (A.2), respectively. The r and θ periods are given by

$$\Lambda_r = 2 \int_{r_p}^{r_a} \frac{dr}{\sqrt{R(r)}}, \quad (\text{A.5})$$

$$\Lambda_\theta = 4 \int_{\theta_{\min}}^{\pi/2} \frac{d\theta}{\sqrt{\Theta(\theta)}}. \quad (\text{A.6})$$

The conjugate frequencies are

$$\Upsilon_{r,\theta} = 2\pi/\Lambda_{r,\theta}, \quad (\text{A.7})$$

and the corresponding angles are defined as

$$w^{r,\theta} = \Upsilon_{r,\theta}\lambda. \quad (\text{A.8})$$

We use this parametrization of the r and θ motion to define Υ_t , the averaged value of the function $T(r, \theta)$,

$$\Upsilon_t = \frac{1}{(2\pi)^2} \int_0^{2\pi} dw^r \int_0^{2\pi} dw^\theta T[r(w^r), \theta(w^\theta)]. \quad (\text{A.9})$$

The long-time average of any black hole orbit functional $f(r, \theta)$ is given by

$$\begin{aligned} \langle f \rangle &\equiv \lim_{T \rightarrow \infty} \frac{1}{2T} \int_{-T}^T f[r(t), \theta(t)] dt \\ &= \frac{1}{(2\pi)^2 \Upsilon_t} \int_0^{2\pi} dw^r \int_0^{2\pi} dw^\theta f[r(w^r), \theta(w^\theta)] T[r(w^r), \theta(w^\theta)]. \end{aligned} \quad (\text{A.10})$$

This is the procedure we use to compute $\langle \mathcal{H}_1 \rangle$ in Sec. 2.4.

Appendix B

Newtonian precession frequencies

For weak-field orbits, we expect that the bumpy black hole frequency shifts in Sec. 2.4 [Eqs. (2.66) – (2.68)] are described well using Newtonian gravity. In this appendix, we compute the Newtonian frequency shifts; in Secs. 2.5 and 2.6, we show that the frequency shifts limit to the results we develop here for weak-field orbits.

As in the relativistic calculation in Sec. 1.3.3, we compute frequency shifts due to multipolar “bumps” by examining the variation of a perturbed Hamiltonian with respect to the action variables:

$$m \delta\Omega^i = \frac{\partial \langle \mathcal{H}_1 \rangle}{\partial J_i}. \quad (\text{B.1})$$

(Note that in Newtonian gravity, there is no distinction between coordinate time and proper time.) The actions are defined by Eqs. (1.38) – (1.40). For a body of mass m orbiting a mass M , in Newtonian gravity the action variables are

$$J_r = Mm\sqrt{p} \left(\frac{1}{\sqrt{1-e^2}} - 1 \right), \quad (\text{B.2})$$

$$J_\theta = Mm\sqrt{p} (1 - \sin \theta_{\min}), \quad (\text{B.3})$$

$$J_\phi = Mm\sqrt{p} \sin \theta_{\min}. \quad (\text{B.4})$$

We define the perturbation to the Hamiltonian as

$$\mathcal{H}_1^{\text{Newt}} = m \delta V_l(r, \theta) = \frac{m B_l M^{l+1}}{r^{l+1}} Y_{l0}(\cos \theta) . \quad (\text{B.5})$$

To perform the averaging, first we reparameterize the radial and angular motion in a manner similar to the parametrization we use for black hole orbits:

$$r = \frac{pM}{1 + e \cos \psi} , \quad (\text{B.6})$$

$$\cos \theta = \cos \theta_{\min} \cos(\psi - \psi_0) . \quad (\text{B.7})$$

Notice that the radial and angular motions vary in phase with one another in the Newtonian limit. The angle ψ_0 is an offset phase between these motions. The equation of motion for ψ is

$$\frac{d\psi}{dt} = \frac{(1 + e \cos \psi)^2}{p^{3/2} M} . \quad (\text{B.8})$$

The averaged Hamiltonian is given by

$$\begin{aligned} \langle \mathcal{H}_1^{\text{Newt}} \rangle &= \frac{m}{T_K} \int_0^{T_K} \delta V_l[r(t), \theta(t)] dt \\ &= \frac{m}{T_K} \int_0^{2\pi} \left(\frac{d\psi}{dt} \right)^{-1} \delta V_l[r(\psi), \cos \theta(\psi)] d\psi , \end{aligned} \quad (\text{B.9})$$

where T_K is the Keplerian orbital period,

$$T_K = 2\pi M \left(\frac{p}{1 - e^2} \right)^{3/2} . \quad (\text{B.10})$$

We can put the orbital period in a more familiar form if we replace the semilatus rectum p with the semi-major axis $a = pM/(1 - e^2)$:

$$T_K = 2\pi M \left(\frac{a}{M} \right)^{3/2} . \quad (\text{B.11})$$

Using these results, we now compute the effects of $l = 2, 3,$ and 4 perturbations in Newtonian gravity.

B.1 Quadrupole shift ($l = 2$)

The quadrupole bump is given by the potential

$$\delta V^{l=2} = \frac{B_2 M^3}{4r^3} \sqrt{\frac{5}{\pi}} (3 \cos^2 \theta - 1) , \quad (\text{B.12})$$

for which we find

$$\langle \mathcal{H}_1 \rangle = \frac{m B_2}{8p^3} \sqrt{\frac{5}{\pi}} (1 - e^2)^{3/2} (1 - 3 \sin^2 \theta_{\min}) . \quad (\text{B.13})$$

Varying this averaged Hamiltonian with respect to $J_{r,\theta,\phi}$, we find

$$\delta \Omega^r = \omega_K \frac{3B_2}{8p^2} \sqrt{\frac{5}{\pi}} \sqrt{1 - e^2} (3 \sin^2 \theta_{\min} - 1) , \quad (\text{B.14})$$

$$\delta \Omega^\theta = \omega_K \frac{3B_2}{8p^2} \sqrt{\frac{5}{\pi}} \left[\sin^2 \theta_{\min} (5 + 3\sqrt{1 - e^2}) - \sqrt{1 - e^2} - 1 \right] , \quad (\text{B.15})$$

$$\delta \Omega^\phi = \omega_K \frac{3B_2}{8p^2} \sqrt{\frac{5}{\pi}} \left[\sin^2 \theta_{\min} (5 + 3\sqrt{1 - e^2}) - \sqrt{1 - e^2} - 1 - 2 \sin \theta_{\min} \right] . \quad (\text{B.16})$$

These frequencies are written using the Kepler frequency $\omega_K = 2\pi/T_K$.

Equations (B.14) – (B.16) reproduce well-known results for motion in a spherical potential augmented by a quadrupole perturbation. To facilitate comparison with the literature, it is useful to change our description of the orientation of the orbital plane from θ_{\min} , the minimum angle θ reaches over an orbit, to the inclination angle $\iota = \pi/2 - \theta_{\min}$. We then construct the precession frequencies

$$\Omega^{\text{apsis}} = \delta \Omega^\theta - \delta \Omega^r = \omega_K \frac{3B_2}{8p^2} \sqrt{\frac{5}{\pi}} (5 \cos^2 \iota - 1) , \quad (\text{B.17})$$

$$\Omega^{\text{plane}} = \delta \Omega^\phi - \delta \Omega^\theta = -\omega_K \frac{3B_2}{4p^2} \sqrt{\frac{5}{\pi}} \cos \iota ; \quad (\text{B.18})$$

Ω^{apsis} describes the frequency of the orbit's apsidal precession within its orbital plane, and Ω^{plane} the frequency at which the orbital plane precesses around the symmetry

axis. These frequencies reproduce expressions that can be found in the literature; cf. Sec. 12.3C of Ref. [39]. The precession of the orbit's periastron, which is due to a beat between the azimuthal and radial motions, is given by

$$\Omega^{\text{peri}} = \delta\Omega^\phi - \delta\Omega^r = \omega_K \frac{3B_2}{8p^2} \sqrt{\frac{5}{\pi}} (5 \cos^2 \iota - 2 \cos \iota - 1) . \quad (\text{B.19})$$

In the equatorial limit ($\iota = 0$), this result agrees with Eq. (A4) of [25] if we identify their parameter Q with $B_2 M^3 \sqrt{5/4\pi}$.

B.2 Octupole shift ($l = 3$)

The octupole bump is given by the potential

$$\delta V^{l=3} = \frac{B_3 M^4}{4r^4} \sqrt{\frac{7}{\pi}} (5 \cos^3 \theta - 3 \cos \theta) , \quad (\text{B.20})$$

leading to

$$\langle \mathcal{H}_1 \rangle = \frac{3mB_3 e}{16p^4} \sqrt{\frac{7}{\pi}} (1 - e^2)^{3/2} \cos \theta_{\min} (5 \cos^2 \theta_{\min} - 4) \cos \psi_0 . \quad (\text{B.21})$$

The value of $\langle \mathcal{H}_1 \rangle$ is proportional to $\cos \psi_0$, and so it depends on the phase offset of the radial and angular motions. Over very long timescales, this dependence averages out due to precession effects; however, on timescales that are not long enough for ψ_0 to vary over its full range, there is a residual impact. For black hole orbits, the r and θ motions do not vary in phase with one another, and so this averaging is much stronger, and we can treat $\langle \mathcal{H}_1 \rangle = 0$. Therefore, on average there is no influence from the $l = 3$ perturbation, nor from any odd l multipolar bump; however, the instantaneous impact of odd l bumps is non-zero.

B.3 Hexadecapole shift ($l = 4$)

Finally, for the hexadecapole bump, we have

$$\delta V^{l=4} = \frac{B_4 M^5}{16r^5} \sqrt{\frac{9}{\pi}} (35 \cos^4 \theta - 30 \cos^2 \theta + 3) , \quad (\text{B.22})$$

leading to

$$\begin{aligned} \langle \mathcal{H}_1 \rangle = & \frac{3mB_4}{256p^5} \sqrt{\frac{9}{\pi}} (1 - e^2)^{3/2} [8(2 + 3e^2) - 20 \cos^2 \theta_{\min}(4 + 3e^2 \\ & + 6e^2 \cos^2 \psi_0) + 35 \cos^4 \theta_{\min}(2 + e^2 + 4e^2 \cos^2 \psi_0)] . \end{aligned} \quad (\text{B.23})$$

We focus on the secular (long-time average) precessions, and average this over ψ_0 , leaving

$$\langle \mathcal{H}_1 \rangle = \frac{3mB_4}{256p^5} \sqrt{\frac{9}{\pi}} (1 - e^2)^{3/2} (2 + 3e^2) (8 - 40 \cos^2 \theta_{\min} + 35 \cos^4 \theta_{\min}) . \quad (\text{B.24})$$

The precession frequencies which arise from this are

$$\delta \Omega^r = -\omega_K \frac{45B_4}{256p^4} \sqrt{\frac{9}{\pi}} e^2 \sqrt{1 - e^2} (8 - 40 \cos^2 \theta_{\min} + 35 \cos^4 \theta_{\min}) , \quad (\text{B.25})$$

$$\begin{aligned} \delta \Omega^\theta = & -\omega_K \frac{15B_4}{256p^4} \sqrt{\frac{9}{\pi}} \left\{ 8 \left[8 + 3e^2 \left(3 + \sqrt{1 - e^2} \right) \right] \right. \\ & - 4 \cos^2 \theta_{\min} \left[62 + e^2 \left(63 + 30\sqrt{1 - e^2} \right) \right] \\ & \left. + 7 \cos^4 \theta_{\min} \left[28 + 3e^2 \left(9 + 5\sqrt{1 - e^2} \right) \right] \right\} , \end{aligned} \quad (\text{B.26})$$

$$\begin{aligned} \delta \Omega^\phi = & \omega_K \frac{15B_4}{256p^4} \sqrt{\frac{9}{\pi}} \left\{ -8 \left[8 + 3e^2 \left(3 + \sqrt{1 - e^2} \right) \right] \right. \\ & + 4 \cos^2 \theta_{\min} \left[62 + e^2 \left(63 + 30\sqrt{1 - e^2} \right) \right] \\ & - 7 \cos^4 \theta_{\min} \left[28 + 3e^2 \left(9 + 5\sqrt{1 - e^2} \right) \right] \\ & \left. + 4 \left(4 - 7 \cos^2 \theta_{\min} \right) \left(2 + 3e^2 \right) \sin \theta_{\min} \right\} . \end{aligned} \quad (\text{B.27})$$

,

Appendix C

Definitions of the modified gravity bumpy Kerr metrics

Here we provide explicit expressions for the polynomials appearing in the conditions that guarantee the existence of a Carter constant in Chapter 3. The polynomials that appear in the Carter conditions for the bumpy Kerr metric [Eq. (3.10)] are

$$P_1^{\text{BK}} = r^6 + 5a^2r^4 + 2a^4r^2 - 2a^2 \cos^2 \theta (2r^4 + a^2r^2 + a^4) - a^4 \cos^4 \theta (r^2 - a^2), \quad (\text{C.1})$$

$$P_2^{\text{BK}} = r^4M + a^2r^2(r + 2M) - a^2 \cos^2 \theta [r^2(r + 2M) - a^2(r - 2M)] - a^4 \cos^4 \theta (r - M), \quad (\text{C.2})$$

$$P_3^{\text{BK}} = r[r^3 + a^2(r + 4M)] + a^2 \cos^2 \theta (r^2 - 4Mr + a^2), \quad (\text{C.3})$$

$$P_4^{\text{BK}} = r^3[r^2(r - 2M) + a^2(3r - 4M)] - 2r^2a^2 \cos^2 \theta (r^2 - 2Mr - a^2) - a^4 \cos^4 \theta (3r^2 - 2Mr + a^2), \quad (\text{C.4})$$

$$P_5^{\text{BK}} = r^3(r - 2M)[r^2(r + 2M) + a^2(r + 4M)] - r^3 \cos^2 \theta [r^4 - 4M^2r^2 - a^2(r^2 - 6Mr + 16M^2) - 2a^4] - a^2 \cos^4 \theta [2r^3(r^2 - 2Mr + 4M^2) + a^2r(r^2 + 4Mr - 4M^2) - a^4(r - 2M)] - a^4 \cos^6 \theta (r - 2M)\Delta, \quad (\text{C.5})$$

$$P_6^{\text{BK}} = -\frac{\Delta \sin^2 \theta (\Sigma \Delta - 2Mr\Sigma + 4Mra^2 + 4Mr^3)}{2\Sigma^2}, \quad (\text{C.6})$$

$$P_7^{\text{BK}} = -\frac{a\Delta \sin^2 \theta (\Sigma - 4Mr)}{2\Sigma^2}, \quad (\text{C.7})$$

$$\begin{aligned}
P_8^{\text{BK}} = & -\sin^2 \theta (8r^{11} - 4r^7 \Sigma^2 + 16M^2 r^9 + 2r^9 \Sigma - 44a^6 M \Sigma \Delta - 8a^{10} M \\
& -68a^4 Mr^4 \Sigma + 128a^4 M^2 r^3 \Sigma - 56a^6 M^2 r \Sigma - 12a^4 r^5 \Sigma - 16a^6 r^3 \Sigma \\
& -6a^8 r \Sigma - 36a^2 Mr^6 \Sigma + 40a^2 Mr^4 \Sigma^2 + 32a^2 r^9 - 3r^5 \Sigma^3 - 8Mr^{10} \\
& -20a^2 M^2 r^3 \Sigma^3 - 16a^2 Mr^8 - 16a^2 M^2 r^7 - 48a^6 M^2 r^3 + 16a^6 Mr^4 \\
& -56a^2 M^2 r^3 \Sigma^2 + 64a^2 M^2 r^5 \Sigma + 72a^4 M^2 r \Sigma^2 - 32M^2 r^7 \Sigma \\
& -4Mr^8 \Sigma - 12a^4 r^3 \Sigma^2 - 12a^2 r^5 \Sigma^2 - 4Mr^6 \Sigma^2 - 4a^6 r \Sigma^2 \\
& -44a^6 M \Sigma^2 + 12Mr^4 \Sigma^3 - 8M^2 r^3 \Sigma^3 + 24M^2 r^5 \Sigma^2 + 2a^2 r^3 \Sigma^3 \\
& +5a^4 r \Sigma^3 + 12a^4 M \Sigma^3), \quad (\text{C.8})
\end{aligned}$$

$$\begin{aligned}
P_9^{\text{BK}} = & a \sin^2 \theta (-16M^2 r^5 \Sigma + 8M^2 r^3 \Sigma^2 - 4Mr^4 \Sigma^2 - 20Mr^6 \Sigma \\
& -32a^2 M^2 r^5 + 24Mr^8 - 24a^4 r^5 - 8a^8 M - 8r^9 + 56a^2 Mr^6 \\
& +40a^4 Mr^4 - 24a^2 r^7 - 8a^6 r^3 + 8a^6 M \Delta + 16a^6 M^2 r - 12a^4 M \Sigma^2 \\
& +28a^6 M \Sigma - 36a^4 M \Sigma \Delta + 12a^2 M \Sigma^2 \Delta - 48a^4 M^2 r^3 + 8a^2 M^2 r \Sigma^2 \\
& -3a^2 r \Sigma^3 + 16M^2 r^7 + 2a^2 M \Sigma^3 + 18a^2 r^5 \Sigma + 6r^7 \Sigma + 18a^4 r^3 \Sigma \\
& +6a^6 r \Sigma + r^3 \Sigma^3 + 48a^2 M^2 r^3 \Sigma - 40a^4 M^2 r \Sigma - 48a^2 Mr^4 \Sigma), \quad (\text{C.9})
\end{aligned}$$

$$\begin{aligned}
P_{10}^{\text{BK}} = & \sin^2 \theta (-12a^4 Mr \Sigma^2 - 48a^2 r^8 + 6a^2 r^4 \Sigma^2 - 48a^4 r^6 + 16a^6 M^2 \Delta \\
& +32a^6 M^3 r + 8a^6 \Sigma \Delta - 8a^2 M^2 \Sigma^3 - 16r^{10} - 16M^2 r^8 \\
& +6a^2 Mr \Sigma^3 + 24a^4 r^4 \Sigma + 32Mr^9 - 32a^2 Mr^3 \Sigma^2 - 8a^8 \Sigma \\
& +8a^6 M^2 \Sigma + 40M^2 r^6 \Sigma + 16a^6 Mr \Sigma - 32a^2 Mr^5 \Sigma + 8r^8 \Sigma \\
& -16a^8 M^2 + 96a^2 M^2 r^4 \Sigma - 16a^6 r^4 + 32a^4 Mr^5 - 80a^2 M^2 r^6 \\
& -48a^4 M^2 r^4 + 16a^4 Mr^3 \Sigma + 24a^2 r^6 \Sigma - 6Mr^3 \Sigma^3 + 3r^4 \Sigma^3 \\
& +2r^6 \Sigma^2 + 5a^4 \Sigma^3 + 64a^2 Mr^7 + 24Mr^5 \Sigma^2 - 24M^2 r^4 \Sigma^2 \\
& -48Mr^7 \Sigma - 24a^6 M^2 \Sigma \sin^2 \theta - 6a^2 \Sigma^3 \Delta + 6a^4 \Sigma^2 \Delta - 4a^6 \Sigma^2), \quad (\text{C.10})
\end{aligned}$$

$$\begin{aligned}
P_{11}^{\text{BK}} = & -8aM \sin^2 \theta (r^3 \Sigma^2 - 5r^5 \Sigma + 4r^7 - 3ar \Sigma^2 + 6a^2 r^3 \Sigma + a^2 M \Sigma^2 \\
& +a^2 M \Sigma \Delta + 2a^2 M^2 r \Sigma - 3a^4 M \Sigma - 8a^2 Mr^4 + 3a^4 r \Sigma - 2Mr^6 \\
& -4a^4 r^3 + 3Mr^4 \Sigma + 2a^4 M \Delta + 4a^4 M^2 r - 2a^6 M), \quad (\text{C.11})
\end{aligned}$$

$$P_{12}^{\text{BK}} = -2r(-28a^2\Sigma\Delta - 56a^2Mr\Sigma + 18a^4\Sigma + \Sigma^3 + 2\Sigma^2\Delta + 4Mr\Sigma^2 + 4a^2\Sigma^2 - 18r^4\Sigma + 16r^6 + 32a^2r^4 + 16a^4\Delta + 32a^4Mr - 16a^6), \quad (\text{C.12})$$

$$P_{13}^{\text{BK}} = 2a^2 \sin^2 \theta (8a^2\Sigma\delta + 16a^2Mr\Sigma - 8a^4\Sigma - \Sigma^3 - 6\Sigma^2\Delta - 12Mr\Sigma^2 + 8a^2\Sigma^2 + 24r^4\Sigma - 16r^6 - 16a^2r^4), \quad (\text{C.13})$$

$$P_{14}^{\text{BK}} = 4aMr \sin^2 \theta (4r^4 - \Sigma\Delta + 2Mr\Sigma - 4a^2\Sigma + 4a^2r^2), \quad (\text{C.14})$$

$$P_{15}^{\text{BK}} = \Sigma^2(4r^6 + 2a^2\Sigma^2 - 4a^2\Sigma\Delta - 8a^2Mr\Sigma + 2a^4\Sigma + 8a^2r^4 - \Sigma^2\Delta - 2Mr\Sigma^2 - 2r^4\Sigma + 4a^4\Delta + 8a^4Mr - 4a^6). \quad (\text{C.15})$$

The polynomial functions that appear in the Carter conditions for the deformed Kerr metric [Eq. (3.24)] are

$$P_1^{\text{DK}} = r^2(r^4 + 5a^2r^2 + 2a^4) - 2a^2 \cos^2 \theta (2r^4 + a^2r^2 + a^4) - a^4 \cos^4 \theta (r^2 - a^2), \quad (\text{C.16})$$

$$P_2^{\text{DK}} = r^2(r^2M + a^2r + 2a^2M) - a^2 \cos^2 \theta [r^2(r + 2M) - a^2(r - 2M)] - a^4 \cos^4 \theta (r - M), \quad (\text{C.17})$$

$$P_3^{\text{DK}} = r^3(r - 2M)[r^2(r + 2M) + a^2(r + 4M)] + 2r^3a^2 \cos^2 \theta (r^2 - 2Mr + 4M^2 + a^2) + a^4 \cos^4 \theta (r - 2M)\Delta, \quad (\text{C.18})$$

$$P_4^{\text{DK}} = r^3[r^2(r - 2M) + a^2(3r - 4M)] - 2r^2a^2 \cos^2 \theta (r^2 - 2Mr - a^2) - a^4 \cos^4 \theta (3r^2 - 2Mr + a^2), \quad (\text{C.19})$$

$$P_5^{\text{DK}} = r^4(r^6 + 3a^2r^4 + 8a^4r^2 + 2a^6) - 3a^4r^4 \cos^2 \theta (3r^2 - a^2) + a^4 \cos^4 \theta (5r^6 - 3a^2r^4 + 6a^4r^2 + 2a^6) + a^6 \cos^6 \theta (2r^4 - 3a^2r^2 - a^4), \quad (\text{C.20})$$

$$P_6^{\text{DK}} = r^4(r^2 - 6a^2) + 3r^2a^2 \cos^2 \theta (3r^2 + 4a^2) - a^4 \cos^2 \theta (9r^2 - 2a^2) - a^6 \cos^6 \theta, \quad (\text{C.21})$$

$$P_7^{\text{DK}} = r^6 + 10a^2r^4 + 6a^4r^2 - a^2 \cos^2 \theta (11r^4 + 16a^2r^2 + 10a^4) + a^4 \cos^4 \theta (5r^2 + 6a^2) + a^6 \cos^6 \theta, \quad (\text{C.22})$$

$$P_8^{\text{DK}} = r^2(3r^2 - a^2) - a^2 \cos^2 \theta (r^2 - 3a^2), \quad (\text{C.23})$$

$$P_9^{\text{DK}} = r^2(3r^4 + 5a^2r^2 - 2a^4) - 2a^2 \cos^2 \theta (r^2 + a^2)(2r^2 - 3a^2) + a^4 \cos^4 \theta (r^2 - 3a^2), \quad (\text{C.24})$$

$$P_{10}^{\text{DK}} = r^2(3r^2 - a^2) - 3 \cos^2 \theta (r^4 - a^4) + a^2 \cos^4 \theta (r^2 - 3a^2), \quad (\text{C.25})$$

$$P_{11}^{\text{DK}} = -r^4(3r^6 - 2Mr^5 + 24a^2r^4 - 18a^2Mr^3 - 8a^2M^2r^2 + 19a^4r^2 - 24a^4Mr + 48a^4M^2 + 6a^6) + a^2 \cos^2 \theta (21r^8 - 18Mr^7 - 8M^2r^6 + 18a^2r^6 - 42a^2Mr^5 + 72a^2M^2r^4 + 33a^4r^4 - 32a^4Mr^3 + 24a^4M^2r^2 + 12a^6r^2 - 16a^6M^2) + a^4 \cos^4 \theta (11r^6 + 6Mr^5 - 24M^2r^4 - 12a^2r^4 + 22a^2Mr^3 - 24a^2M^2r^2 + 3a^4r^2 - 24a^4Mr + 24a^4M^2 + 2a^6) + a^6 \cos^6 \theta (3r^4 - 6Mr^3 - 6a^2r^2 + 18a^2Mr - 8a^2M^2 - a^4), \quad (\text{C.26})$$

$$P_{12}^{\text{DK}} = r^3(r^3M + 3a^2r^2 - 6a^2Mr - a^4) - a^2 \cos^2 \theta (3r^5 - 3Mr^4 - 3a^2Mr^2 - 3a^4r + 2a^4M) + a^4 \cos^4 \theta (r^3 - 3a^2r + a^2M), \quad (\text{C.27})$$

$$P_{13}^{\text{DK}} = r^3(r^6 + 9a^2r^4 - 10a^2Mr^3 + 6a^4r^2 - 8a^4Mr + 2a^6) - \cos^2 \theta r(r^8 + 18a^2r^6 - 22a^2Mr^5 + 15a^4r^4 - 26a^4Mr^3 + 20a^6r^2 - 12a^6Mr + 6a^8) + a^2 \cos^4 \theta (9r^7 - 12Mr^6 + 6a^2r^5 - 22a^2Mr^4 + 27a^4r^3 - 18a^4Mr^2 + 6a^6r + 4a^6M) + a^4 \cos^6 \theta (3r^5 + 4Mr^4 - 10a^2r^3 + 6a^2Mr^2 + 3a^4r - 6a^4M) + a^6 \cos^8 \theta (r^3 - 3a^2r + 2a^2M), \quad (\text{C.28})$$

$$P_{14}^{\text{DK}} = r^3(3r^8 + 4Mr^7 + 22a^2r^6 - 30a^2Mr^5 + 8a^2M^2r^4 + 29a^4r^4 - 14a^4Mr^3 + 12a^6r^2 - 12a^6Mr - 16a^6M^2 + 2a^8) - a^2 \cos^2 \theta (15r^9 - 24Mr^8 + 8M^2r^7 + 10a^2Mr^6 + 21a^4r^5 - 34a^4Mr^4 - 32a^4M^2r^3 + 24a^6r^3 + 12a^6Mr^2 - 32a^6M^2r + 6a^8r + 8a^8M) - a^4 \cos^4 \theta (13r^7 - 32Mr^6 + 6a^2r^5 + 14a^2Mr^4 + 8a^2M^2r^3 - 3a^4r^3 - 42a^4Mr^2 + 48a^4M^2r + 4a^6r - 16a^6M) - a^6 \cos^6 \theta (3r^5 - 12Mr^4 + 8M^2r^3 - 2a^2r^3 + 18a^2Mr^2 - 16a^2M^2r - 5a^4r + 6a^4M), \quad (\text{C.29})$$

$$\begin{aligned}
P_{15}^{\text{DK}} = & r^3(r^6 - 8M^2r^4 + 9a^2r^4 - 22a^2Mr^3 + 6a^4r^2 - 4a^4Mr \\
& + 16a^4M^2 + 2a^6) - a^2 \cos^2 \theta(9r^7 - 28Mr^6 + 9a^2r^5 - 18a^2Mr^4 \\
& + 16a^2M^2r^3 + 16a^2M^2r^3 + 18a^4r^3 - 36a^4Mr^2 + 6a^6r - 8a^6M) \\
& - a^4 \cos^4 \theta[3r^4 - 4Mr^3 + r^2(8M^2 - 9a^2) + 18a^2Mr - 16a^2M^2] \\
& - a^6 \cos^6 \theta(r^3 - 3a^2r + 2a^2M). \tag{C.30}
\end{aligned}$$

Bibliography

- [1] S. Alexander and N. Yunes. Chern-Simons modified general relativity. *Physics Reports*, 480:1–55, August 2009.
- [2] P. Amaro-Seoane, J. R. Gair, M. Freitag, M. C. Miller, I. Mandel, C. J. Cutler, and S. Babak. TOPICAL REVIEW: Intermediate and extreme mass-ratio inspirals – astrophysics, science applications and detection using LISA. *Classical and Quantum Gravity*, 24:113, September 2007.
- [3] T. A. Apostolatos, G. Lukes-Gerakopoulos, and G. Contopoulos. How to Observe a Non-Kerr Spacetime Using Gravitational Waves. *Physical Review Letters*, 103(11):111101, September 2009.
- [4] T. Bäckdahl and M. Herberthson. Explicit multipole moments of stationary axisymmetric spacetimes. *Classical and Quantum Gravity*, 22:3585–3594, September 2005.
- [5] L. Barack. TOPICAL REVIEW: Gravitational self-force in extreme mass-ratio inspirals. *Classical and Quantum Gravity*, 26(21):213001, November 2009.
- [6] L. Barack and C. Cutler. LISA capture sources: Approximate waveforms, signal-to-noise ratios, and parameter estimation accuracy. *Physical Review D*, 69:082005, Apr 2004.
- [7] L. Barack and N. Sago. Gravitational self-force on a particle in eccentric orbit around a Schwarzschild black hole. *Physical Review D*, 81(8):084021, April 2010.
- [8] E. Barausse and A. Buonanno. Improved effective-one-body hamiltonian for spinning black-hole binaries. *Physical Review D*, 81:084024, Apr 2010.
- [9] E. Barausse, A. Buonanno, S. A. Hughes, G. Khanna, S. O’Sullivan, and Y. Pan. Modeling multipolar gravitational-wave emission from small mass-ratio mergers. *Physical Review D*, 85(2):024046, January 2012.
- [10] P. Bender et al. Laser Interferometer Space Antenna for the Detection and Observation of Gravitational Waves: An International Project in the Field of Fundamental Physics in Space. LISA Pre-Phase A Report, Max-Planck-Institut für Quantenoptik, Garching, July 1998. MPQ 233.

- [11] B. Bertotti, L. Iess, and P. Tortora. A test of general relativity using radio links with the Cassini spacecraft. *Nature*, 425:374–376, September 2003.
- [12] L. Blanchet. Gravitational Radiation from Post-Newtonian Sources and Inspiral Compact Binaries. *Living Reviews in Relativity*, 9:4, June 2006.
- [13] J. Brink. Spacetime encodings. I. A spacetime reconstruction problem. *Physical Review D*, 78(10):102001, November 2008.
- [14] J. Brink. Spacetime encodings. II. Pictures of integrability. *Physical Review D*, 78(10):102002, November 2008.
- [15] J. Brink. Spacetime encodings. III. Second order Killing tensors. *Physical Review D*, 81(2):022001, January 2010.
- [16] J. Brink. Spacetime encodings. IV. The relationship between Weyl curvature and Killing tensors in stationary axisymmetric vacuum spacetimes. *Physical Review D*, 81(2):022002, January 2010.
- [17] J. Brink. Formal solution of the fourth order Killing equations for stationary axisymmetric vacuum spacetimes. *Physical Review D*, 84(10):104015, November 2011.
- [18] A. E. Broderick, V. L. Fish, S. S. Doeleman, and A. Loeb. Estimating the Parameters of Sagittarius A*’s Accretion Flow Via Millimeter VLBI. *The Astrophysical Journal*, 697:45–54, May 2009.
- [19] D. A. Brown, J. Brink, H. Fang, J. R. Gair, C. Li, G. Lovelace, I. Mandel, and K. S. Thorne. Prospects for Detection of Gravitational Waves from Intermediate-Mass-Ratio Inspirals. *Physical Review Letters*, 99(20):201102, November 2007.
- [20] L. M. Burko. Orbital evolution of a test particle around a black hole. II. Comparison of contributions of spin-orbit coupling and the self-force. *Physical Review D*, 69(4):044011, February 2004.
- [21] B. A. Campbell, N. Kaloper, and K. A. Olive. Classical hair for Kerr-Newman black holes in string gravity. *Physics Letters B*, 285:199–205, July 1992.
- [22] B. Carter. Global Structure of the Kerr Family of Gravitational Fields. *Physical Review*, 174:1559–1571, October 1968.
- [23] B. Carter. Axisymmetric Black Hole Has Only Two Degrees of Freedom. *Physical Review Letters*, 26:331–333, February 1971.
- [24] E. J. M. Colbert and M. C. Miller. Observational Evidence for Intermediate-Mass Black Holes in Ultra-Luminous X-Ray Sources. In M. Novello, S. Perez Bergliaffa, and R. Ruffini, editor, *The Tenth Marcel Grossmann Meeting. On recent developments in theoretical and experimental general relativity, gravitation and relativistic field theories*, page 530, February 2005.

- [25] N. A. Collins and S. Hughes. Towards a formalism for mapping the spacetimes of massive compact objects: Bumpy black holes. *Physical Review D*, 69:124022, 2004.
- [26] M. Colpi, S. L. Shapiro, and I. Wasserman. Boson stars - Gravitational equilibria of self-interacting scalar fields. *Physical Review Letters*, 57:2485–2488, November 1986.
- [27] K. Danzmann. LISA - An ESA cornerstone mission for the detection and observation of gravitational waves. *Advances in Space Research*, 32:1233–1242, October 2003.
- [28] K. Danzmann and A. Rüdiger. LISA technology - concept, status, prospects. *Classical and Quantum Gravity*, 20:1, May 2003.
- [29] W. G. Dixon. Dynamics of Extended Bodies in General Relativity. I. Momentum and Angular Momentum. *Royal Society of London Proceedings Series A*, 314:499–527, January 1970.
- [30] S. S. Doeleman, J. Weintroub, A. E. E. Rogers, R. Plambeck, R. Freund, R. P. J. Tilanus, P. Friberg, L. M. Ziurys, J. M. Moran, B. Corey, K. H. Young, D. L. Smythe, M. Titus, D. P. Marrone, R. J. Cappallo, D. C.-J. Bock, G. C. Bower, R. Chamberlin, G. R. Davis, T. P. Krichbaum, J. Lamb, H. Maness, A. E. Niell, A. Roy, P. Strittmatter, D. Werthimer, A. R. Whitney, and D. Woody. Event-horizon-scale structure in the supermassive black hole candidate at the Galactic Centre. *Nature*, 455:78–80, September 2008.
- [31] S. P. Drake and P. Szekeres. Uniqueness of the Newman-Janis Algorithm in Generating the Kerr-Newman Metric. *General Relativity and Gravitation*, 32:445–458, March 2000.
- [32] S. Drasco and S. A. Hughes. Rotating black hole orbit functionals in the frequency domain. *Physical Review D*, 69(4):044015, February 2004.
- [33] F. J. Ernst. New Formulation of the Axially Symmetric Gravitational Field Problem. *Physical Review D*, 167:1175–1177, March 1968.
- [34] G. Fodor, C. Hoenselaers, and Z. Perjés. Multipole moments of axisymmetric systems in relativity. *Journal of Mathematical Physics*, 30:2252–2257, October 1989.
- [35] J. R. Gair, C. Li, and I. Mandel. Observable properties of orbits in exact bumpy spacetimes. *Physical Review D*, 77(2):024035, January 2008.
- [36] R. Geroch. Multipole Moments. II. Curved Space. *Journal of Mathematical Physics*, 11:2580–2588, August 1970.

- [37] A. M. Ghez, B. L. Klein, M. Morris, and E. E. Becklin. High Proper-Motion Stars in the Vicinity of Sagittarius A*: Evidence for a Supermassive Black Hole at the Center of Our Galaxy. *The Astrophysical Journal*, 509:678–686, December 1998.
- [38] K. Glampedakis and S. Babak. Mapping spacetimes with LISA: inspiral of a test body in a 'quasi-Kerr' field. *Classical and Quantum Gravity*, 23:4167–4188, June 2006.
- [39] H. Goldstein, C. Poole, and J. Safko. *Classical mechanics*. Addison Wesley, 2002.
- [40] S. E. Gralla. Motion of small bodies in classical field theory. *Physical Review D*, 81(8):084060, April 2010.
- [41] W.-B. Han. Gravitational radiation from a spinning compact object around a supermassive Kerr black hole in circular orbit. *Physical Review D*, 82(8):084013, October 2010.
- [42] R. O. Hansen. Multipole moments of stationary space-times. *Journal of Mathematical Physics*, 15:46–52, January 1974.
- [43] J. B. Hartle. Slowly Rotating Relativistic Stars. I. Equations of Structure. *The Astrophysical Journal*, 150:1005, December 1967.
- [44] J. B. Hartle and K. S. Thorne. Slowly Rotating Relativistic Stars. II. Models for Neutron Stars and Supermassive Stars. *The Astrophysical Journal*, 153:807, September 1968.
- [45] A. Heger, C. L. Fryer, S. E. Woosley, N. Langer, and D. H. Hartmann. How Massive Single Stars End Their Life. *The Astrophysical Journal*, 591:288–300, July 2003.
- [46] T. Hinderer and É. É. Flanagan. Two-timescale analysis of extreme mass ratio inspirals in Kerr spacetime: Orbital motion. *Physical Review D*, 78(6):064028, September 2008.
- [47] E. A. Huerta and J. R. Gair. Importance of including small body spin effects in the modelling of extreme and intermediate mass-ratio inspirals. *Physical Review D*, 84(6):064023, September 2011.
- [48] W. Israel. Event Horizons in Static Vacuum Space-Times. *Physical Review*, 164:1776–1779, December 1967.
- [49] P. Jaranowski and A. Królak. Gravitational-Wave Data Analysis. Formalism and Sample Applications: The Gaussian Case. *Living Reviews in Relativity*, 8:3, March 2005.

- [50] T. Johannsen and D. Psaltis. Testing the No-hair Theorem with Observations in the Electromagnetic Spectrum. I. Properties of a Quasi-Kerr Spacetime. *The Astrophysical Journal*, 716:187–197, June 2010.
- [51] T. Johannsen and D. Psaltis. Testing the No-hair Theorem with Observations in the Electromagnetic Spectrum. II. Black Hole Images. *The Astrophysical Journal*, 718:446–454, July 2010.
- [52] G. Jones and J. E. Wang. Weyl card diagrams. *Physical Review D*, 71(12):124019, June 2005.
- [53] P. Kanti, N. E. Mavromatos, J. Rizos, K. Tamvakis, and E. Winstanley. Dilatonic black holes in higher curvature string gravity. *Physical Review D*, 54:5049–5058, October 1996.
- [54] P. Kanti, N. E. Mavromatos, J. Rizos, K. Tamvakis, and E. Winstanley. Dilatonic black holes in higher curvature string gravity. II. Linear stability. *Physical Review D*, 57:6255–6264, May 1998.
- [55] J. Kormendy and D. Richstone. Inward Bound—The Search For Supermassive Black Holes In Galactic Nuclei. *Annual Review of Astronomy and Astrophysics*, 33:581, 1995.
- [56] M. Kramer, I. H. Stairs, R. N. Manchester, M. A. McLaughlin, A. G. Lyne, R. D. Ferdman, M. Burgay, D. R. Lorimer, A. Possenti, N. D’Amico, J. M. Sarkissian, G. B. Hobbs, J. E. Reynolds, P. C. C. Freire, and F. Camilo. Tests of General Relativity from Timing the Double Pulsar. *Science*, 314:97–102, October 2006.
- [57] K. Liu, N. Wex, M. Kramer, J. M. Cordes, and T. J. W. Lazio. Prospects for Probing the Spacetime of Sgr A* with Pulsars. *The Astrophysical Journal*, 747:1, March 2012.
- [58] J. Magorrian, S. Tremaine, D. Richstone, R. Bender, G. Bower, A. Dressler, S. M. Faber, K. Gebhardt, R. Green, C. Grillmair, J. Kormendy, and T. Lauer. The Demography of Massive Dark Objects in Galaxy Centers. *The Astronomical Journal*, 115:2285–2305, June 1998.
- [59] V. S. Manko and I. D. Novikov. Generalizations of the Kerr and Kerr-Newman metrics possessing an arbitrary set of mass-multipole moments. *Classical and Quantum Gravity*, 9:2477–2487, November 1992.
- [60] D. Merritt, T. Alexander, S. Mikkola, and C. M. Will. Testing properties of the Galactic center black hole using stellar orbits. *Physical Review D*, 81(6):062002, March 2010.
- [61] S. Mignemi and N. R. Stewart. Dilaton-axion hair for slowly rotating Kerr black holes. *Physics Letters B*, 298:299–304, January 1993.

- [62] C. W. Misner, K. S. Thorne, and J. A. Wheeler. *Gravitation*. W. H. Freeman and Co., 1973.
- [63] D. J. Mortlock, S. J. Warren, B. P. Venemans, M. Patel, P. C. Hewett, R. G. McMahon, C. Simpson, T. Theuns, E. A. González-Solares, A. Adamson, S. Dye, N. C. Hambly, P. Hirst, M. J. Irwin, E. Kuiper, A. Lawrence, and H. J. A. Röttgering. A luminous quasar at a redshift of $z = 7.085$. *Nature*, 474:616–619, June 2011.
- [64] R. Narayan, J. E. McClintock, and R. Shafee. Estimating the Spins of Stellar-Mass Black Holes by Fitting Their Continuum Spectra. In Y.-F. Yuan, X.-D. Li, and D. Lai, editor, *Astrophysics of Compact Objects*, volume 968 of *American Institute of Physics Conference Series*, pages 265–272, January 2008.
- [65] E. T. Newman and A. I. Janis. Note on the Kerr Spinning-Particle Metric. *Journal of Mathematical Physics*, 6:915–917, June 1965.
- [66] F. Özel, D. Psaltis, R. Narayan, and J. E. McClintock. The Black Hole Mass Distribution in the Galaxy. *The Astrophysical Journal*, 725:1918–1927, December 2010.
- [67] P. Pani and V. Cardoso. Are black holes in alternative theories serious astrophysical candidates? The case for Einstein-dilaton-Gauss-Bonnet black holes. *Physical Review D*, 79(8):084031, April 2009.
- [68] A. Papapetrou. Spinning Test-Particles in General Relativity. I. *Royal Society of London Proceedings Series A*, 209:248–258, October 1951.
- [69] A. Z. Petrov. *Einstein spaces*. Pergamon Press, 1969.
- [70] E. Poisson. The Motion of Point Particles in Curved Spacetime. *Living Reviews in Relativity*, 7:6, May 2004.
- [71] E. Poisson, A. Pound, and I. Vega. The Motion of Point Particles in Curved Spacetime. *Living Reviews in Relativity*, 14:7, September 2011.
- [72] M. Pomazanov, V. Kolubasova, and S. Alexeyev. The problem of singularities of higher order curvature corrections in four dimensional string gravity. arXiv:gr-qc/0301029. January 2003.
- [73] S. F. Portegies Zwart and S. L. W. McMillan. The Runaway Growth of Intermediate-Mass Black Holes in Dense Star Clusters. *The Astrophysical Journal*, 576:899–907, September 2002.
- [74] R. H. Price. Nonspherical Perturbations of Relativistic Gravitational Collapse. I. Scalar and Gravitational Perturbations. *Physical Review D*, 5:2419–2438, May 1972.

- [75] R. H. Price. Nonspherical Perturbations of Relativistic Gravitational Collapse. II. Integer-Spin, Zero-Rest-Mass Fields. *Physical Review D*, 5:2439–2454, May 1972.
- [76] T. Prince. LISA: The Laser Interferometer Space Antenna. In *American Astronomical Society Meeting Abstracts #202*, volume 35 of *Bulletin of the American Astronomical Society*, page 751, May 2003.
- [77] D. Psaltis. Private communication.
- [78] D. Psaltis. Probes and Tests of Strong-Field Gravity with Observations in the Electromagnetic Spectrum. *Living Reviews in Relativity*, 11:9, November 2008.
- [79] D. C. Robinson. Uniqueness of the Kerr black hole. *Physical Review Letters*, 34:905, April 1975.
- [80] F. D. Ryan. Gravitational waves from the inspiral of a compact object into a massive, axisymmetric body with arbitrary multipole moments. *Physical Review D*, 52:5707–5718, November 1995.
- [81] F. D. Ryan. Spinning boson stars with large self-interaction. *Physical Review D*, 55:6081–6091, May 1997.
- [82] W. Schmidt. Celestial mechanics in Kerr spacetime. *Classical and Quantum Gravity*, 19:2743–2764, May 2002.
- [83] B. F. Schutz, J. Centrella, C. Cutler, and S. A. Hughes. Will Einstein Have the Last Word on Gravity? In *Astro2010: The Astronomy and Astrophysics Decadal Survey*, page 265, 2009.
- [84] A. Sesana, M. Volonteri, and F. Haardt. The imprint of massive black hole formation models on the LISA data stream. *Monthly Notices of the Royal Astronomical Society*, 377:1711–1716, June 2007.
- [85] R. Smits, M. Kramer, B. Stappers, D. R. Lorimer, J. Cordes, and A. Faulkner. Pulsar searches and timing with the Square Kilometre Array. *Astronomy and Astrophysics*, 493:1161–1170, January 2009.
- [86] C. F. Sopuerta. A Roadmap to Fundamental Physics from LISA EMRI Observations. *GW Notes, Vol. 4, p. 3-47*, 4:3–47, September 2010.
- [87] C. F. Sopuerta and N. Yunes. Extreme- and intermediate-mass ratio inspirals in dynamical Chern-Simons modified gravity. *Physical Review D*, 80(6):064006, September 2009.
- [88] I. H. Stairs. Testing General Relativity with Pulsar Timing. *Living Reviews in Relativity*, 6:5, September 2003.

- [89] J. F. Steiner, R. C. Reis, J. E. McClintock, R. Narayan, R. A. Remillard, J. A. Orosz, L. Gou, A. C. Fabian, and M. A. P. Torres. The spin of the black hole microquasar XTE J1550-564 via the continuum-fitting and Fe-line methods. *Monthly Notices of the Royal Astronomical Society*, 416:941–958, September 2011.
- [90] J. Steinhoff and D. Puetzfeld. Multipolar equations of motion for extended test bodies in general relativity. *Physical Review D*, 81(4):044019, February 2010.
- [91] T. Torii, H. Yajima, and K.-I. Maeda. Dilatonic black holes with a Gauss-Bonnet term. *Physical Review D*, 55:739–753, January 1997.
- [92] S. Vigeland. Multipole moments of bumpy black holes. *Physical Review D*, 82(10):104041, November 2010.
- [93] S. Vigeland and S. A. Hughes. Spacetime and orbits of bumpy black holes. *Physical Review D*, 81(2):024030, January 2010.
- [94] S. Vigeland, N. Yunes, and L. C. Stein. Bumpy black holes in alternative theories of gravity. *Physical Review D*, 83(10):104027, May 2011.
- [95] N. Warburton and L. Barack. Self-force on a scalar charge in Kerr spacetime: Eccentric equatorial orbits. *Physical Review D*, 83:124038, Jun 2011.
- [96] C. M. Will. *Theory and Experiment in Gravitational Physics*. Cambridge University Press, 1993.
- [97] N. Yunes. Gravitational Wave Modelling of Extreme Mass Ratio Inspirals and the Effective-One-Body Approach. *GW Notes, Vol. 2, p. 3-47*, 2:3–47, November 2009.
- [98] N. Yunes and E. Berti. Accuracy of the post-Newtonian approximation: Optimal asymptotic expansion for quasicircular, extreme-mass ratio inspirals. *Physical Review D*, 77(12):124006, June 2008.
- [99] N. Yunes, A. Buonanno, S. A. Hughes, M. C. Miller, and Y. Pan. Modeling Extreme Mass Ratio Inspirals within the Effective-One-Body Approach. *Physical Review Letters*, 104(9):091102, March 2010.
- [100] N. Yunes, A. Buonanno, S. A. Hughes, Y. Pan, E. Barausse, M. C. Miller, and W. Thorne. Extreme mass-ratio inspirals in the effective-one-body approach: Quasicircular, equatorial orbits around a spinning black hole. *Physical Review D*, 83(4):044044, February 2011.
- [101] N. Yunes and F. Pretorius. Dynamical Chern-Simons modified gravity: Spinning black holes in the slow-rotation approximation. *Physical Review D*, 79(8):084043, April 2009.

- [102] N. Yunes and F. Pretorius. Fundamental theoretical bias in gravitational wave astrophysics and the parametrized post-Einsteinian framework. *Physical Review D*, 80(12):122003, December 2009.
- [103] N. Yunes and L. C. Stein. Nonspinning black holes in alternative theories of gravity. *Physical Review D*, 83(10):104002, May 2011.
- [104] J. Ziółkowski. Evolutionary constraints on the masses of the components of the HDE 226868/Cyg X-1 binary system. *Monthly Notices of the Royal Astronomical Society*, 358:851–859, April 2005.